Coop-
Agreement
Honeywell Inc

THESIS/
REPORTS
SWANSON,
D.H.

EXTENDED HIGH-ALTITUDE RETARDANT DROP MECHANIZATION STUDY

Final Report

to

UNITED STATES DEPARTMENT OF AGRICULTURE
FOREST SERVICE
INTERMOUNTAIN FOREST & RANGE EXPERIMENT STATION
OGDEN, UTAH 84401

A report of research performed under the auspices of the Intermountain Forest and Range Experiment Station

Honeywell
600 2ND STREET NORTH
HOPKINS, MINNESOTA 55343

Honeywell

EXTENDED HIGH-ALTITUDE RETARDANT DROP MECHANIZATION STUDY

FINAL REPORT

by

D. H. Swanson and T. N. Helvig

Contract 26-2888

10 January 1974

United States Department of Agriculture
Forest Service
Intermountain Forest & Range Experiment Station
Ogden, Utah 84401

Approved by:

D. H. Swanson
Program Manager

Submitted by:

R. Biscoe
Marketing Representative

Government and Aeronautical Products Division
2600 RIDGWAY PARKWAY, MINNEAPOLIS, MINNESOTA 55413

TABLE OF CONTENTS

Section		Page
I	INTRODUCTION	1
II	EXECUTIVE SUMMARY	3
	Methodology and Results	3
	Determination of Vertical Fuel Coverage	5
	Contained Delivery Versus Cascade	8
	Retardant Breakup Physics	11
	Flow-Rate Distribution Effect on Pattern Formation	11
	Effect of Altitude on the Pattern	15
	Importance of Retardant Form Over Altitude	19
	Simulation Models	24
	Simulation Program Description	24
	Input Variables	26
	Processing Steps	29
	Output	35
	Conclusions	43
III	TASK 1 - FLOW-RATE CALIBRATION	44
	Background	44
	Summary	45
	Conclusions	45
	Discussion	46
	Program Changes	46
	DC6B Test and Analysis	48

LIST OF ILLUSTRATIONS

Figure		Page
1	Basic Problem: Effect of Tank Design on Ground Pattern	4
2	Pattern Test Data in Isoplethic Form	6
3	Model View of Vertical Fuel Structure	7
4	Tree Loading for Thick and Thin Redardant	7
5	Reduction in Spread Rate or Intensity Afforded by Various Coverage Levels	9
6	Retardant Coverage Levels Desired for Various Fuel Complexes	10
7	Retardant Forms Evaluation	10
8	Taylor Instabilities	12
9	Retardant Breakup Process	13
10	Flow-Rate Distribution	14
11	Three-Dimensional Pattern	16
12	Pattern/Flow-Rate Distribution Comparison	16
13	Effect of Altitude on Retardant Cloud	17
14	Pattern Change with Altitude	18
15	Pattern Cross-Section as Modified by Altitude	18
16	Marginal Distribution Definition	20
17	Altitude Effect on Crossrange Distribution	21
18	Phases of Retardant Breakup	22
19	Importance of Retardant Breakup Phases	23
20	Simulation Overview	25
21	Tank Geometry Descriptors	27

LIST OF ILLUSTRATIONS (Continued)

Figure		Page
22	Inputs Describing Door Opening	27
23	Aircraft Inputs	28
24	Simulated and Measured Volume Flow-Rate Distribution	29
25	Breakup Physical Processes	30
26	Simulated Ground Pattern	31
27	Stored Rules for Estimating Uniform Distribution of Simulated Pattern	33
28	Rules for Estimating Normal Distribution of Pattern	34
29	Pattern Data Output in "Computer Scale"	36
30	Pattern Data Output in True Scale	37
31	Pattern Data Output in True Scale with Grid Overlay	38
32	Summary Data Output	39
33	Simulated and Actual Pattern Data Comparison	40
34	Simulated and Actual Pattern Data Comparison in Isoplethic Form	40
35	Centerline-to-Centerline Comparison of Simulated and Actual Pattern Data Example	41
36	Trail-Drop Pattern Performance	42
37	Door-Opening Data Comparison – DC6B Test	49
38	Flow Rate Prediction Comparison – DC6B Test	49
39	Door-Opening Data Comparison – P2V Test	50
40	Measured Flow Rate versus Time – CL-125 Test	53
41	Measured Door Opening versus Time – CL-125	53

LIST OF ILLUSTRATIONS (Continued)

Figure		Page
42	Comparison of Simulated and Measured Flow Rate – CL-125	55
43	Exit Velocity versus Time Simulation Using Cubic Polynomial – CL-125	55
44	Approximated Flow Rate	58
45	Comparison of Simulated and Real Patterns Using Approximate Measured Flow Rate	59
46	Pattern Forms	67
47	Typical MIX-2 Program Output	71
48	Simulated Marginal Range Distribution – 100% Recovery	72
49	Simulated Marginal Range Distribution – 78% Recovery	72
50	Simulated Uniform Range Distribution – $\lambda = 0.2$	73
51	Simulated "Normal" Range Distribution – $(1 - \lambda) = 0.8$	73
52	Combined Uniform and Normal Range Distribution	74
53	Three-Dimensional Pattern Simulation	74
54	Run 51 Test Data	76
55	Run 51 Test Data with Densities ≤ 0.1 gpc Removed	77
56	Simulated Data	78
57	Differenced Data	78
58	Flow Chart of MIX2/RETARD Comparison Process	80
59	Factorial Computer Experiment Setup	84
60	Comparison of Test and Simulation Data – CL-215 Drop at 173 Feet	85
61	Comparison of Test and Simulation Data – CL-215 Drops at 311 and 315 Feet	86

LIST OF ILLUSTRATIONS (Continued)

Figure		Page
62	Comparison of Test and Simulation Data – CL-125 Drop at 539 Feet	87
63	Comparison of Test and Simulation Data – CL-215 Drop at 1046 Feet	88
64	Comparison of Test and Simulation Data – DC6B Drop at 150 Feet	90
65	Comparison of Test and Simulation Data – DC6B Drop at 300 Feet	91
66	Comparison of Test and Simulation Data – P2V Drop at 150 Feet	92
67	Comparison of Test and Simulation Data – P2V Drops at 300 Feet	93
68	Simulation Results Scattergraph	95
69	Comparison of Test and Simulation Data – Aero Union B-17 Drop at 300 Feet	96
70	Comparison of Test and Simulation Data – Intermountain B-17 Drop at 500 Feet	97
71	Comparison of Test and Simulation Data – Intermountain B-17 Drop at 268 Feet	98
72	Comparison of Test and Simulation Data – Aero Union C-119 Drop at 150 Feet	99
73	Comparison of Test and Simulation Data – Aero Union Drop at 300 Feet	100
74	Comparison of Test and Simulation Data – Aero Union B-17 Trail Drop	102
75	Three-Dimensional Patterns of One- and Two-Tank Drops	103
76	Film Tracing of 1400-Gallon Drop	110
77	Frame Detail of Film Tracing	110

LIST OF ILLUSTRATIONS (Concluded)

Figure		Page
78	Time-Series Analysis Program	115
79	Single-Filter Type Power Spectral Density Analyzer	116
80	Simplified Example of the Hypothetical Interpretation of Pattern Frequency Data with Respect to Unstable Breakup	118
81	Marginal Difference Series (Range) – P2V Drop No. 2	119
82	Marginal Difference Series (Range) – P2V Drop No. 6	119
83	Marginal Difference Series (Range) – DC6B Drop No. 1	120
84	Marginal Difference Series (Range) – DC6B Drop No. 2	120
85	Power Spectrum for Three P2V Drops	121
86	Power Spectrum Gain Factor Associated with 125-Foot Altitude Increase	122

LIST OF TABLES

Table		Page
1	Measured Flow Data	54
2	Comparison of Polynomial Fit	56
3	Comparison of Match with Original Simulated and Measured Flow Data	60
4	Selected Parameter Sets	84
5	Comparison of PB4Y2 Simulation with Test Results	101
6	Simulation Applied to Multiple-Tank Drop	104

I. INTRODUCTION

This report documents effort on a change order resulting in a six-month extension to Contract 26-2888 for the High-Altitude Drop Mechanization Study. The particular effort was a logical extension of work summarized in a two-volume final report (Ref. 1). The technical content of the change order consisted of three specific work tasks:

- Task 1 - Flow-Rate Calibration, in which the retardant flow-rate prediction subroutine of the MacPherson simulation was checked against actual flow measured by the Forest Service in static and flight drops.

- Task 2 - Crossrange Development, in which the altitude-related rules for expanding the simulated distribution of retardant on the ground into a predicted pattern similar to those generated in grid tests was developed.

- Task 3 - Bond Number Studies, in which the study of physical theory of retardant breakup was continued for application to methods of controlling patterns and increasing understanding of the modeling.

A fourth task required program documentation, including a formal viewgraph presentation, to summarize contract findings.

Completion of the above tasks resulted in a substantial refinement of the ability to simulate airtanker performance and improvement of the analytic programs to extract information from recovered pattern data. Specifically, the simulation now offers the possibility of conducting air tanker evaluations over a full range of delivery altitudes, velocities, and tank release options, starting with measured flow rate parameters obtained in relatively inexpensive ground

tests. Capabilities and limitations of a given air tanker can then be defined without resorting to full-scale evaluation tests.

The three programs developed during the study have been furnished to the Northern Forest Fire Laboratory.

- MIX2, a research simulation program, evolving from original work by MacPherson, that develops a retardant pattern based on tank and aircraft parameters. (See Appendix A.)

- Modified RETARD, a program that accepts pattern data from MIX2 and/or actual card data from grid tests; conducts a wide range of statistical tests on the pattern; or, by comparison, produces similar statistical characterization of the differences between any two patterns. This feature allows optimization of empirical simulation rules or resolution of differences between closely related real patterns. (See Appendix B.)

- PATSIM, a simplified version of the MIX2/RETARD research program that accepts simplified tank and mission inputs to develop both detailed and summary pattern data output for ease of assessment. (See Appendix C.)

Section II of this report is an executive summary of program results, including a description of the operation of the simulation program. This summary is followed by individual sections which detail the results of the three tasks called out in the contract change order.

II. EXECUTIVE SUMMARY

This summary review of the High-Altitude Retardant Drop Mechanization Study includes information from both the original contract and the subsequent change order. It is particularly relevant because of the viewpoints in the earlier two-volume report have been modified slightly by increased resolution of delivery phenomena acquired in the continued effort. The narrative follows the organization of the visual presentation material (Task 4 of the Work Statement). For additional information on supporting studies, including delivery accuracy, hydrodynamic theory, preliminary tank designs and related material, refer to the prior report (Ref. 1).

METHODOLOGY AND RESULTS

The High-Altitude Retardant Mechanization Study was undertaken to determine the most effective way to improve air tanker performance against fires and particularly to assess techniques for increasing the permissible delivery altitude for increased safety and/or effective pattern generation (Figure 1).

A considerable amount of experimental data was available from two important Forest Service Test Series known as the Porterville and Marana Tests. This data base provided the basic input to address two interrelated questions:

- By what mechanisms in the design of the tank and gating system can bulk release (cascade) of retardant as currently practiced be improved?

- Can alternative delivery techniques such as the use of containers improve delivery capability?

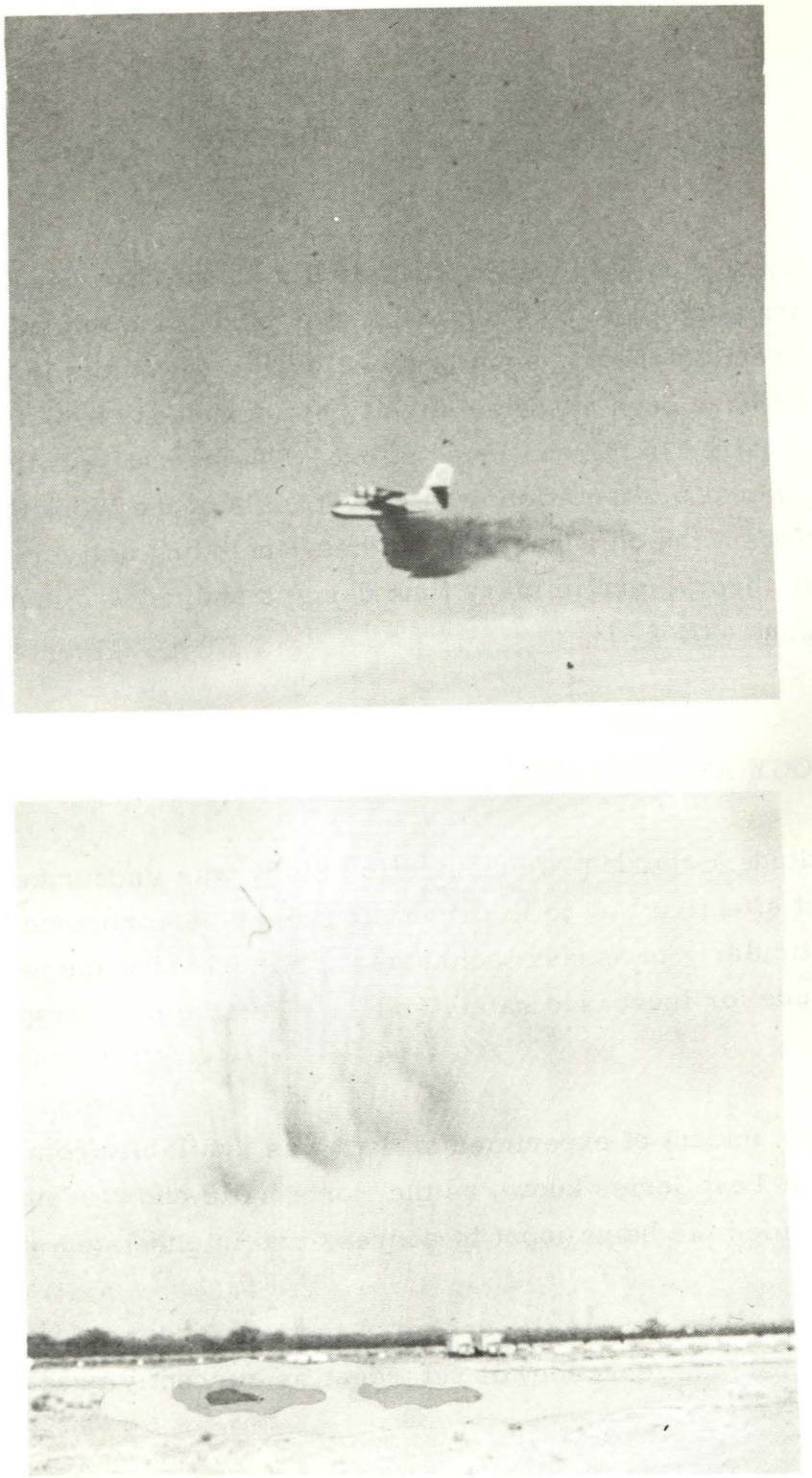

Figure 1. Basic Problem: Effect of Tank Design on Ground Pattern

The test results available were isoplethic representations of recovered retardant patterns developed on the ground for a range of aircraft, tanks, altitudes, velocities, and retardants (Figure 2). (The term isopleth refers to lines on a map connecting points at which a given variable, in this case, gallons per 100 sqaure feet, or gpc, has a specified constant value.)

Determination of Vertical Fuel Coverage

The first problem was to assess the collected retardant pattern based on effectiveness against various fire situations and mission intent. Since the patterns are collected on a flat surface and, since most of the quantitative estimates of appropriate coverage levels are developed in essentially two-dimensional fuel beds, an initial task under the contract was to estimate the effect of three-dimensional fuel structures on pattern effectiveness.

A vertical fuel coverage model was developed as a method of providing estimates of the vertical fuel effect on required retardant quantities. (This model is documented in Volume 2 of Reference 1 and is briefly described here.) The model views the vertical fuel structure as a series of geometrical segments (Figure 3). Each segment is described in terms of measured fuel parameters, geometry, surface area and fuel volume. Retardant entering vertically is allowed to pass through the segment, be captured and retained, or drip to the next section when the surface is saturated. The model is conceptually related to forest hydrological studies, and can be calibrated for waterlike materials against experimental studies.

With the model, the effect of various retardant characteristics including thickness (determining the limits of the amount that can be retained on fuel surface), salt content, and fuel types can be evaluated as a function of the amount of retardant applied to the top of the fuel structure. Figure 4 shows tree loading achieved for a thick and thin retardant as a function of gpc.

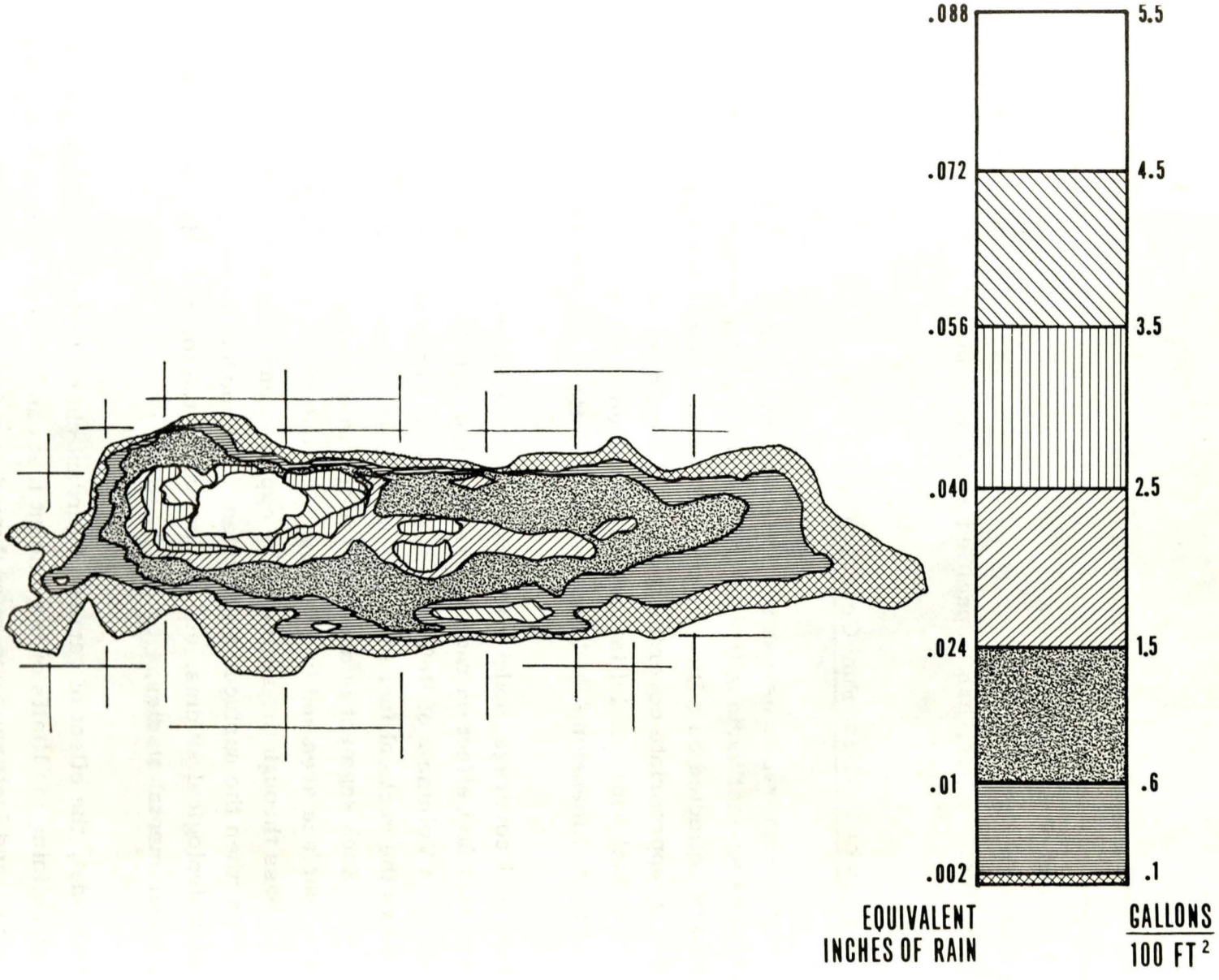

Figure 2. Pattern Test Data in Isoplethic Form

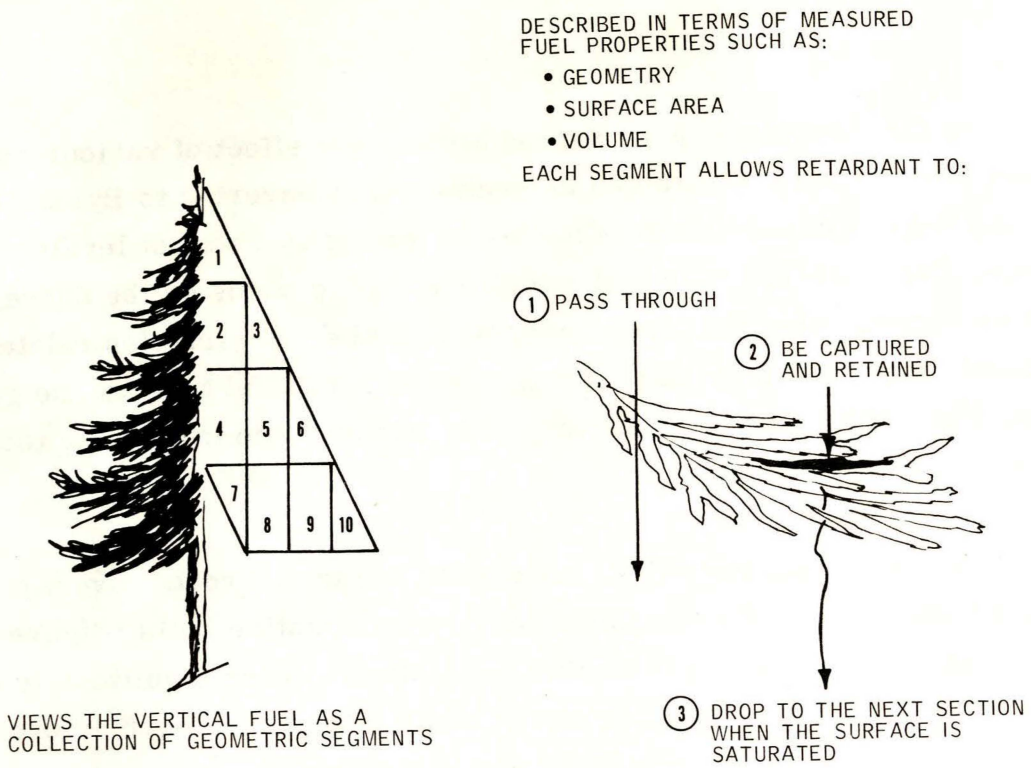

Figure 3. Model View of Vertical Fuel Structure

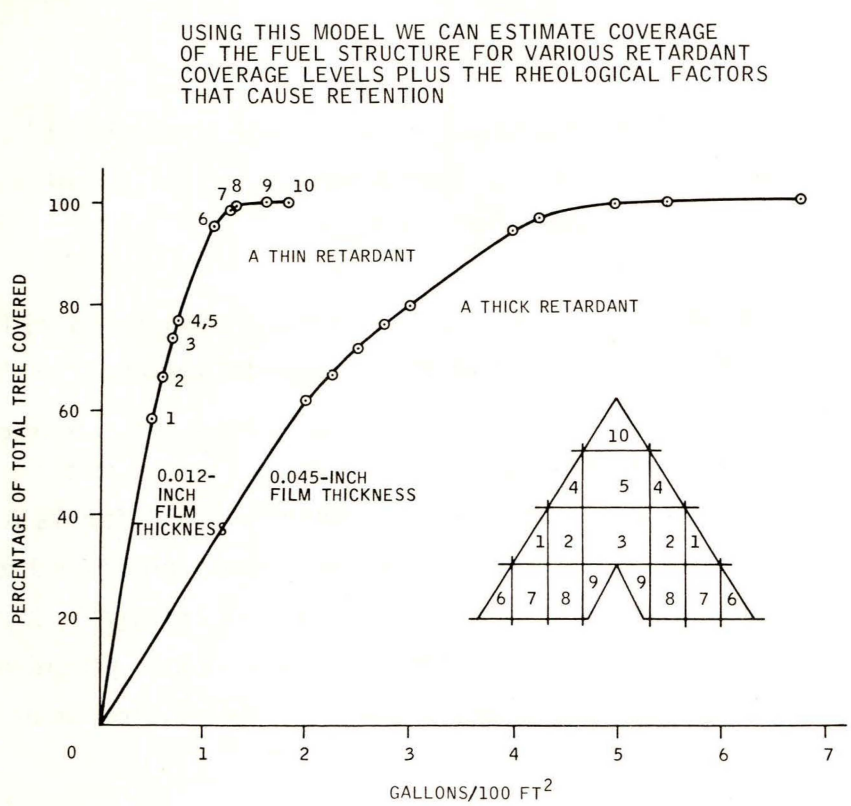

Figure 4. Tree Loading for Thick and Thin Retardant

By applying the Rothermel Fire Spread Model, the effect of various coverage levels on the fire spread rate can be evaluated. Converted to Byram's intensity scale, the degree of knockdown afforded by various treatment levels can be estimated (Figure 5) for four fuel situations. (The bands on the curve may be viewed as representing the uncertainty in a number of variables related to fire spread and suppression by retardants.) It is also useful to show the general intensity characteristics of fires subject to suppression in direct attack as extrapolated from Canadian data.

Results of the program permit an estimation of the retardant coverage levels associated with effective use against four representative fuels (Figure 6). Although the levels inferred from this study do not differ significantly from those previously thought adequate on the basis of experience, they provide a reasonable point of departure for tradeoff studies.

Contained Delivery Versus Cascade

A key point in this study is the necessity to achieve distribution of retardant films over a considerable area, i. e., to convert an initial quantity (gallons per foot) into a gallons-per-100-square-foot film.

On this basis, the hydrodynamic breakup phenomena associated with cascade delivery is an essentially free source of the energy to accomplish the area expansion. The ability of containers to break and splash to appropriate uniform coverage levels is limited by impact energy, which in turn is limited by ground safety requirements. As a result, the retardant forms for delivery may be organized as shown in Figure 7. The physically contained methods of delivery gain advantages over bulk release only where relatively high coverage levels must be achieved from high altitudes. Drop size can potentially be increased up to those approaching small containers by manipulation of retardant rheology.

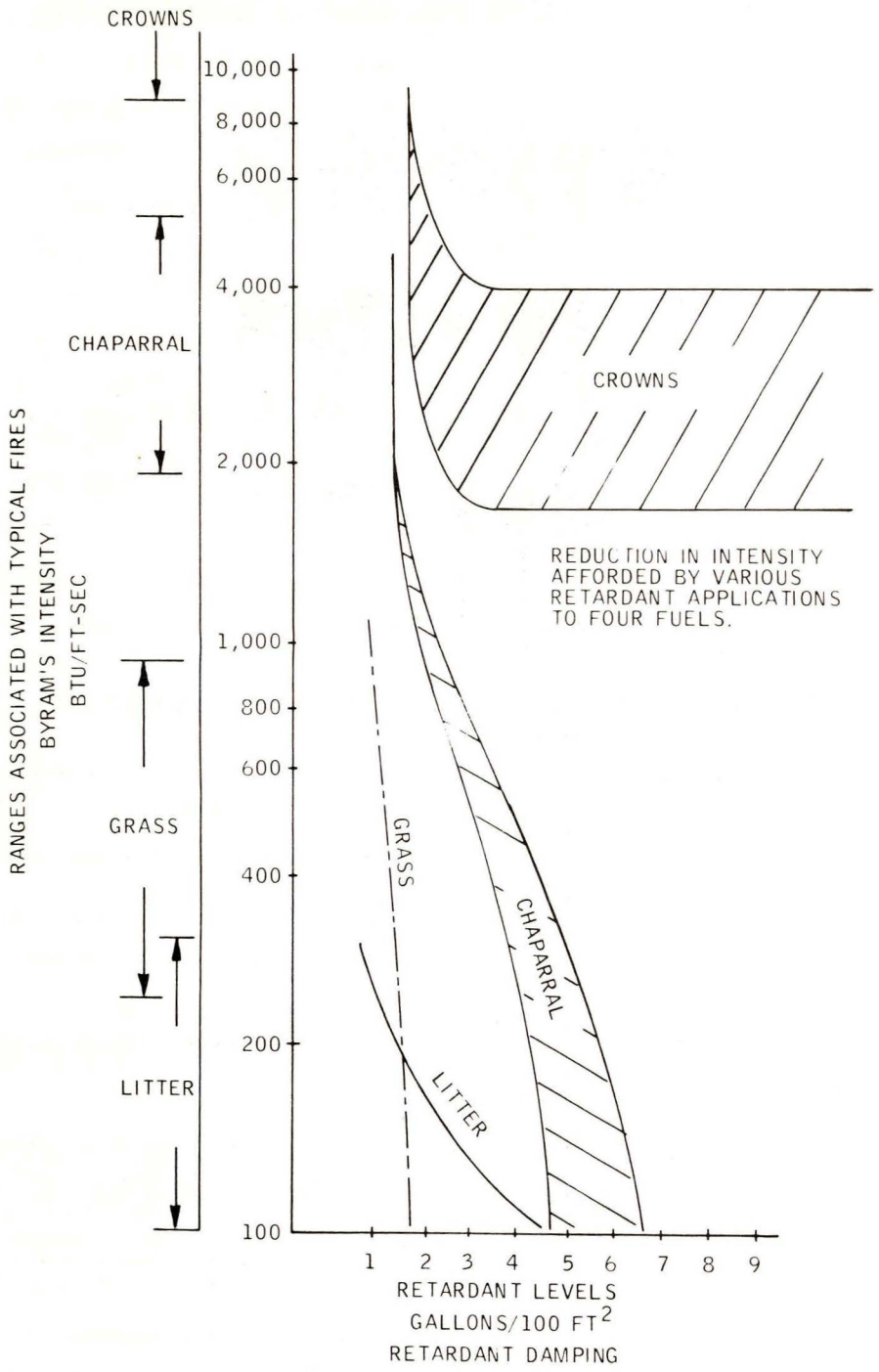

Figure 5. Reduction in Spread Rate or Intensity Afforded by Various Coverage Levels

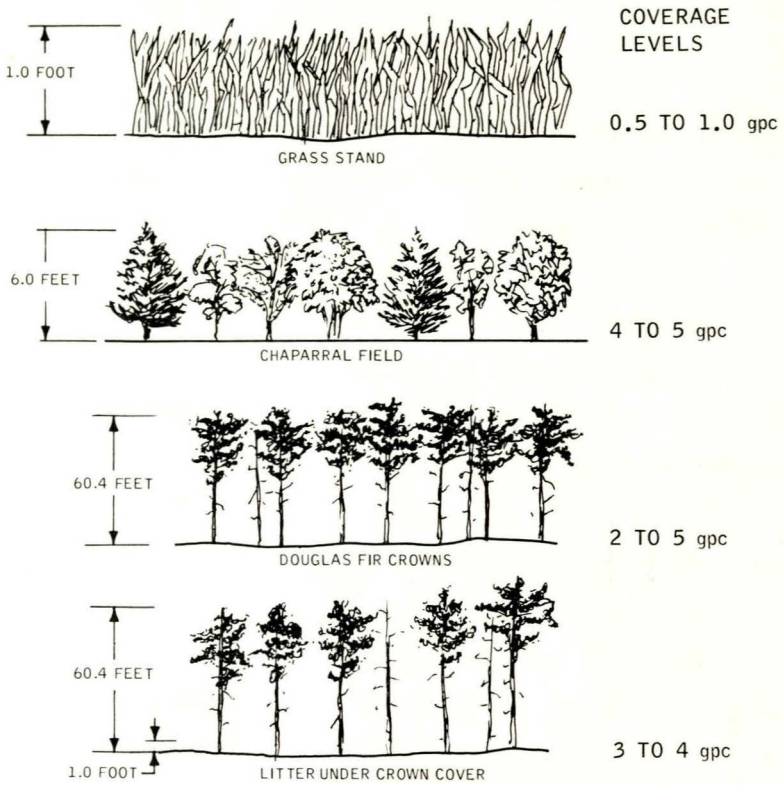

Figure 6. Retardant Coverage Levels Desired for Various Fuel Complexes

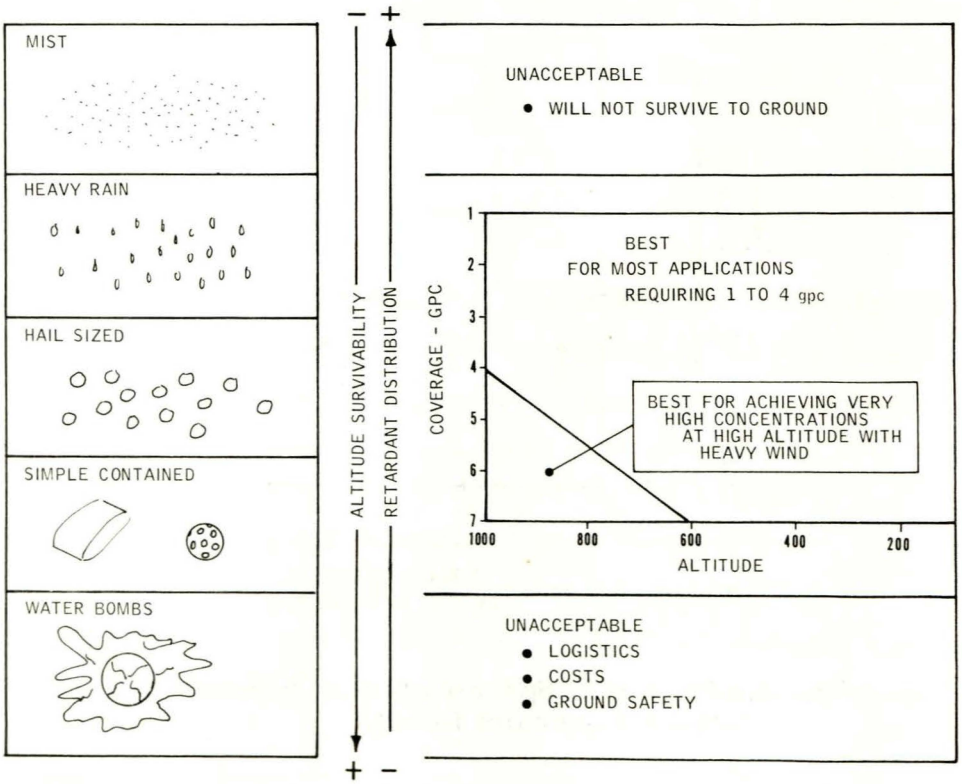

Figure 7. Retardant Forms Evaluation

Retardant Breakup Physics

There are two separable parts to the development of appropriate coverage levels. The rate at which the aircraft releases the retardant, and the processes whereby the aerodynamic breakup occurs. Considerable study was conducted (Ref 1, Vol 1) to determine the physics of breakup. It was found that the breakup takes two forms: (1) peripheral stripping, which contributes losses in the recovered retardant and adds little to the meaningful pattern; and (2) unstable breakup by virtue of Taylor instabilities that develop on the frontal face of the retardant mass. These instabilities are visible as the spike and bubble formations shown in Figure 8.

Extension of this theory to release condition identifies the stages in the process (Figure 9) for the CL-215. They are (1) a discharge phase during which fluid is released continuously from the tank, (2) a deformation phase characterized by by frontal area expansion that contributes width to the pattern, and (3) a sudden breakup due to amplifying instabilities after which the retardant trajectory is essentially straight downward. Higher aircraft velocity or smaller release quantities both have the effect of reducing the time to breakup and limiting pattern width.

Flow-Rate Distribution Effect on Pattern Formation

The basic controllable factor that determines pattern characteristics is the volume flow rate from the tank, i. e., the starting point that is modified by aerodynamic influences. This flow rate is the gallons per second released for each second of aircraft travel as shown in Figure 10. In the figure, the measured flow from the CL-215 tank is juxtaposed against the retardant as it appears during the release phase. The flow-rate distribution is determined by tank geometry, door geometry, door opening rate, and venting, and is therefore subject to control.

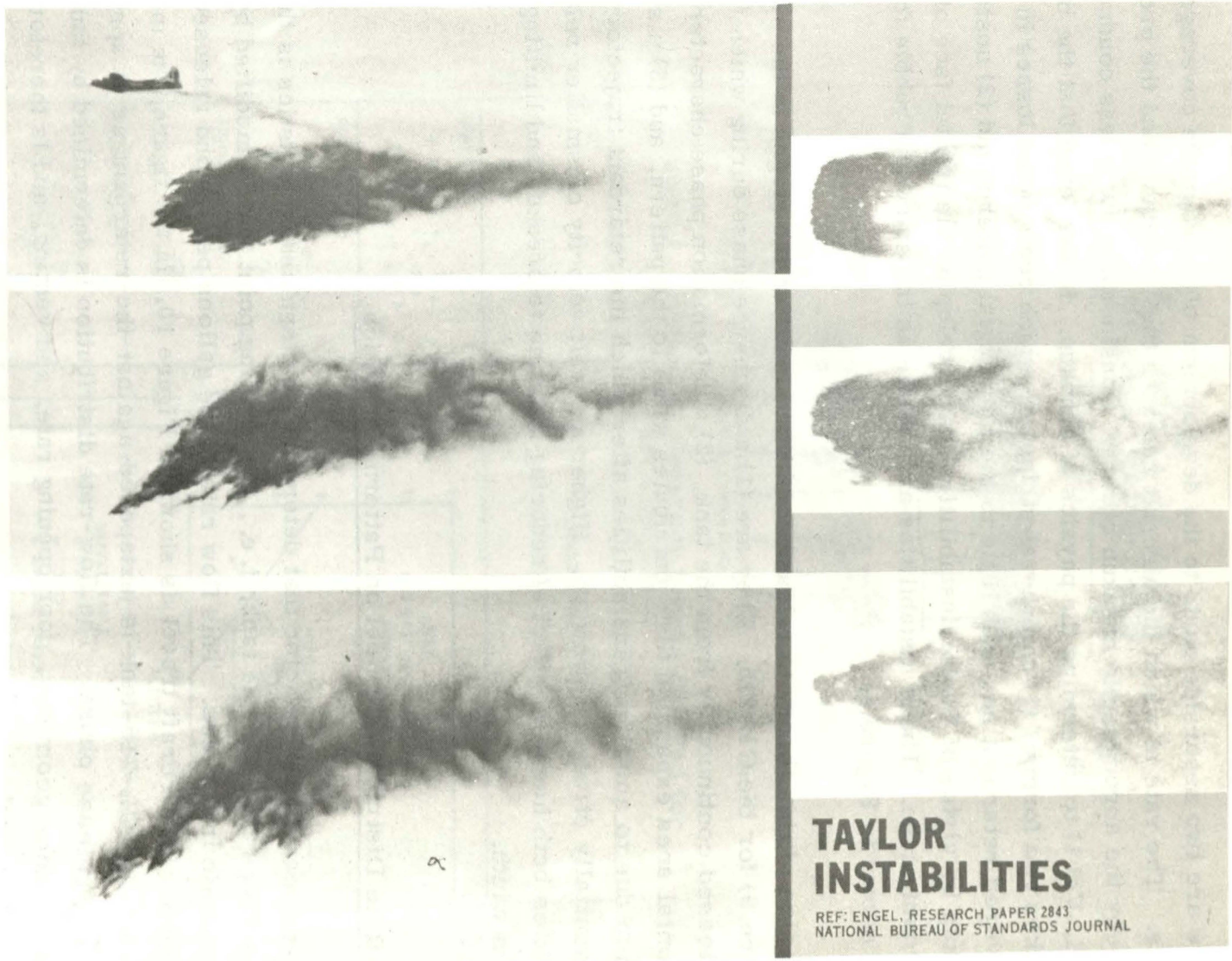

Figure 8. Taylor Instabilities

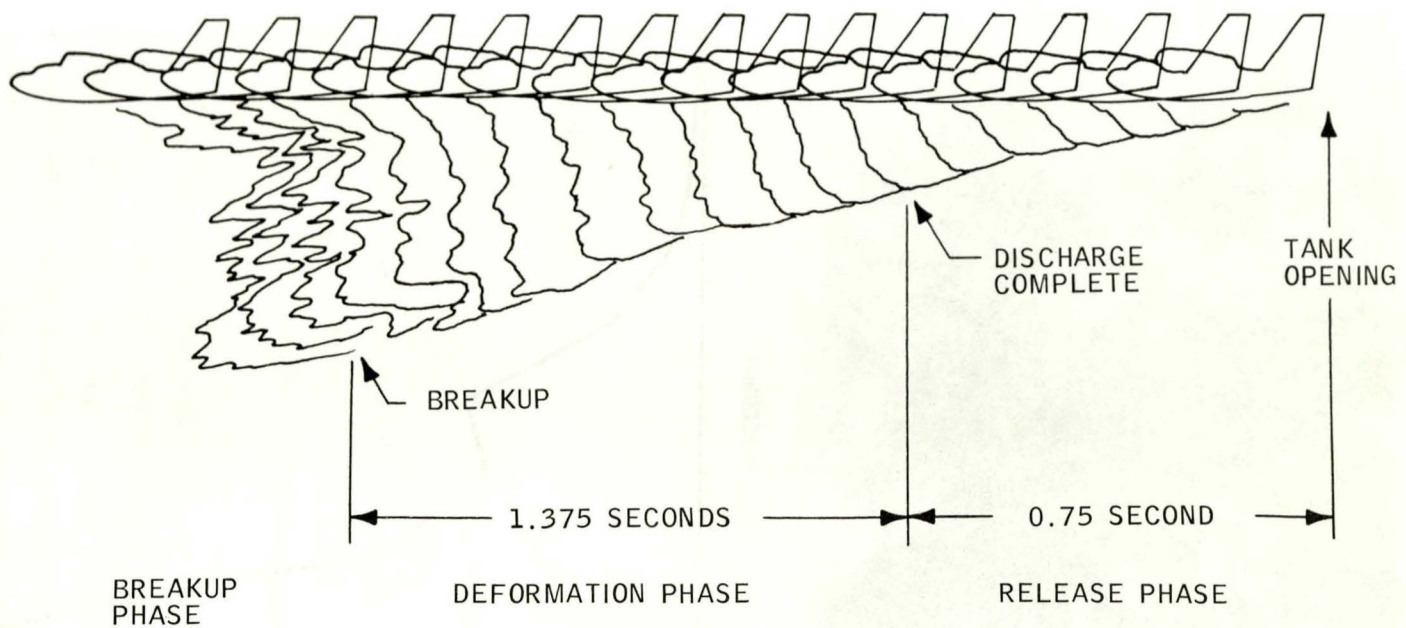

Figure 9. Retardant Breakup Process

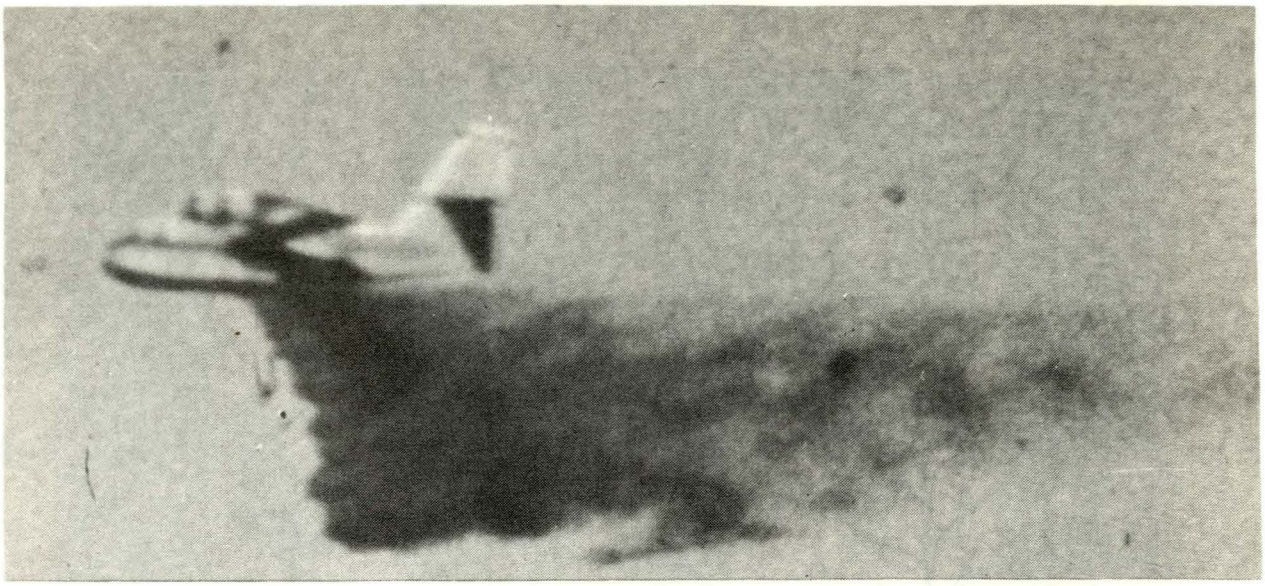

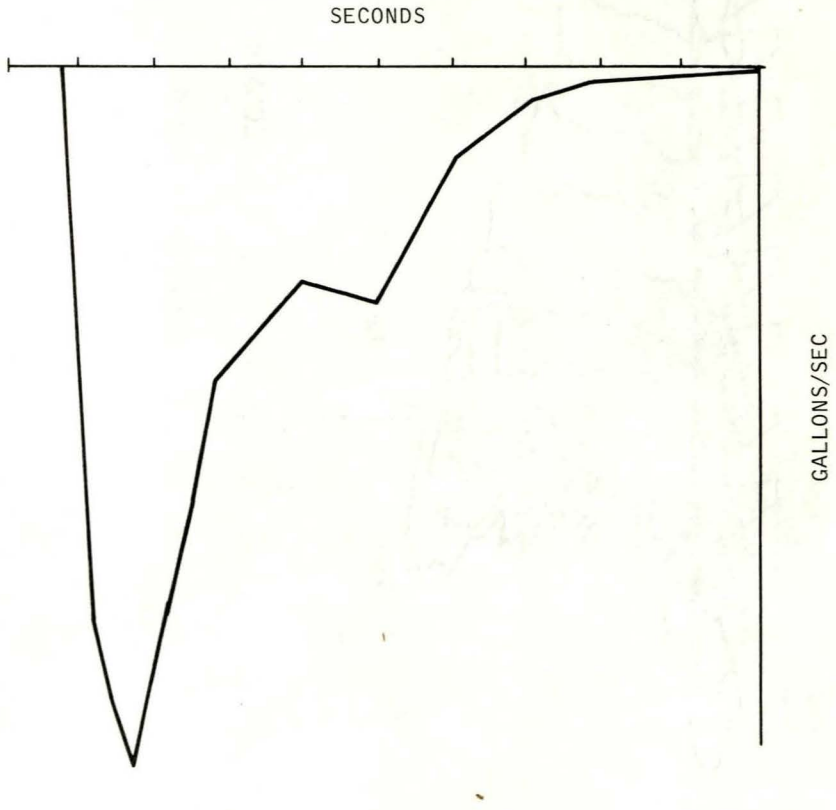

Figure 10. Flow-Rate Distribution

The significance of the volume flow-rate distribution on the pattern is shown most dramatically when the pattern is viewed not as the traditional isopleth (Figure 2) but as a three-dimensional (3D) graph of coverage (Figure 11). The pattern thus viewed has the look of a mountain range on a plateau. In this example the plateau or pattern fringe is generated primarily by peripheral stripping, seldom contributes meaningful coverage levels, and is subject to wind drift indicated by the offset of the fringe toward the leeward side. The mountains, on the other hand, are formed by the unstable breakup which produces the meaningful coverage area.

The central cross section of the pattern (conditional distribution) shown in Figure 12 bears a striking resemblance to the flow-rate distribution curve. This scalar transformation convolutes flow rate (gallons per second^2) to gallons per 100 square feet^2 and this is the primary task of the simulation program.

Effect of Altitude on the Pattern

Figure 13 shows the change in the nature of the retardant cloud as it falls. During this period, the retardant undergoes a continuing transformation as the initial products of Taylor breakup continue toward a quasi-stable state. This change is significant both in the form of the retardant cloud (which will be discussed later) and in the uniformity of the developing pattern.

Figure 14 shows graphically the form of the 3D pattern as it is modified by altitude. Peak values (overcoverage) are reduced, and lateral spread drives the pattern toward more uniform coverage levels. At the same time, some loss in quantity is taken as smaller particles evaporate. We can show this in terms of the central cross section of the patterns shown comparatively in Figure 15. The form of the cross section, determined initially by the flow-rate

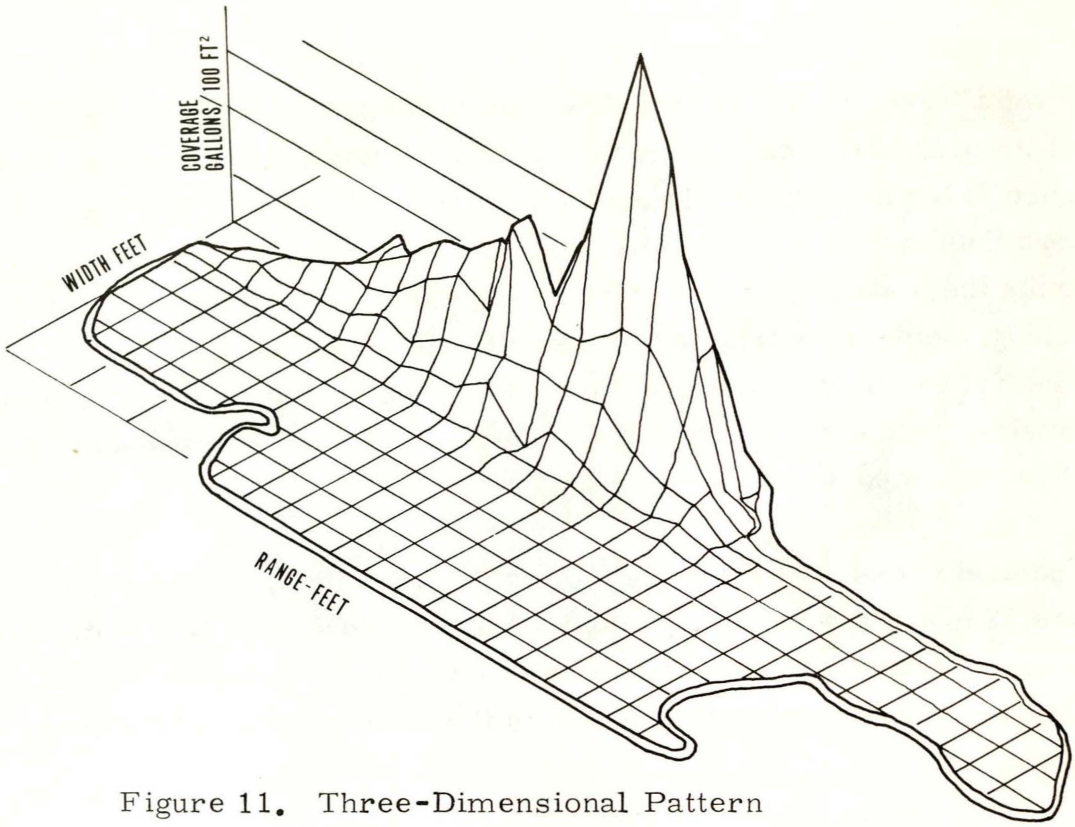

Figure 11. Three-Dimensional Pattern

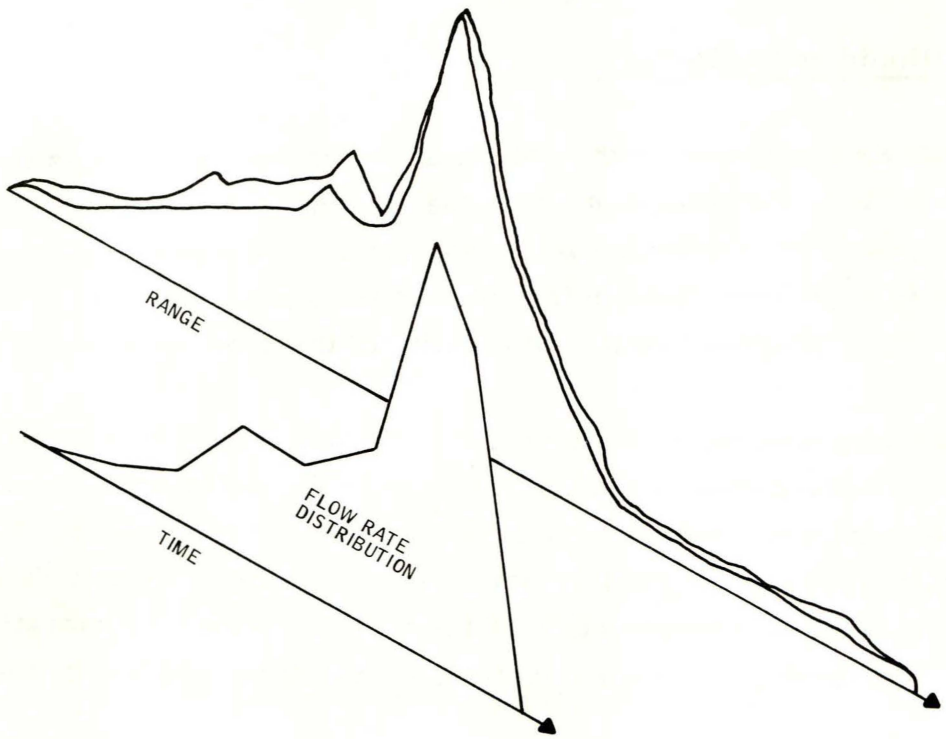

Figure 12. Pattern/Flow-Rate Distribution Comparison

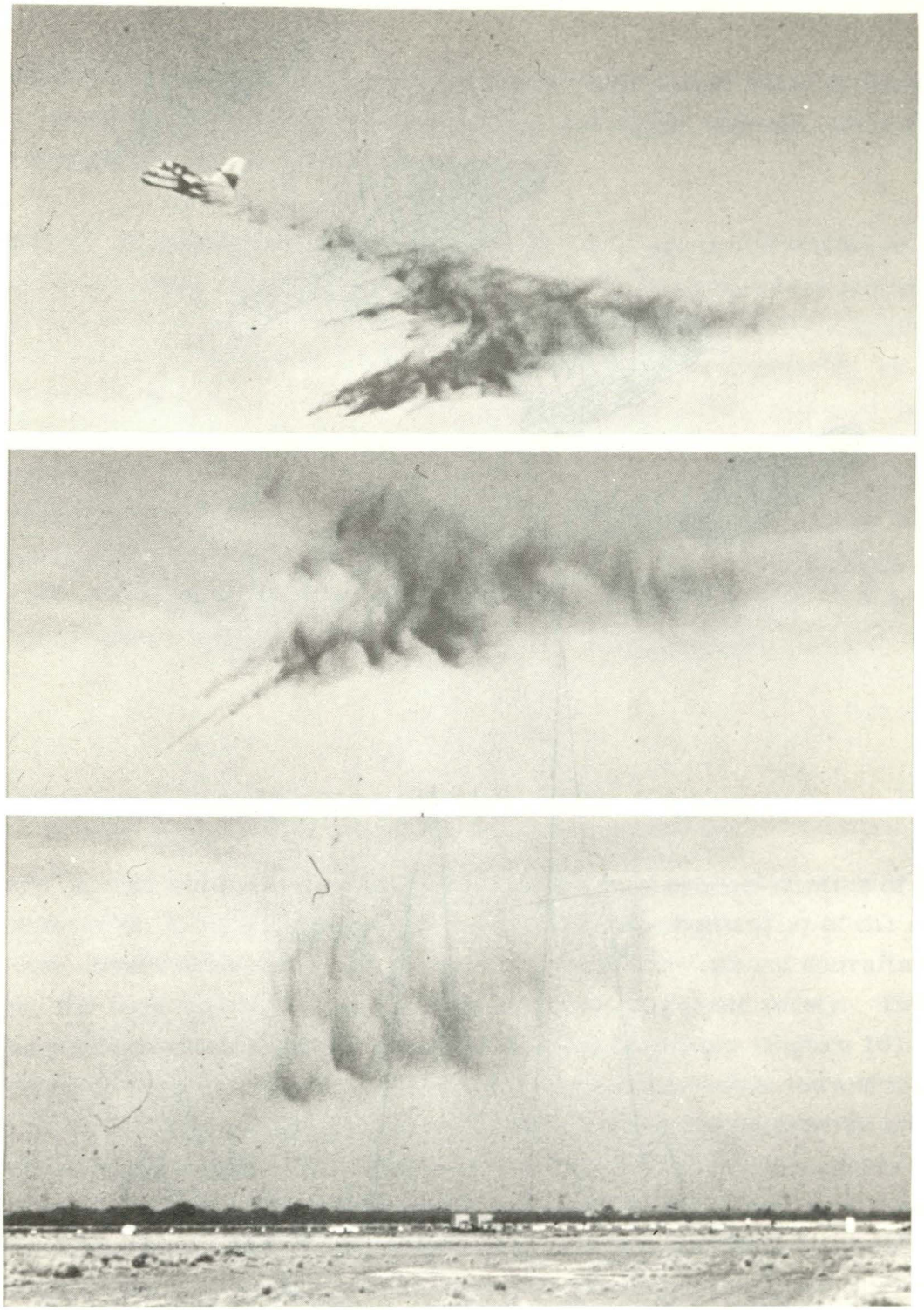

Figure 13. Effect of Altitude on Retardant Cloud

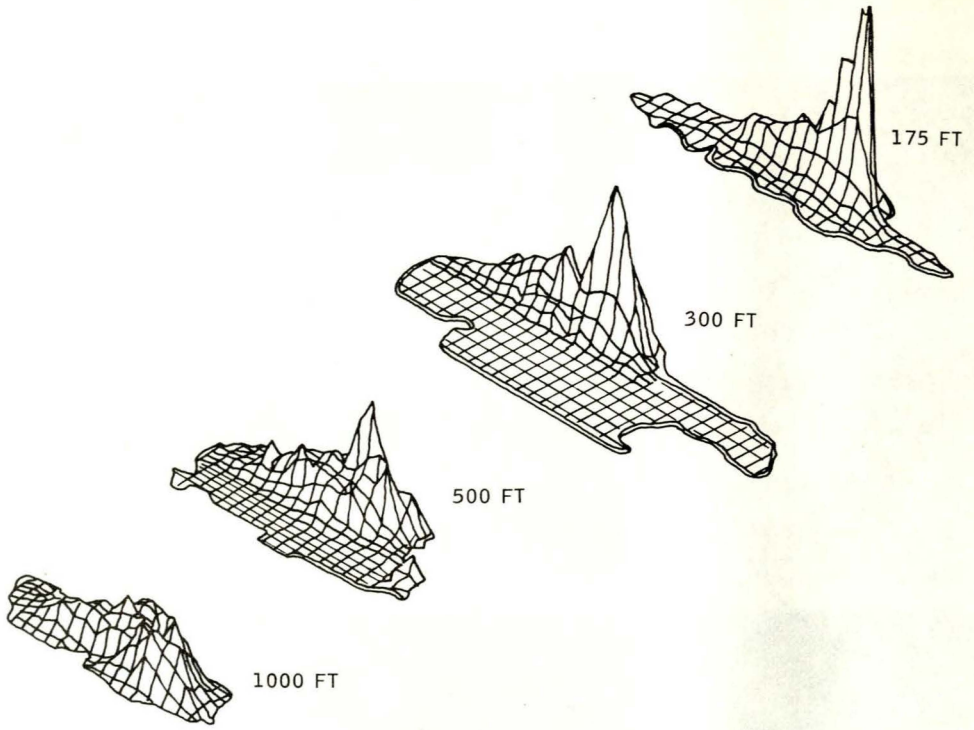

Figure 14. Pattern Change with Altitude

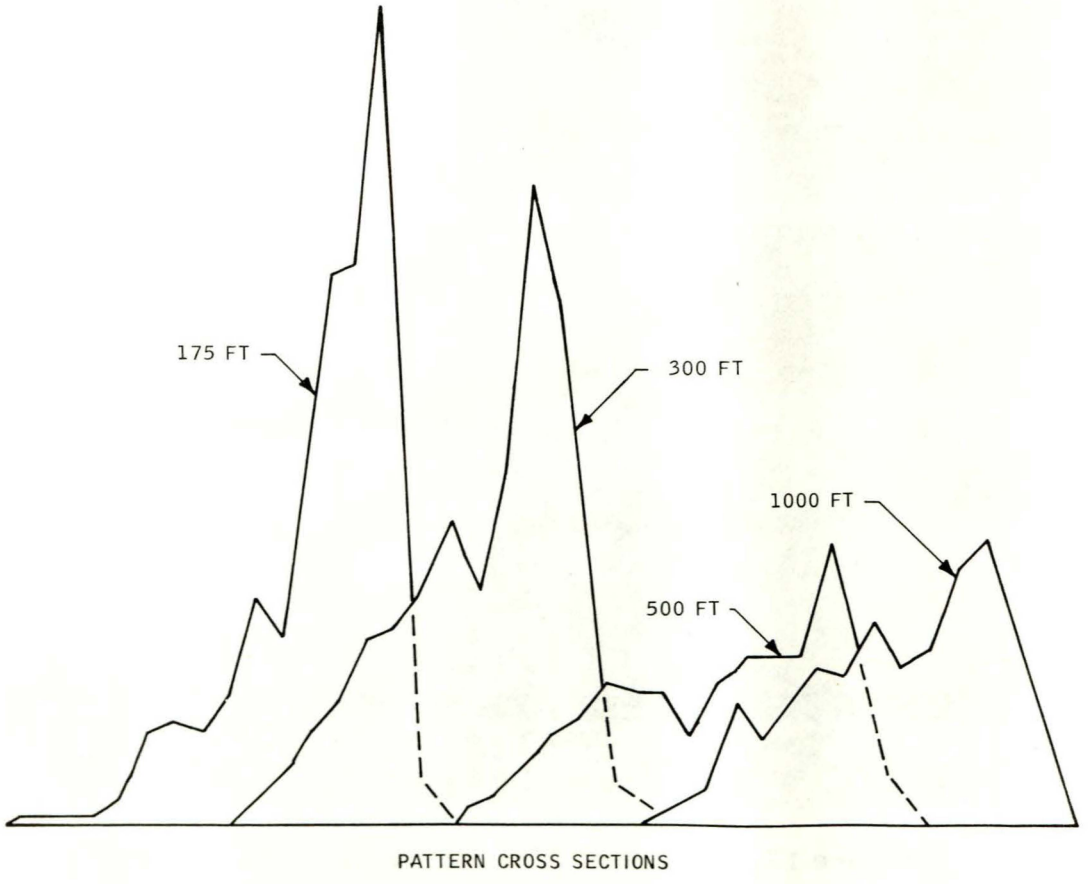

Figure 15. Pattern Cross-Section as Modified by Altitude

distribution, continues to retain its characteristic shape; there is little change in the length of the pattern, but peak values are being reduced, not strictly from loss, but from a general spreading out.

To explore the spreading phenomenon and to facilitate the precision of modeling this process, some additional meaningful statistical parameters are required. Specifically, the cross section (conditional distribution) is only a qualitative representation of the total pattern. The total pattern is, however, characterized based on marginal distributions defined in Figure 16. The distribution is derived from summing the rows (or columns) of a matrix in the margin. With this concept, we can examine the spreading out of the pattern without regard to quantity losses (Figure 17). This confirms the observation in the earlier studies that the effect of altitude on retardant dispersion is predominantly to increase crossrange spread of the pattern rather than range (or length) spread. This principle is applied in the development of the simulation model.

Importance of Retardant Form Over Altitude

Pattern spread and coverage levels are not the only characteristics of a drop that determine its effectiveness. In particular, the momentum of the retardant can have considerable influence ability to breach fire-induced updrafts for direct attack, the accuracy in the face of high wind, or on ground safety. These can be qualitatively related to phases of pattern formation (Figure 18). They are related to the transition from initial products of breakup toward the steady-state or heavy-rain condition. Their relative values are altered by mission conditions (Figure 19). The significance of this relationship suggests a tailoring of the delivery mission to the fire control intent and conditions. It further explains the indications in Marana tests that optimum altitudes for coverage areas may be higher than currently flown and indicates where high-quantity, low-altitude delivery can top trees or be exceedingly dangerous to ground personnel.

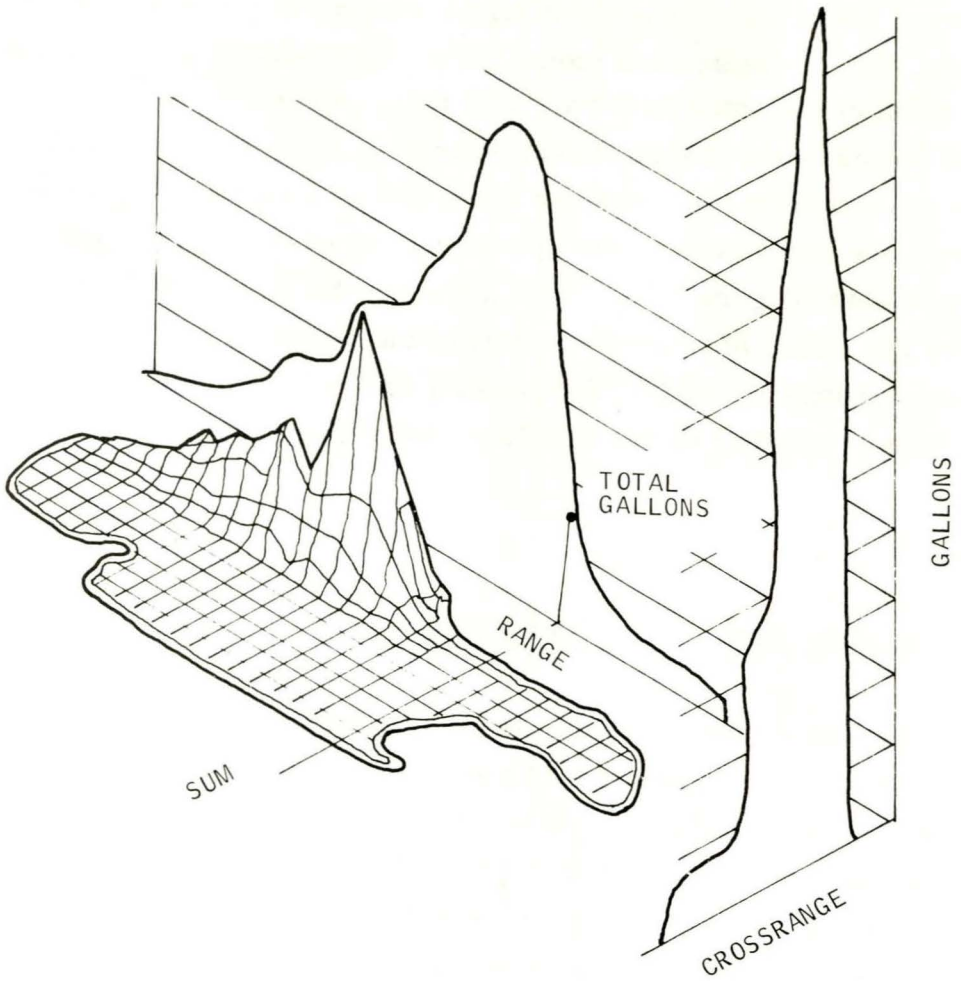

Figure 16. Marginal Distribution Definition

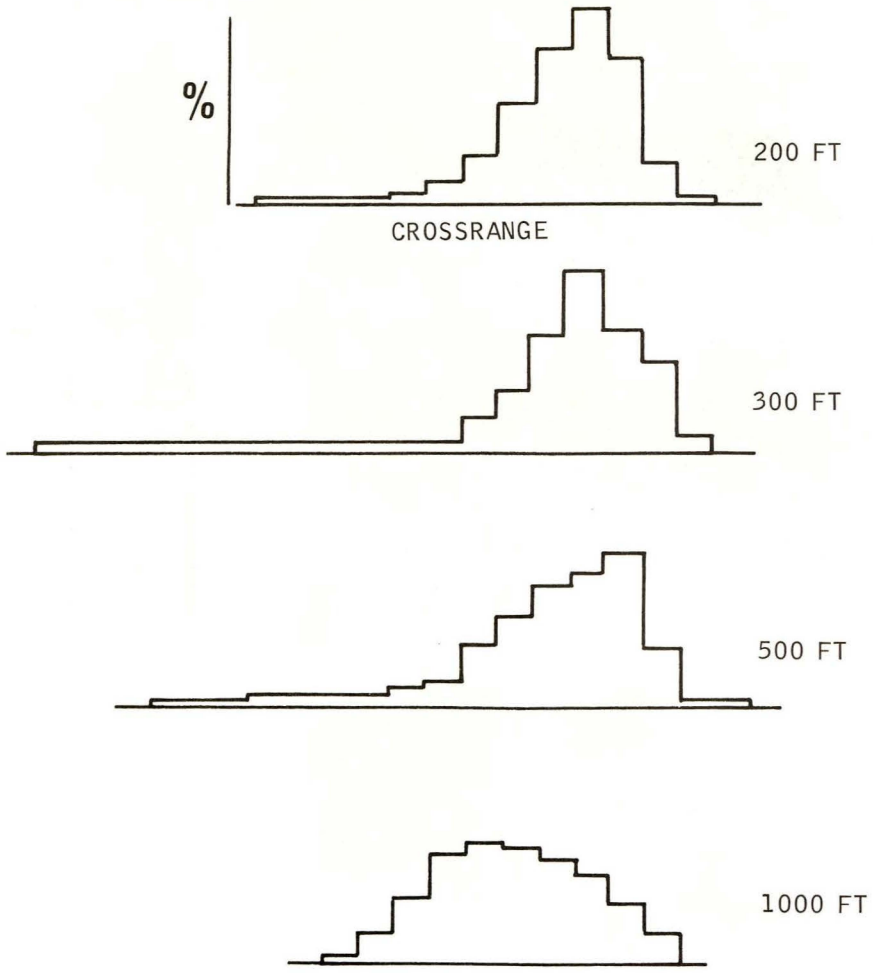

Figure 17. Altitude Effect on Crossrange Distribution

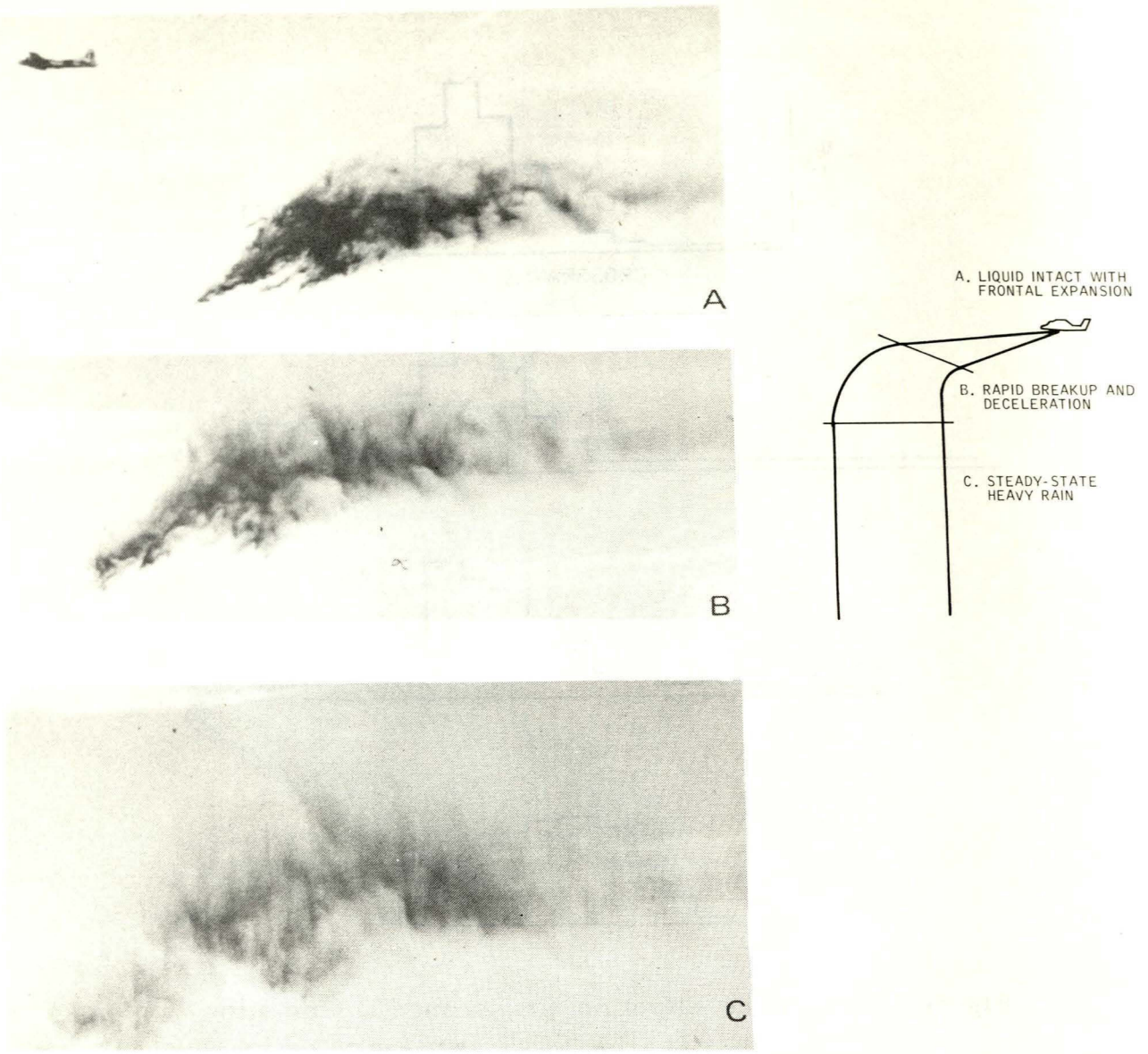

Figure 18. Phases of Retardant Breakup

HIGHEST MOMENTUM ⟵
BEST ACCURACY ⟵
⟵ BEST DISPERSION
⟵ SAFEST DELIVERY

	DIRECT ATTACK	LINE BUILDING
HIGH CONCENTRATION, DROP ALTITUDE A	MOST FAVORABLE AGAINST SMALL BUT INTENSE FIRES OR FIRES IN TIMBER CANOPIES. BEST WIND PENETRATION. MOST REPEATABLE TRAJECTORY. MOST HAZARDOUS TO GROUND PERSONNEL.	POOR LINE-BUILDING CHARACTERISTICS BECAUSE OF POOR DISPERSION.
AFTER INITIAL BREAKUP, DROP ALTITUDE B	USE WHEN MORE AREA COVERAGE IS REQUIRED AT LOWER CONCENTRATIONS THAN AT DROP DISTANCE A. MAY NOT PENETRATE STRONG CONVECTION COLUMN.	GOOD LINE-BUILDING CHARACTERISTICS NEAR A FIRE FRONT. LESS DRIFT THAN WITH DROP DISTANCE C.
CLOUD DISPERSION, DROP ALTITUDE C	PROBABLY ACCEPTABLE AGAINST LARGE LOW-INTENSITY FIRES IN LOW WIND CONDITIONS.	MOST FAVORABLE FOR BUILDING CONTINUOUS LINE FROM HIGH ALTITUDES UNDER LOW WIND CONDITIONS WHEN ACCURACY IS NOT CRITICAL.

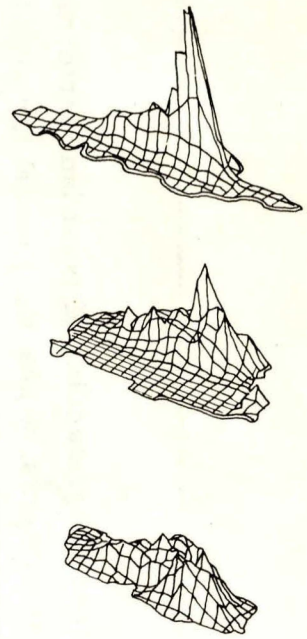

Figure 19. Importance of Retardant Breakup Phases

Simulation Models

To apply the generalized understanding of retardant performance to design or evaluation of airtanker systems, a practical model for simulation is required. Two related models have been developed to trace tank and aircraft parameters to ground-pattern formation. One is essentially a research tool with a computational capacity to conduct a number of experiments in developing or calibrating the predictive capability.

The second is a simplified replica of the resulting process. Both follow the same fundamental operation described in the following subsection.

SIMULATION PROGRAM DESCRIPTION

Both the research simulation and its simplified counterpart follow the basic principle of generating ground patterns from tank geometry, door-opening rate, aircraft velocity, and altitude (Figure 20).

There are four basic steps in the program:

- Generation of the flow-rate prediction from tank geometry and door opening rates.
- Generation of a marginal range distribution from flow rate and aircraft velocity.
- Development of the crossrange distribution from the marginal range distribution as a function of altitude.
- Summarization of the simulated pattern as a scaled pattern plot, gallons, area, and lengths associated with various coverage levels.

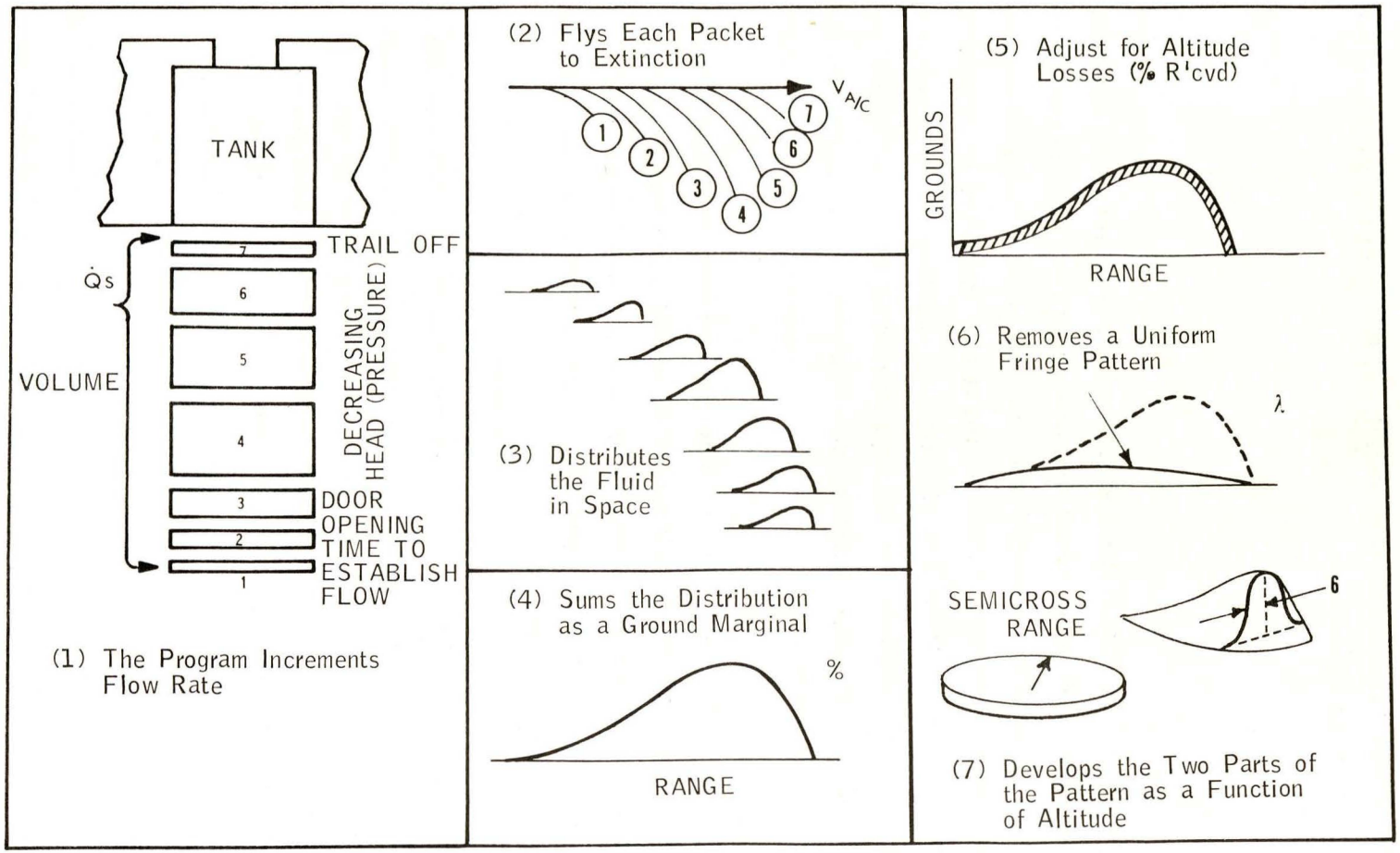

Figure 20. Simulation Overview

Each part of the simulation is discussed, with examples given of the input, output, and processes involved.

Input Variables

Tank Geometry -- The simulation starts with a geometrical representation of the tank geometry, involving seven basic values for a simple tank (Figure 21). Additional input capacity is provided to accommodate more complex tanks with up to four sections. (Detailed data on input are included in Appendix A.) Although the descriptive data are supplied in rectangular coordinates, cylindrical tanks or tank sections can be approximated by "equivalent" rectangular tanks. In addition to the geometrical description, the quantity contained in the tank is a required input.

Door Opening Geometry and Rate -- The second important parameter in determining flow-rate distribution is the door-opening rate and geometry. Geometrical data required in addition to door area are the discharge angle, and the angle of the door at maximum opening. A choice of door-opening-rate inputs is provided (Figure 22) as follows:

- Uniform Door Opening -- This approach assumes that the door moves from the closed to maximum open condition at a constant angular velocity. It allows the simulation to be run where door opening time and maximum angle are known, without regard to actual rate measurements. This approach provides a reasonable approximation for most door systems and is appropriate for preliminary design analysis on tanking system parameters.

- Nonuniform Door Opening -- Where actual test measurement data are are available, a more accurate representation of the door-opening characteristics can be determined by fitting measured data to the

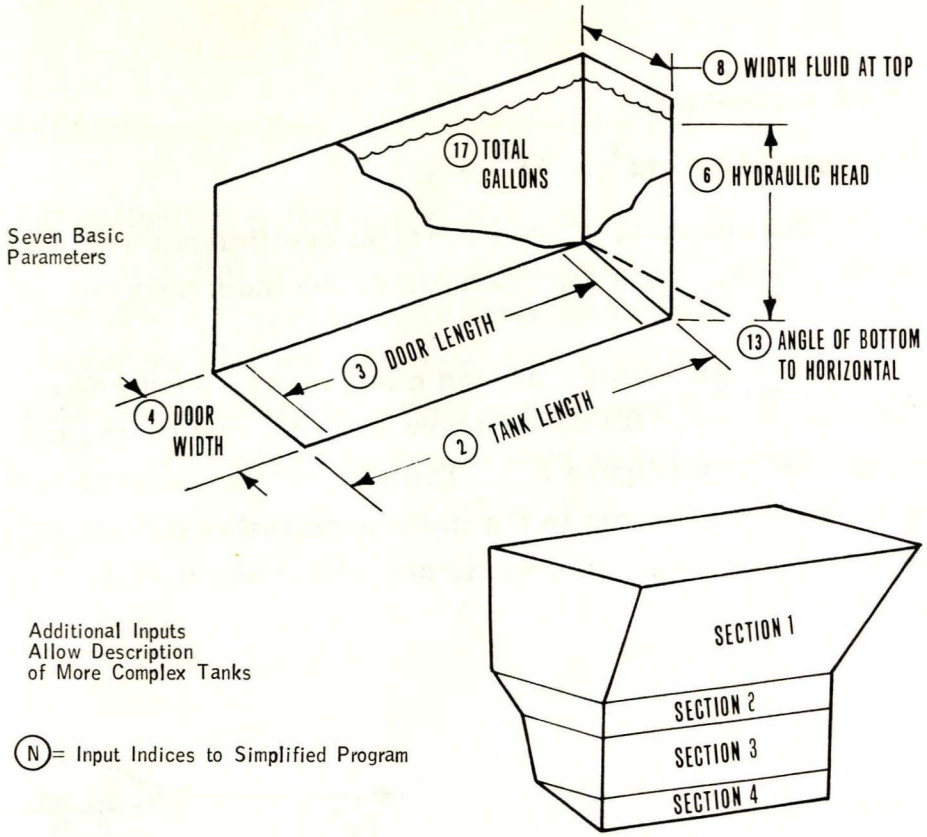

Figure 21. Tank Geometry Descriptors

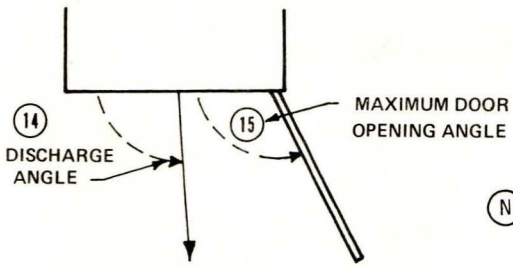

DOOR OPENING RATE		
TYPE	USE	INPUTS
UNIFORM	A REASONABLE APPROXIMATION	(16) DOOR RATE
(OR) NONUNIFORM	ACCOMMODATES MEASURED DATA	(19) OPENING TIME (20) (21) COEFFICIENTS (22) (23) OF POLYNOMIAL FIT TO DATA

Figure 22. Inputs Describing Door Opening

polynomial expression

$$\theta \text{ (degrees)} = at^3 + bt^2 + ct$$

where t is time and a, b, c are empirical coefficients to achieve the best-fit match. This approach yields the most accurate simulation.

Aircraft and Mission Data -- Aircraft and mission data inputs describe (1) the aircraft velocity at release, (2) the delivery altitude, and (3) the number of tanks released in the drop (Figure 23). The aircraft is assumed to be in level flight. (Dive delivery can be run in the more permissive format of the research program, but it is not incorporated in the simplified simulation.)

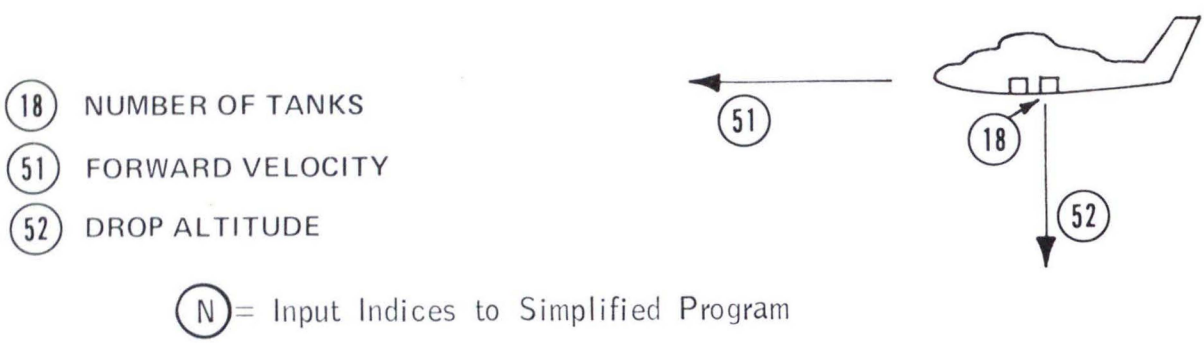

Figure 23. Aircraft Inputs

Multiple-tank salvos are approximated by simply assuming a larger tank of equivalent configuration. The approximation appears valid for directly adjacent tanks and looses precision as the physical separation of the tanks increases. (The rules for improving the simulation in multiple-tank drops have not yet been derived and are a recommended area for further investigation.)

Processing Steps

Flow-Rate Distribution -- The program first calculates a flow-rate distribution from tank geometry and door-opening-rate inputs. The process has two parts: (1) calculation of an ejection velocity based on Bernoulli continuity equations and (2) calculation of the door-opening area as a function of time. In combination, these two time functions define a volume flow-rate distribution as shown in Figure 24. The figure shows both simulated and measured data for the internal DC6B tank.

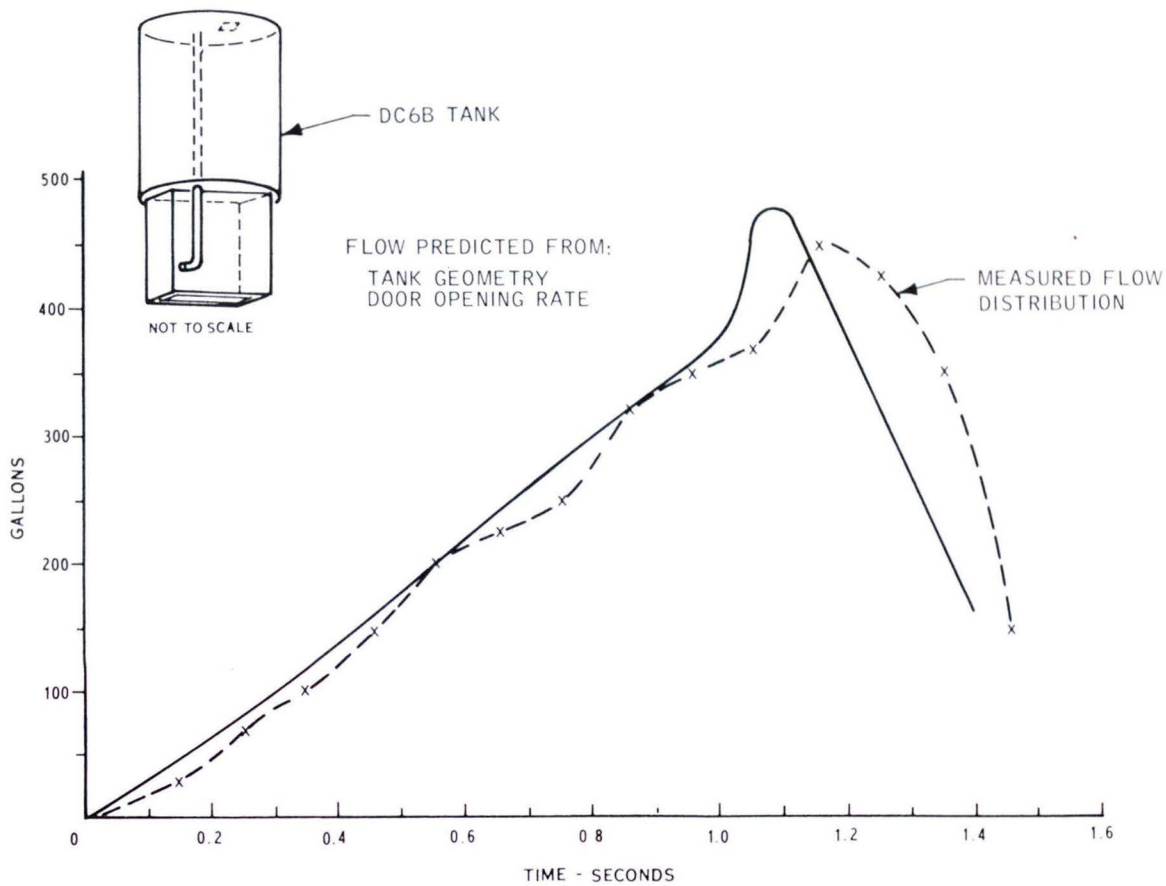

Figure 24. Simulated and Measured Volume Flow-Rate Distribution

Generation of the Range Marginal Distribution -- The flow-rate distribution is artificially broken into fluid packets corresponding to an amount released in each of several small time increments. Each packet is flown on a trajectory starting from a point in space determined by its release time and aircraft velocity and ending at its breakup. The breakup process, though empirically derived, has its analog in the physical processes of breakup (Figure 25). The amount of fluid distributed in space is initially small, probably the products of peripheral stripping while the fluid deforms. At the conclusion of the deformation phase there is a sudden, rapid buildup of instabilities that shatters the packet into relatively large drops. This two-stage process is approximated by an exponential mass-loss equation.

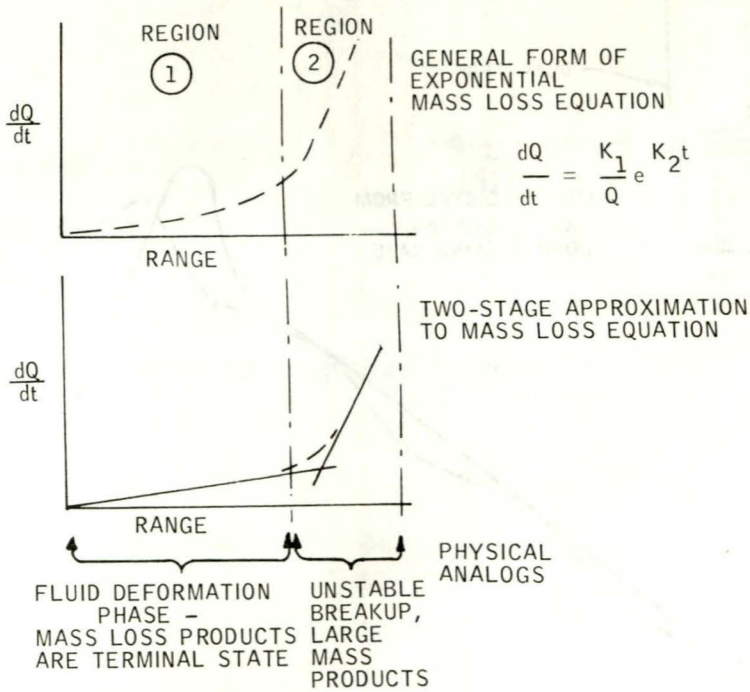

Figure 25. Breakup Physical Processes

The simulation traces each packet to its extinction and sums the distribution of retardant in terms of a range marginal distribution (percent of retardant delivered in each foot of pattern length) from the point of release to the frontal edge of the pattern. The characteristics of this distribution do not change significantly with altitude.

Generation of the Crossrange Expansion -- The marginal range distribution is converted to gallon units by subtracting the amount lost through evaporation, which is viewed as a function of altitude. The remaining retardant is subject to crossrange expansion. First, an amount, λ (%), is removed from the available retardant. This retardant is distributed uniformly over an elliptical area defined by the value: Semi-crossrange. Both λ and Semi-crossrange are varied as a function of altitude. This quantity represents the pattern fringe, seldom contains useful coverage levels, and is subject to wind-drift. It nonetheless gives the simulated pattern its look-alike characteristics with measured pattern data.

The remaining retardant is distributed across the pattern as a normal distribution characterized by its sigma value. The sum of the uniform and normal retardant produces the simulated ground pattern (Figure 26).

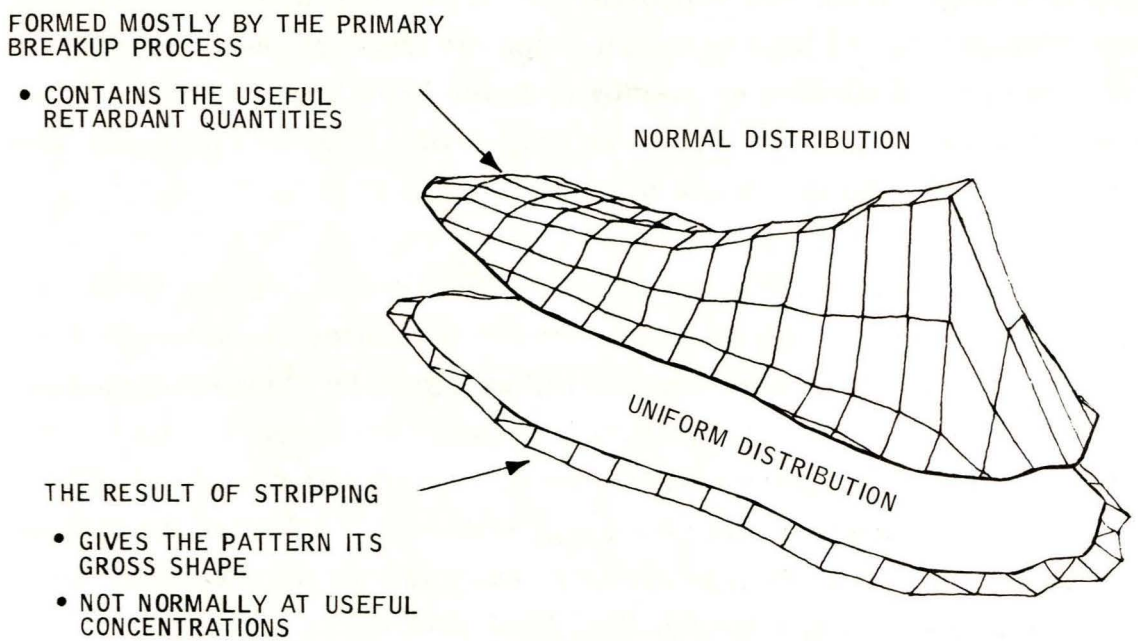
FORMED MOSTLY BY THE PRIMARY BREAKUP PROCESS
• CONTAINS THE USEFUL RETARDANT QUANTITIES
NORMAL DISTRIBUTION
UNIFORM DISTRIBUTION
THE RESULT OF STRIPPING
• GIVES THE PATTERN ITS GROSS SHAPE
• NOT NORMALLY AT USEFUL CONCENTRATIONS

Figure 26. Simulated Ground Pattern

The program uses rules for relating "percent recovered", λ, semi-crossrange, and sigma (σ) derived from optimization on the research program; however, different values can be input to override the built-in rules at the option of the user. Percent recovery as a function of altitude is approximated for most tanks by built-in values set at 90 percent of the recovery values determined for the CL-215.

Rules for the development of the uniform portion of the pattern are shown in Figure 27. Although they are somewhat approximate, when compared with the more formally derived values generated in the optimization program, the technique of estimation is belived adequate. This portion of the pattern seldom contains meaingful retardant levels -- on the order of 0.1 or 0.2 gpc. It is thus significant not in its effect on the fire, but in providing a look-alike character to actual patterns. The program introduces a reduction in semi-crossrange as a function of aircraft velocity which, though based on findings relating to a single drop, are supported by the physical understanding of the breakup phenomena. At higher velocity, the deformation phase contributing to lateral spread is terminated earlier by unstable breakup. Although the simplified model does not provide a rule for trail drops, they can be approximated by using a semi-crossrange value of 30 feet at low altitude.

The rule specified in the computer program for determining the crossrange distribution of the most significant portions of the pattern is shown in Figure 28. The rules here are much more consistent, as shown by comparing these rule curves with data from the optimization program. This consistency is critical since this portion of the pattern substantially determines areas and lengths associated with coverage levels above 1 gpc which are effective for fire-control missions. Again, a reduction in sigma is specified for high-velocity drops. Lower values must be input for handling trail drops.

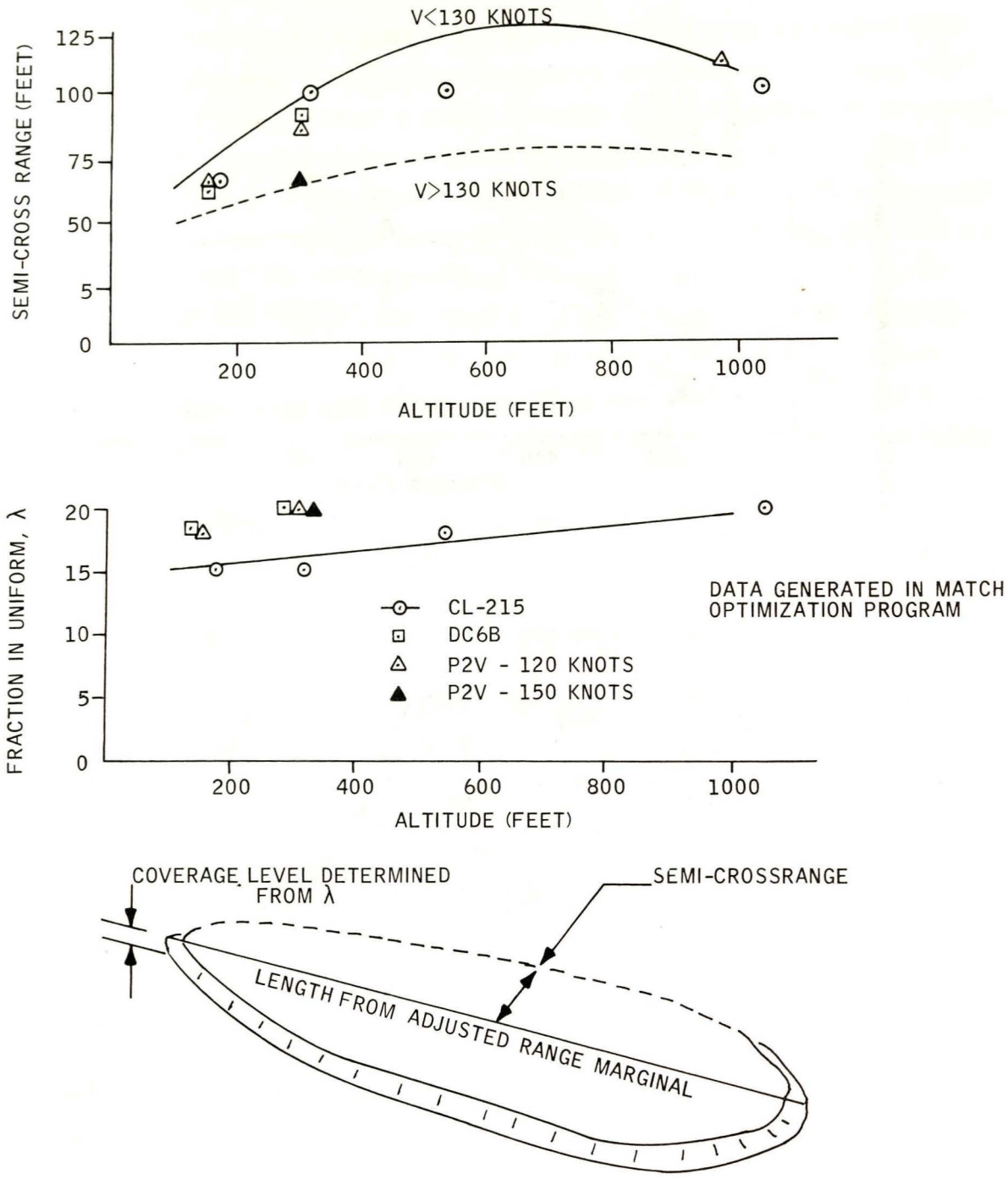

Figure 27. Stored Rules for Estimating Uniform Distribution of Simulated Pattern

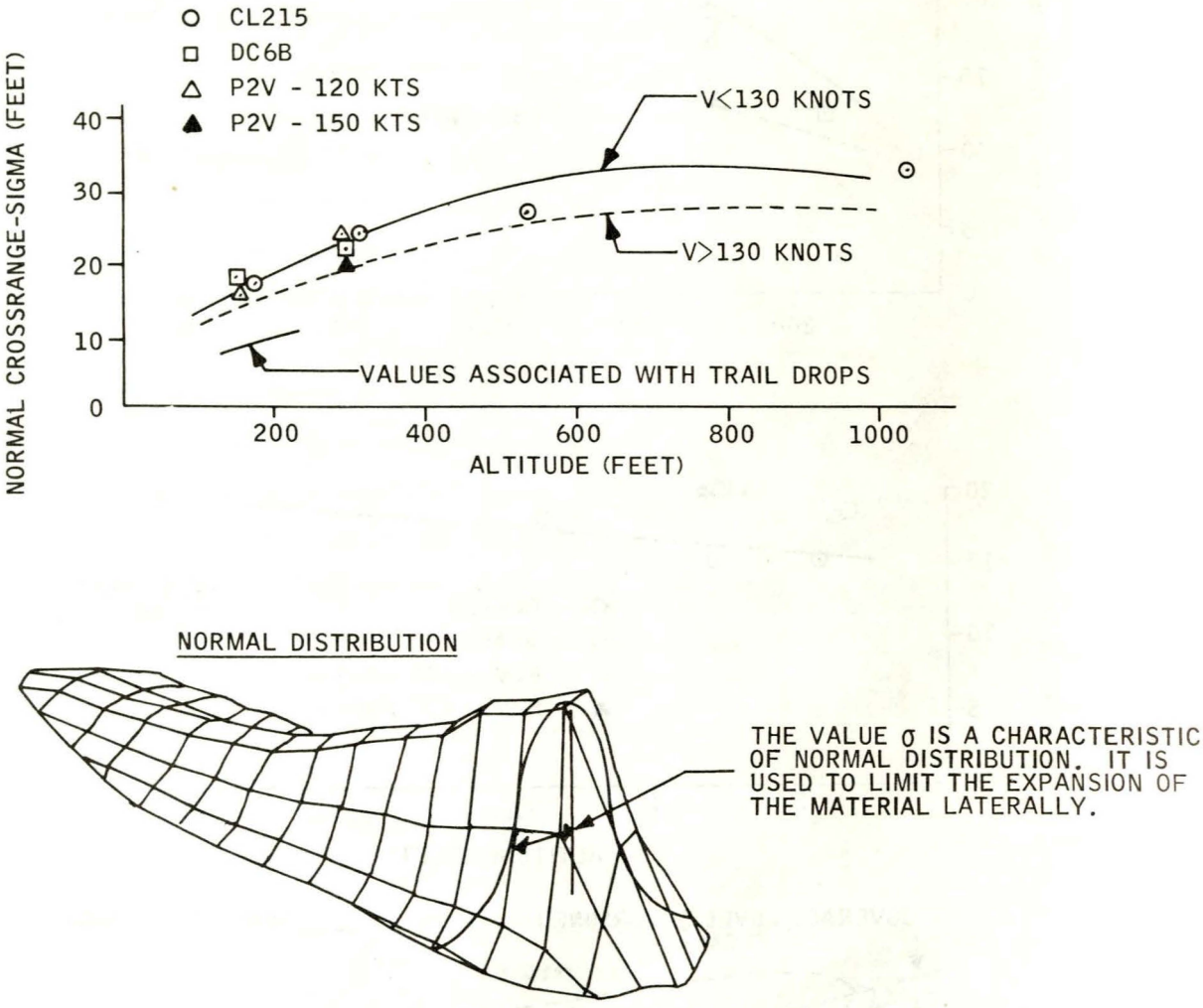

Figure 28. Rules for Estimating Normal Distribution of Pattern

Output

Patterns -- The output of the simplified program is limited to summary data in three forms. First a detailed pattern summary is presented in "computer scale" (Figure 29). This printout yields a quantity (gpc) at each point in a grid. The scale, however, considerably shortens the pattern. Consequently, a second printout is provided that places the pattern in-scale and codes the coverage levels by increments. This display (Figure 30) uses computer line-printer spacing to approximate true scale and thus avoids the use of plotters or other sophisticated peripheral equipment. Each code symbol represents the center of a 15- by-30-foot grid area. A transparent grid overlay simplifies interpretation (Figure 31). Range coordinates printed in the right margin show the position of the pattern, relative to the release point, in ground coordinates.

Summary Data -- Summary data are also calculated and displayed in three forms: (1) gallons within each contour interval, (2) area in each contour interval, and (3) length above each countour interval coverage value (Figure 32). The total gallons on the grid, percent of total dropped, total area covered, and average pattern coverage level are also displayed.

Typical Results -- Figure 33 shows a graphic comparison between simulated and actual pattern data for the DC6B drop. Although the simulation produces a somewhat more regular shape, this characteristic is to be expected. The irregularity in the actual pattern is thought to be imposed on the pattern by the instabilities generated during breakup. Figure 34 compares the same patterns in the more familiar isoplethic representation. The comparison is perhaps more dramatic when the outer area (pattern fringe) is ignored.

A second example of predicted-to-actual pattern comparison is shown in Figure 35. This represents a center-line-to-center-line comparison of a simulated

.0	.0	.0	.2	.2	.2	.2	.0	.0	.0
.0	0.0	.2	.2	.2	.2	.2	.2	0.0	0.0
.0	0.0	.2	.2	.2	.2	.2	.2	0.0	0.0
.0	.2	.2	.2	.2	.2	.2	.2	.2	0.0
.0	.2	.2	.2	.3	.3	.2	.2	.2	.0
.2	.2	.2	.3	.3	.3	.3	.2	.2	.2
.2	.2	.2	.4	.6	.6	.4	.2	.2	.2
.2	.2	.3	.6	.9	.9	.6	.3	.2	.2
.2	.2	.4	.8	1.2	1.2	.8	.4	.2	.2
.2	.2	.5	1,1	1.7	1.7	1.1	.5	.2	.2
.2	.3	.6	1.4	2.3	2.3	1.4	.6	.3	.2
.2	.3	.7	1.7	2.8	2.8	1.7	.7	.3	.2
.2	.3	.9	2.2	3.6	3.6	2.2	.9	.3	.2
.0	.3	.9	2.4	4.0	4.0	2.4	.9	.3	.0
.0	.3	1.0	2.6	4.4	4.4	2.6	1.0	.3	.0
.0	.2	1.0	2.6	4.4	4.4	2.6	1.0	.2	.0
.0	.1	.6	1.6	2.5	2.5	1.6	.6	.1	.0
.0	0.0	0.0	.2	.2	.2	.2	0.0	0.0	0.0

Figure 29. Pattern Data Output in "Computer Scale"

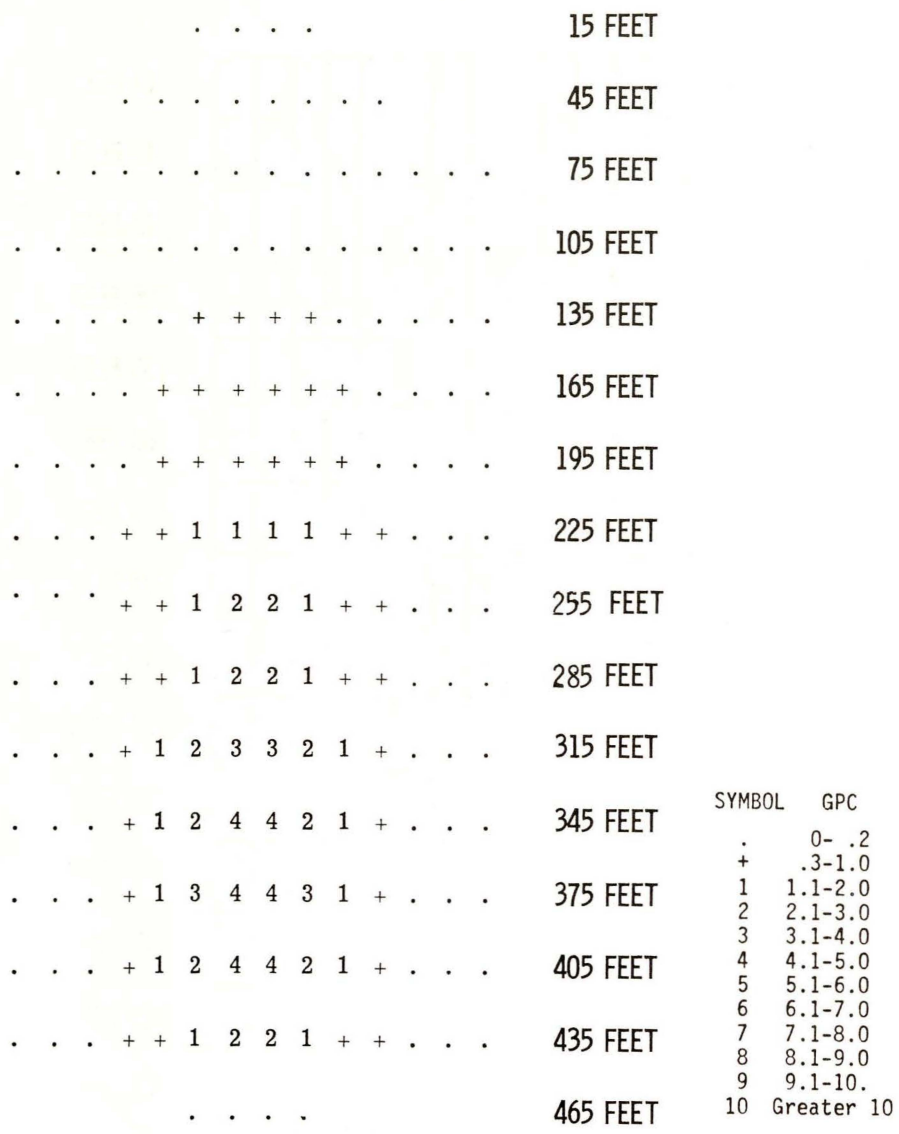

Figure 30. Pattern Data Output in True Scale

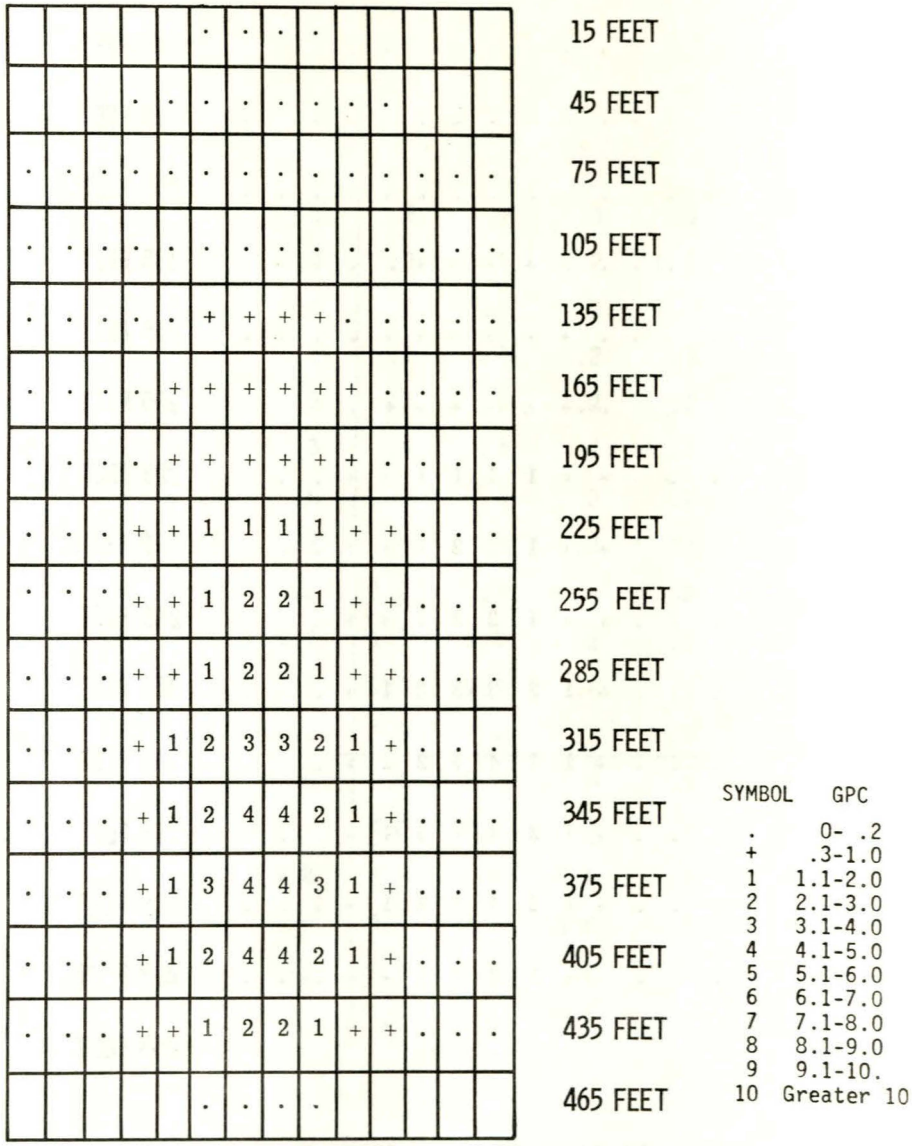

Figure 31. Pattern Data Output in True Scale with Grid Overlay

CONTOUR INTERVALS FOR RETARDANT DISTRIBUTION
(GALLONS/100 SQUARE FEET)
TOTAL WITHIN EACH INTERVAL

0.0-0.2	0.3-1.0	1.1-2.0	2.1-3.0	3.1-4.0	4.1-5.0	5.1-6.0	6.1-7.0	7.1-8.0
48.4064	110.9556	116.5968	136.3993	60.5805	115.2700	0.0000	0.0000	0.0000

8.1-9.0	9.1-10
0.0000	0.0000

> 10
0.0000

TOTAL AMOUNT OF RETARDANT ON GRID = 588.21 GALLONS PERCENT OF TOTAL= 84.030
AVERAGE PATTERN LEVEL IS 2.2 GALLONS PER 100 SQUARE FEET

CONTOUR INTERVALS FOR RETARDANT DISTRIBUTION
(SQUARE-FOOT COVERAGE)
TOTAL WITHIN EACH INTERVAL

0.0-0.2	0.3-1.0	1.1-2.0	2.1-3.0	3.1-4.0	4.1-5.0	5.1-6.0	6.1-7.0	7.1-8.0
46800	24300	8100	5400	1800	2700	0	0	0

8.1-9.0	9.1-10
0	0

TOTAL AREA COVERED 89100 SQUARE FEET

> 10
0

PATTERN LENGTH DATA

480 FEET ABOVE	0.0 GALLONS/100 SQUARE FEET
330 FEET ABOVE	.3 GALLONS/100 SQUARE FEET
240 FEET ABOVE	1.0 GALLONS/100 SQUARE FEET
210 FEET ABOVE	2.0 GALLONS/100 SQUARE FEET
120 FEET ABOVE	3.0 GALLONS/100 SQUARE FEET
90 FEET ABOVE	4.0 GALLONS/100 SQUARE FEET
0 FEET ABOVE	5.0 GALLONS/100 SQUARE FEET
0 FEET ABOVE	6.0 GALLONS/100 SQUARE FEET
0 FEET ABOVE	7.0 GALLONS/100 SQUARE FEET
0 FEET ABOVE	8.0 GALLONS/100 SQUARE FEET
0 FEET ABOVE	9.0 GALLONS/100 SQUARE FEET
0 FEET ABOVE	10.0 GALLONS/100 SQUARE FEET

Figure 32. Summary Data Output (sample)

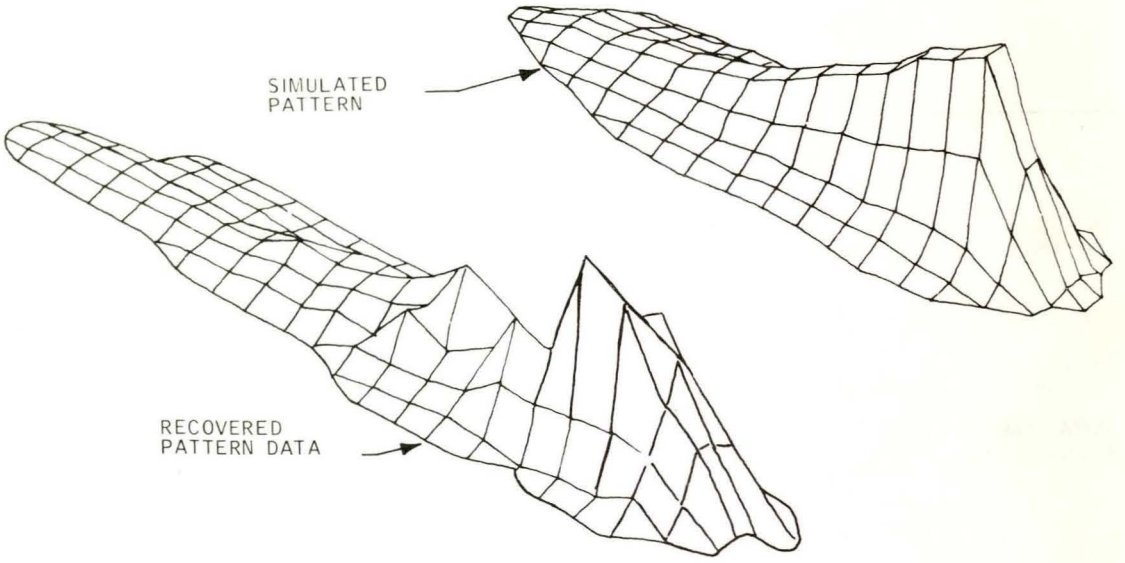

Figure 33. Simulated and Actual Pattern Data Comparison

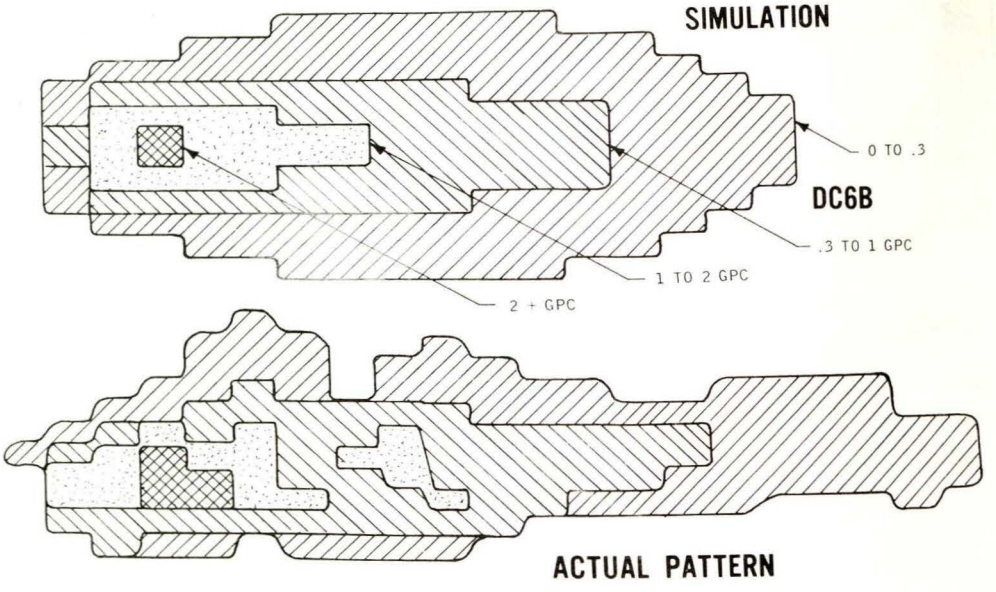

Figure 34. Simulated and Actual Pattern Data Comparison in Isoplethic Form

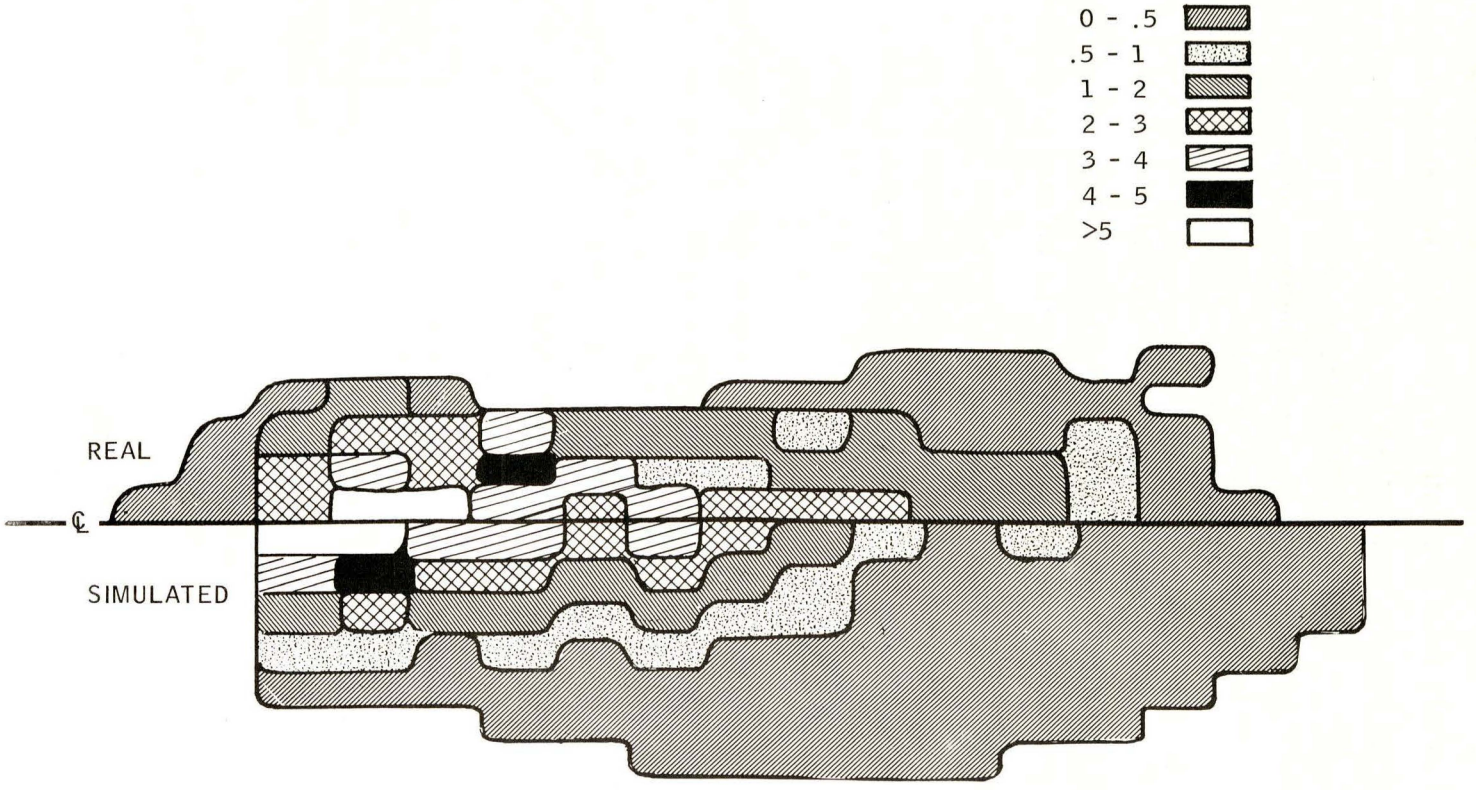

Figure 35. Centerline-to-Centerline Comparison of Simulated and Actual Pattern Data Example

and actual pattern for the CL-215. The comparison used the measured flow rate from USFS static tests, which was hand fed into the research program -- the simplified program does not allow for direct insertion of measured flow data. However, the processing and rules for the simplified program were applied. (It should be noted that the actual pattern at issue had a considerable fringe displacement to the left which is not shown in the display.)

Figure 36 shows the ability of the program to handle trail drops with an appropriate change in the sigma and semi-crossrange rules. The rearward offset of the pattern centroid in the simulation may be related to imprecisions in the available input data.

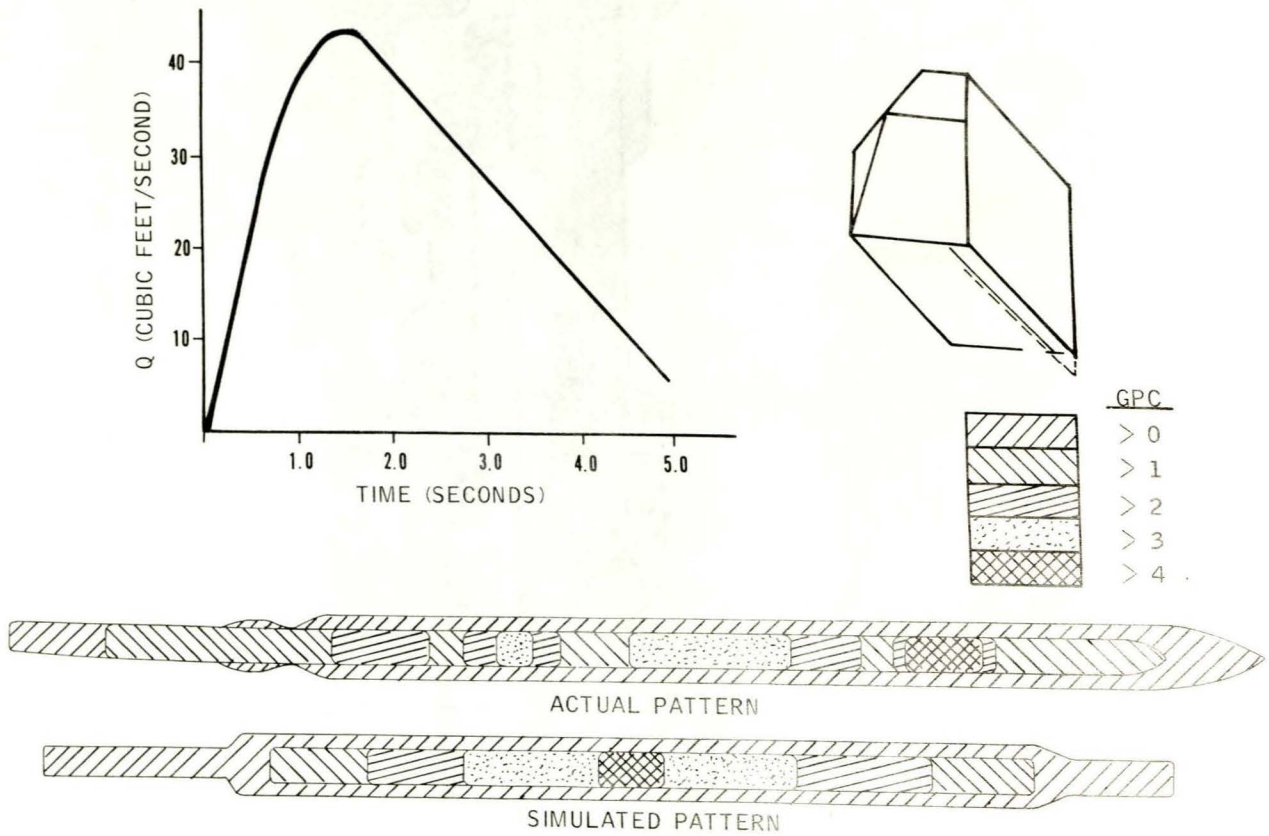

Figure 36. Trail-Drop Pattern Performance

Conclusions

The simulation provides a good estimate of pattern performance over the altitude range. It makes possible the computerized evaluation of aircraft over a wide range of possible delivery conditions similar, for example, to the full test series conducted on the CL-215 at Marana. This feature of the program could well be applied to usage guidelines for airtankers now in operation.

Improvements in the programming capability should be considered in two areas:

- Incorporation of rules to accommodate retardants other than Phoschek XA. * (This retardant, with emphasis on tank designs for high altitude was selected due to its apparently superior survivability over the altitude range.)

- Incorporation of more precise rules for handling multiple tank drops where tanks are physically separated (not directly adjacent) to preserve aircraft center-of-gravity limits or simply to allow direct evaluation of tank-gating sequences. The improvement would replace the current technique of viewing multiple drops as direct multiplication of the quantity emanating from a single tank.

Both improvements appear to be within the current analytic capability using the Research Simulation (MIX 2) with RETARD (pattern analysis program) in an optimization loop, with refinements to be considered after tests on the Experimental Tank and Gating System.

---

*Phoschek XA is a registered trademark of Monsanto Corp.

III. TASK 1 - FLOW-RATE CALIBRATION

Task 1 of the contract change order required completion of the following subtasks:

1.1 Calibrate the MacPherson flow-rate prediction with actual flow rates for a single retardant and water. This effort was to include at least two aircraft tanking systems and possibly two additional tanking systems. (Given tank geometry and actual door opening, adjust α and/or model to provide a good fit to actual flow-rate histories.)

1.2 Check out the sensitivity of marginal distributions to the corrected flow rate from subtask 1.1.

BACKGROUND

The simulation developed in earlier phases of the High Altitude Delivery Program employs a flow-rate distribution model originally developed by J. I. MacPherson (Ref. 2). It is essentially a two-part simulation in which the hydraulic head (or suitable pressurization) determines the fluid ejection velocity based on Bernoulli continuity equations. The volume of flow is then computed associating the velocity with tank exit geometry from door geometry and opening rate. In the prior simulation work, tank evacuation times inferred from photographic records of Marana and Porterville tests were used as the basic input. Door-opening rates were then estimated assuming an appropriate uniform opening rate to match the observed evacuation time. Since the previous effort identified the importance of the volume flow rate, it was recommended that the adequacy of this relatively simple model be tested against actual flow-rate measurements from Marana Aircraft.

SUMMARY

The simple flow-rate model worked well on the first two tanks tested, a DC 6B (internal tank) and the Forest Service P2V. Given the actual (variable) door opening rate and tank geometry, volume flow rates were predictable. Tests showed no significant difference between a retardant (Phoschek XA) and water, nor was there a significant difference between static ground tests and values recorded inflight (DC 6B). Even the adjustment constant (efficiency factor, α) imposed on the flow equations was found to be within a few percent of the "best-fit" value to actual tests. Late in the program, test data on the measured flow from the CL-215 tank became available. The flow-rate model does not adequately predict the flow of this tank. The problem is believed to be caused by a combination of two factors: (1) a highly impulsive fluid release and (2) the particular tank geometry. Specifically, the equations do not incorporate acceleration (the "inertia" of the fluid). Consequently, they predict flow rates higher than those actually achieved. Actual flow-rates introduced into the simulation, nonetheless, yield a "good" match to the real patterns. (A cursory examination of Forest Service work using the flow-rate simulation of measured data on an S2F unfortunately did not yield conclusive evidence of model performance. Data were confounded by a negative pressure developing at release, usually indicative of venting problems. The simulation was overpredicting evacuation times when the negative pressure was ignored, and underpredicting when a constant negative pressure was assumed. Since the actual conditions are intermediate, the result, though inconclusive, was not discouraging.)

CONCLUSIONS

The Task 1 results indicated that:

- The flow-rate simulation appears adequate for most tanks of conventional geometry and volume flow rate. However, where there is an abrupt change

in tank geometry with the fluid moving from a small cross-section to a larger one, particularly at high flow-rate, experimental determination of actual flow rate may be necessary. Since these conditions are generally avoidable in new tank design, the correction to accommodate the specific case at issue is not recommended unless the need for improved flow-rate prediction is indicated in future tests.

- For preliminary analyses, either for design study or application evaluation, the uniform door-opening assumption reasonably approximates experienced flow rates. When actual door-rate data are not available, or if a hypothetical design incorporates no intentional variation in the door rate, the assumption of uniformity can be expected to yield reasonable predictions of tank performance.

- The adequacy of the simulation should be further checked for tanks with considerable restriction of the fluid flow passage, as for example in trail drops. Although application of the total simulation to the Aero Union B-17 trail suggests that the pattern is predictable under these conditions, difficulties in achieving good matches to PB4Y2 data (a tank system with a restricted door area) suggest either a deficiency in the evacuation-time data or a possible deviation in the flow-rate prediction.

DISCUSSION

Program Changes

Three changes were introduced into the flow-rate prediction subroutine:

- Provisions for Handling Nonuniform Door Opening - This change enables the program to accept measured door-opening rate data which

was approximated by a cubic polynomial of the form

$$\theta \text{ degrees} = at^3 + bt^2 + ct$$

where a, b, and c are coefficients determined to best-fit measured data.

- Limit Check on Small Quantity Increments - To achieve the match at low flow rate, a small change was incorporated in the program. This change applies a limit check on the quantity predicted within each time increment to ensure that it does not exceed the quantity available. (Previously, a flow rate was assumed to apply throughout the time increment established in the program regardless of the quantity available. This yielded overestimation of the retardant quantity in the early stages of door opening, i. e., at relatively low flow rates.)

- Corrected Geometrical Derivation - A second minor change was incorporated to correct a geometrical derivation in the original MacPherson work (Ref. 2). The equation originally took the form

$$V_{Z_2} = f \frac{\sin^2 \varphi}{\sin^2 \theta}$$

This was changed to:

$$V_{Z_2} = f \cos 2(\theta - 4)$$

where V_{Z_2} is the velocity of the water leaving the tank to fill the triangular area associated with the opening door.

φ is the angle of the tank bottom from the horizontal in degrees.

θ is the door angle in radians

The effect of this change on the program is minor.

DC 6B Test and Analysis

The DC 6B with internal tanks, as used in the Marana test series, was the first aircraft on which flow rate was measured. The USFS accomplished most of the analysis using a card deck for the MacPherson Simulation furnished by Honeywell. The findings, to be published by the USFS, are abstracted below, based on Honeywell's assessment of the resulting data:

- The door-opening rate with a 350-gallon load of retardant or water was not linear, but followed a polynomial opening rate of the form

  $$\theta \text{ (degrees)} + at^3 + bt^2 + ct$$

  Provision for the simulation program to accept door-opening rates in this form was initially introduced in the program by the USFS and subsequently adopted in the Honeywell program. The constants are selected, to best match measured door-opening data. Figure 37 shows the USFS fit to the DC 6B measurement.

- Given the above door-opening rate and tank geometry, the simulation predicted the measured flow rate within reasonable limits. Figure 38 shows a comparison of the flow-rate predictions using: (1) the linear door-opening assumption and (2) the polynomial door-opening rate. It shows a good fit to measured data.

- There appeared to be no significant difference between the measured door-opening rate or measured flow between retardant and water. Although a difference was recorded, it was less than the variation between two essentially identical tanks. The effect of the retardant, Phoschek XA, was a slightly higher door-opening rate and a consequent increase in the volume flow rate. The curves are approximately parallel with the Phoschek, producing about 0.3 ft^2 more door area and about 15 more gallons than water at the same stage of its release. The door is fully open about 0.05 second faster, which is not significant in the total simulation.

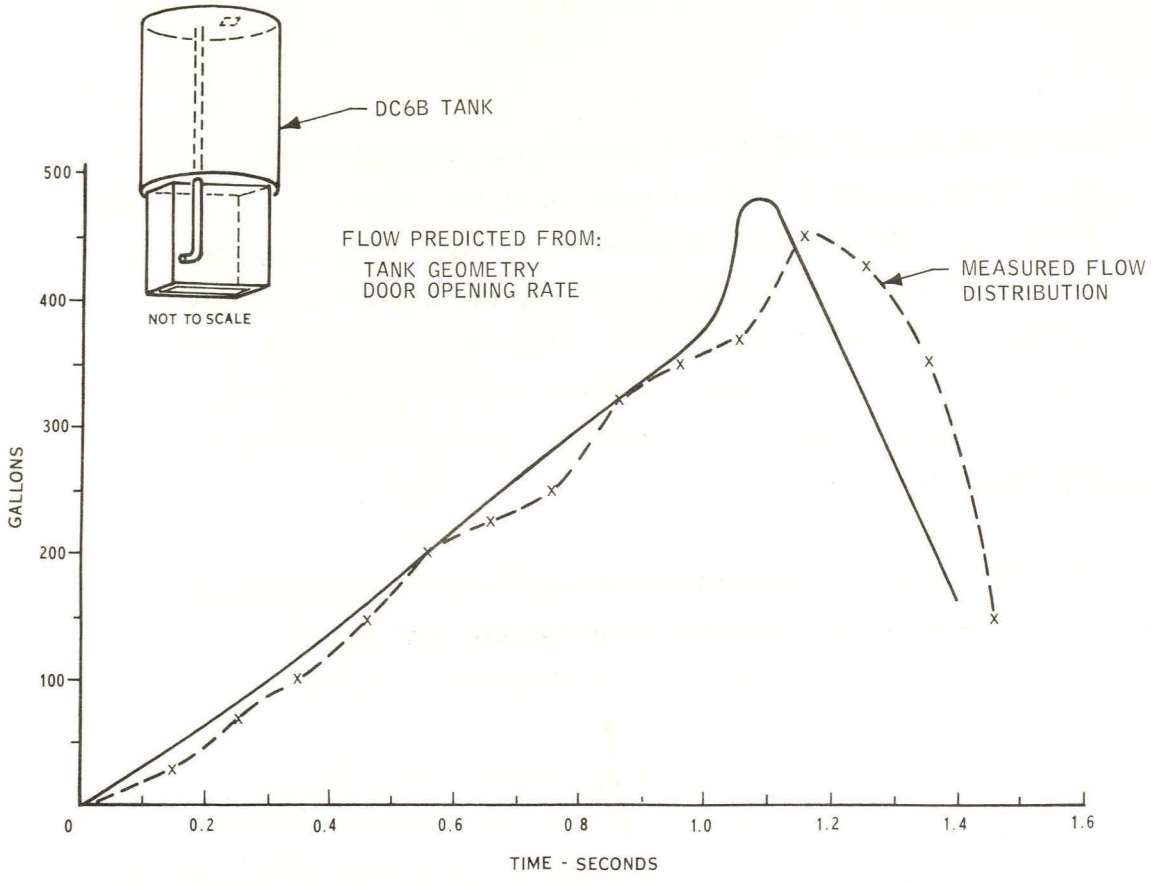

Figure 37. Door-Opening Data Comparison – DC6B Test

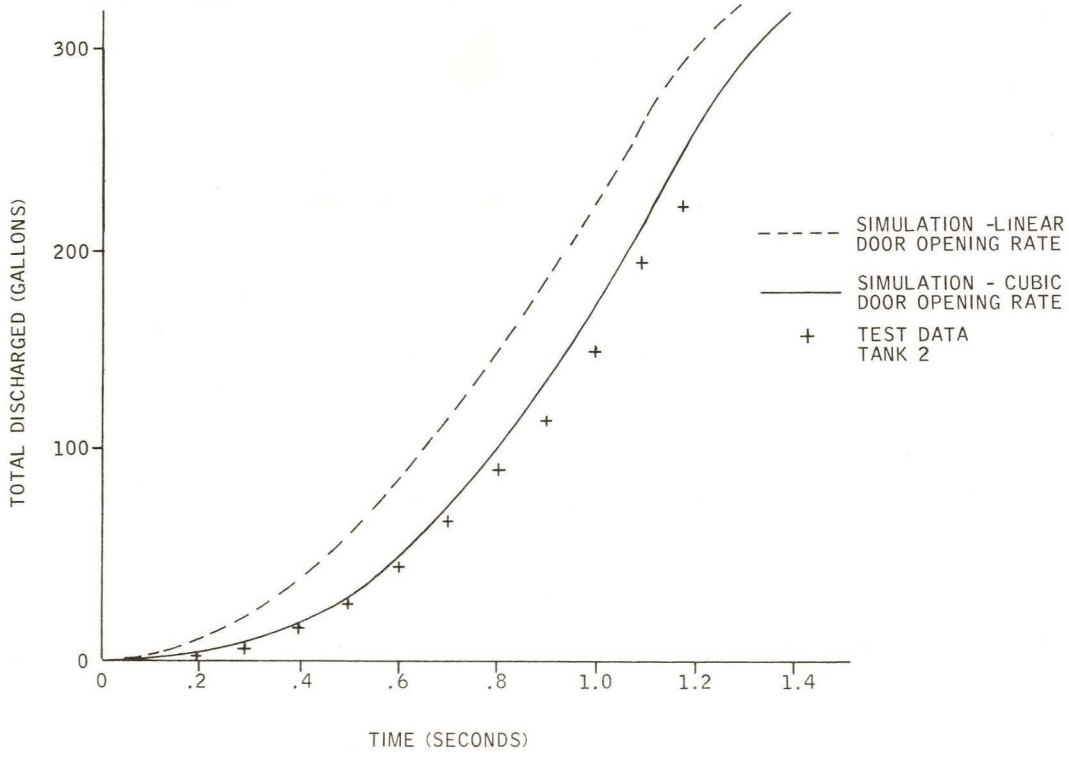

Figure 38. Flow-Rate Prediction Comparison – DC6B Test

- The best fit to the flow-rate prediction was achieved with an α efficiency factor of 0.83 versus the 0.85 inferred from previous studies. There was little difference, however, in the fit with α perturbed from 0.81 to 0.85. Thus, the use of the factor as a constant appears valid.

P2V Test and Analysis

Figure 39 shows the predicted and actual flow rates for a single P2V tank. Again a good match was obtained using the simulation.

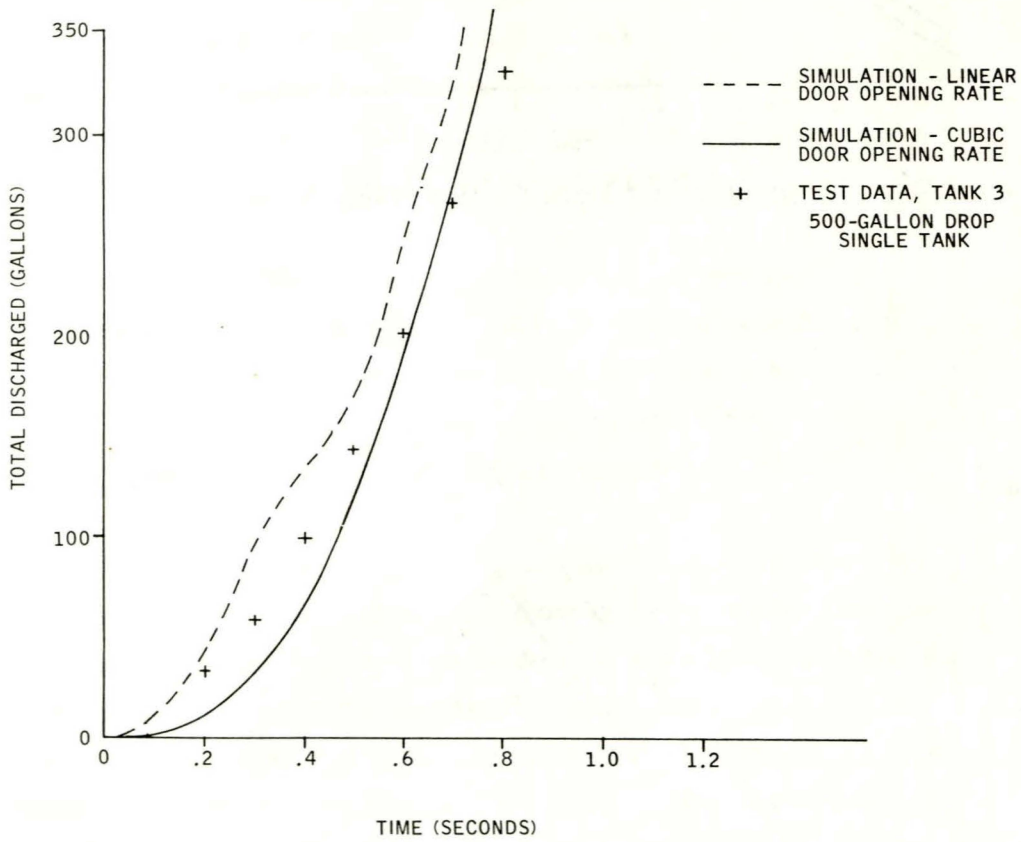

Figure 39. Door-Opening Data Comparison – P2V Test (USFS Data)

A significant finding in these tests was the dependence of door-opening rate on the number of doors actuated, to the extent that in a salvo drop, evacuation occurred before the doors were fully open. This effect might be beneficial under certain circumstances to modulate the very high gross flow from a 3000-gallon drop. It probably accounts for some of the difficulty in evaluating multiple-tank drops encountered in the previous study. For this program, only the single-tank drop was of major interest, since these drops are statistically simple.

Some venting difficulties were encountered in the higher-quantity drops. These were anticipated from prior effort and were one of the reasons that single-tank drops were selected for use in simulation development.

It was concluded as a result of the DC 6B and P2V effort that the flow-rate simulation was performing adequately with the minor changes introduced. This conclusion held until the advent of CL-215 measured flow data which became available late in the program effort.

CL-215 Test and Analysis

A preliminary analysis of the measured flow data obtained from the Northern Forest Fire Laboratory was made. This analysis has shown that the actual CL-215 flow data is substantially different than the predicted flow from the MacPherson simulation. Evacuation times for the CL-215 are complete in 0.7 second, compared with the USFS estimated times of 1.87 seconds (Ref. 3) or with the simulated times of 1.34 seconds. Peak flow rates of 740 gal/sec were predicted in the MacPherson simulation, whereas measured peak flow rates greater than 2000 gal/sec were observed. The implusive nature of the flow is evidenced by the fact that 65% of the fluid is discharged in 0.4 second with an average flow rate of 1200 gal/sec.

The CL-215 has to be considered to be a maximum-flow-rate tank. These extremely high flow rates potentially explain differences that were observed with CL-215 drops. The higher recovery percentage can be associated with the high flow and the lower CL-215 delivery velocity, i.e., 100 knots versus 120 to 150 knots. The onset times of the spike and bubble formations of Taylor instabilities at release are now consistent with other aircraft. Finally, the predicted breakup completion altitude of 500 feet can be traced to this high flow-rate release.

These high flow rates introduce a complication into the MacPherson tank flow simulation. The MacPherson simulation utilizes the continuity equation and a Bernouli equation for an ideal fluid. For these equations to be applicable requires steady, frictionless, incompressible fluid along a streamline. We think the combination of an extremely fast-opening door and the steplike geometry of the tank are causing a nonsteady flow so that a more complicated flow simulation is required. A first step in correcting this difficulty would be to introduce an acceleration term into the momentum equation. The effects of viscosity might have to be examined, which means a more complicated simulation of the Navier Stokes equations. An alternative is to utilize measured flow data for flow rate and exit velocity.

Single-tank data generated by the USFS measurements were used for comparison with the simulation (Table 1).

These data are shown graphically in Figures 40 and 41. Figure 40 shows the measured flow data obtained by simple differencing of the recorded data. (Value from observation 2 minus value from observation 1 divided by Δt.) The extremely high flow rates in the neighborhood of 0.6 second are substantially larger than expected, and the average flow during the time increment $0.3 \leq t \leq .675$ is larger than 1450 gal/sec. The CL-215 discharge is impulsive, with flow rates two to three times those predicted, and exit velocities are also larger. Figure 41 shows the measured door angle as a function of time on the

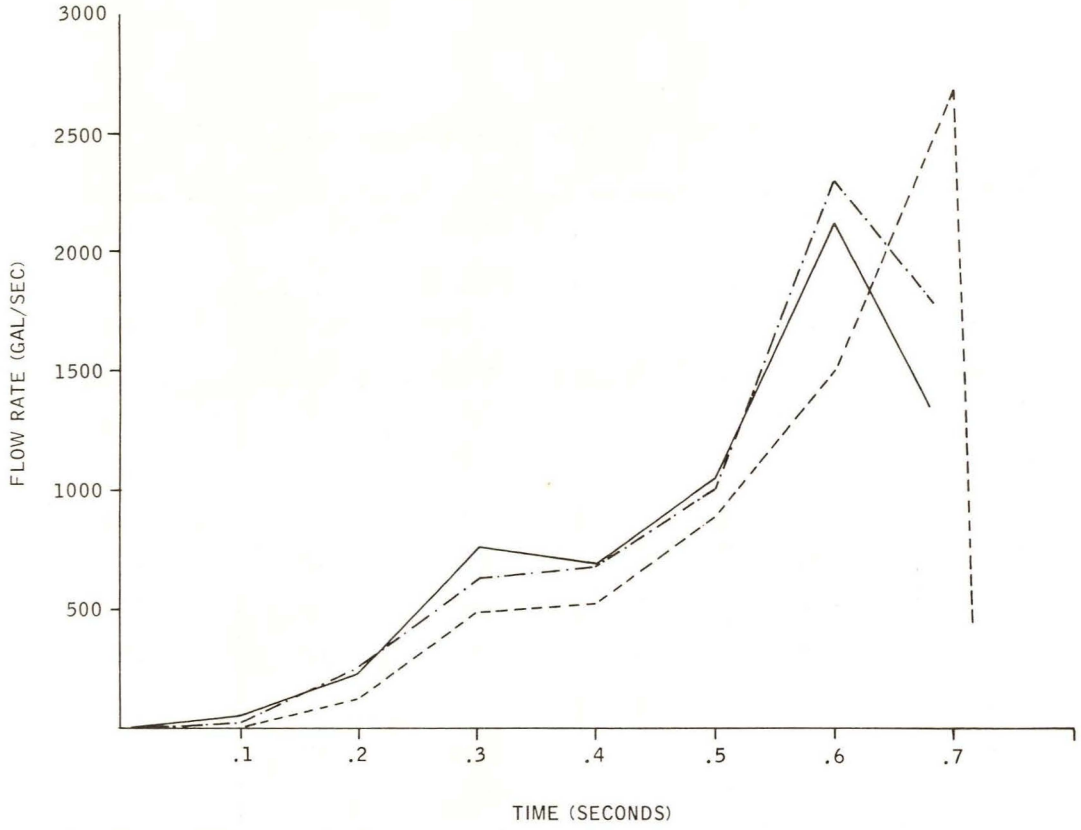

Figure 40. Measured Flow Rate versus Time - CL-215 Test (NFFL Data - Three Tests)

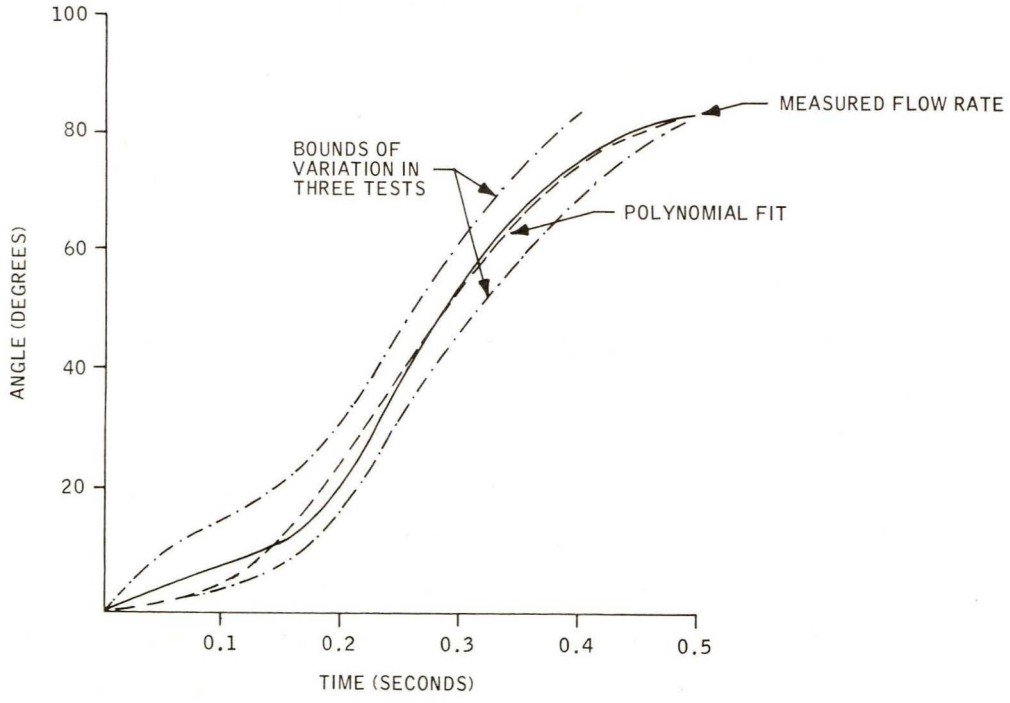

Figure 41. Measured Door Opening versus Time - CL-125

Table 1. Measured Flow Data

Time (sec)	Test 1-14		Test 2-14		Test 3-14	
	Quantity (gal)	Angle (deg)	Quantity (gal)	Angle (deg)	Quantity (gal)	Angle (deg)
.1	6	7	0	15	2	4
.2	29	20	12	30	27	15
.3	105	54	61	60	90	45
.4	174	75	113	82	157	67
.5	278	82	202	82	258	82
.6	484	82	352	82	486	82
.675	620	82	-	-	659	82
.700	-	-	619	82	-	-
.715	-	-	650	-	-	-

three tests and the polynomial fit applied in the simulation. The cubic polynomial fit as a function of time is:

$$f(t) = 0.8934 - 00.69\,t + 1460.\,t^2 - 1870.5\,t^3$$

The curve fit is shown in Table 2.

These coefficients were used to produce a revised MacPherson simulation of flow out of the tank.

When the actual door-opening rate (polynomial) is used in the simulation, the flow-rate distribution shown in Figure 42 results. This is obviously not an adequate fit to the measured flow data. The problem appears to be traceable to the ejection velocity prediction. Figure 43 shows predicted exit velocity plotted against an estimated ejection velocity derived from test results.

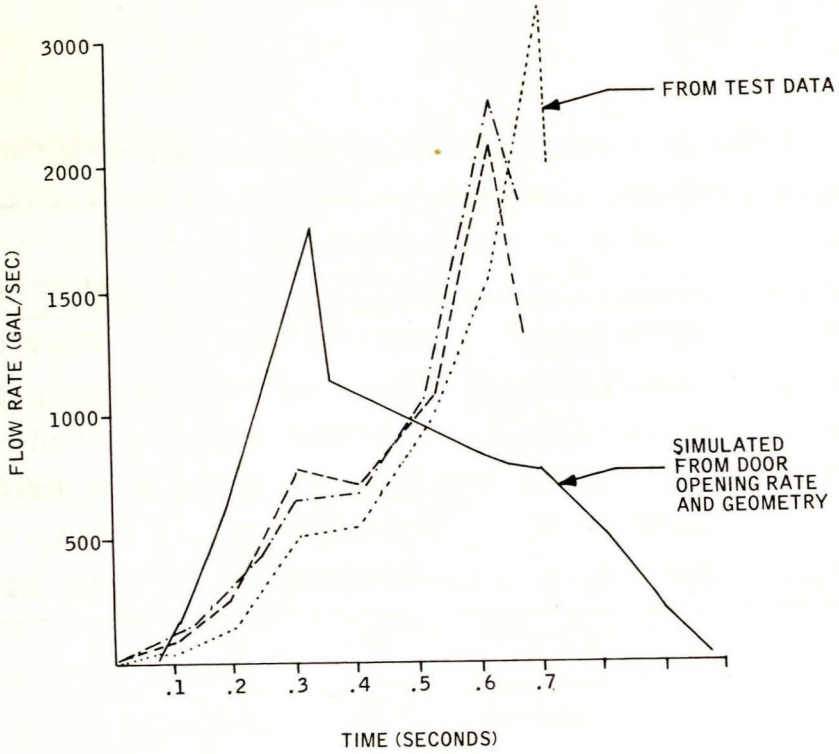

Figure 42. Comparison of Simulated and Measured Flow Rate - CL-125

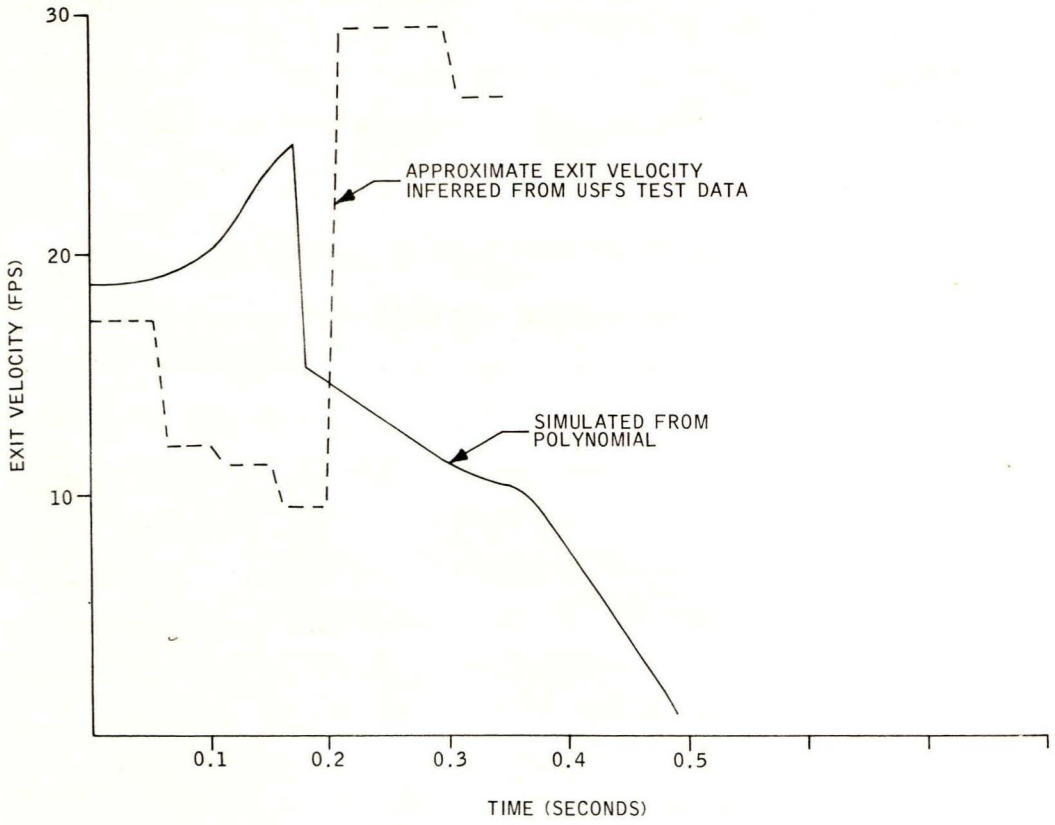

Figure 43. Exit Velocity versus Time Simulation Using Cubic Polynomial - CL-125

Table 2. Comparison of Polynomial Fit

Actual Time (sec)	Actual Opening (deg)	Calculated Opening (deg)	Difference
.000000E 00	.000000E 00	.897337E 00	-.897337E 00
.100000E 00	.700000E 01	.365882E 01	.334178E 01
.200000E 00	.200000E 02	.243965E 02	-.439645E 01
.300000E 00	.540000E 02	.518891E 02	.211091E 01
.400000E 00	.750000E 02	.749132E 02	.868378E-01
.500000E 00	.820000E 02	.822457E 02	-.245712E 00

The exit velocity was estimated for each time increment by calculating the flow velocity during the discharge and applying the equation of continuity:

$$V_T A_T = V_E A_E$$

where

V_T is the estimated float vertical velocity

A_T is the area of the top of the fluid

A_E is the exit area

It is this condition that suggests a problem in the failure to account for fluid acceleration. Apparently, the bulk of the tank carried below the floor of the aircraft cannot flow freely until the upper section clears. This would account for the drop in velocity, followed by a surge, not now accommodated in the model. (There is some evidence of this phenomena in DC 6B data where the radical change in tank cross section occurs sufficiently late in the evacuation cycle that it does not significantly change the flow-rate calculation.)

The significance of the inability to simulate flow rate from the CL-215 is not entirely clear. If the explanation relates to the abrupt change in geometry coupled with the exceedingly fast release, as currently believed, the inability to handle this kind of situation is of no major consequence. Most tanks avoid this condition by virture of their design. There is little indication that tanks of less abrupt geometry are not adequately simulated. As a consequence, it would be enough to know the characteristics of a tank that reduce confidence in the model so that actual flow rates can be substituted for predicted values.

The true test of the model rests on the above proposition that, given the measured flow rate, a pattern can be adequately predicted. To test this contention, the measured flow rate was approximated numerically and inserted in the program. (Figure 44)

Preliminary calculations utilizing measured flow data in conjunction with the marginal distribution calculations show the existing model applies without major modification. A single run with measured data and the constants developed during the contract produced comparable results in the simulated patterns.

Using the approximated flow rate, the pattern was generated (Figure 45). Note that this center-line-to-center-line comparison tests the major portion of the pattern. Since the actual flow-rate distribution derives from Drop 4, where the skirt was considerably offset, this is belived to be a reasonable comparison. Table 3 presents data on both the original simulation and the modified simulation. Both achieved a comparable mean and variance. Since the approximated flow rate was run without iterative optimization on the constants, it is expected that a better match could be achieved with the actual flow-rate distribution than was achieved with the erroneous one. In particular, the hand-fed flow rate elevated more gallons into the higher coverage area. In addition, the low-altitude drop is, in general, the more difficult simulation for this program because the breakup for the CL-215 is not complete as it appears to be for other aircraft.

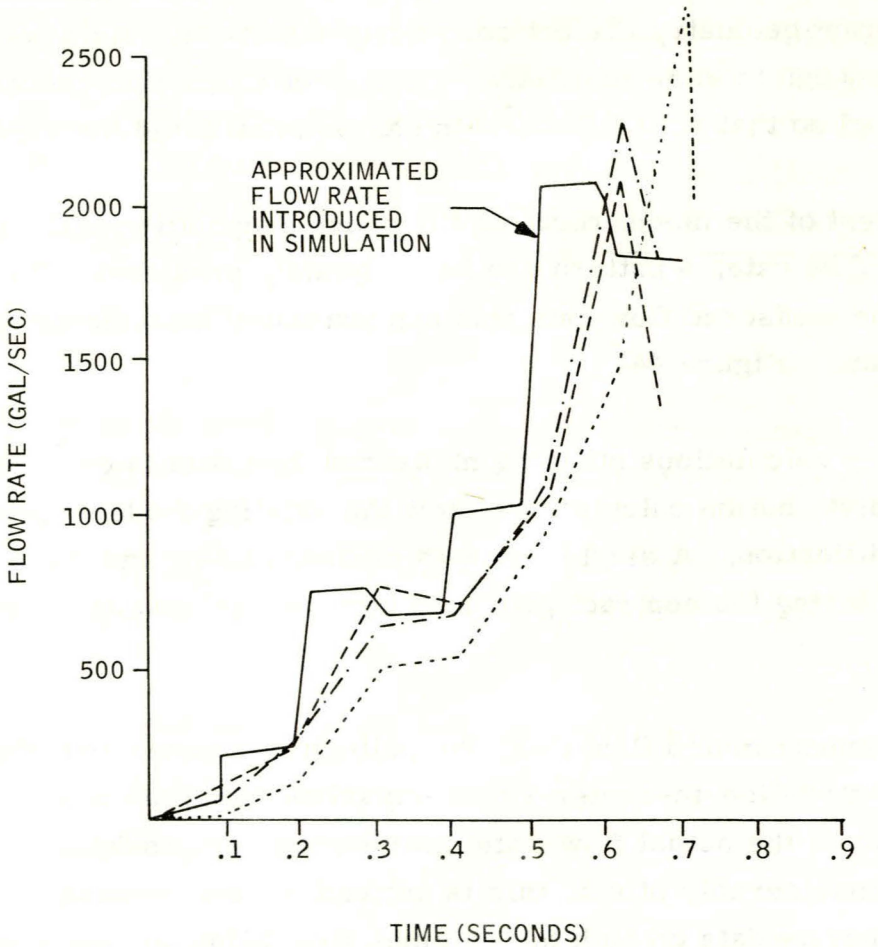

Figure 44. Approximated Flow Rate

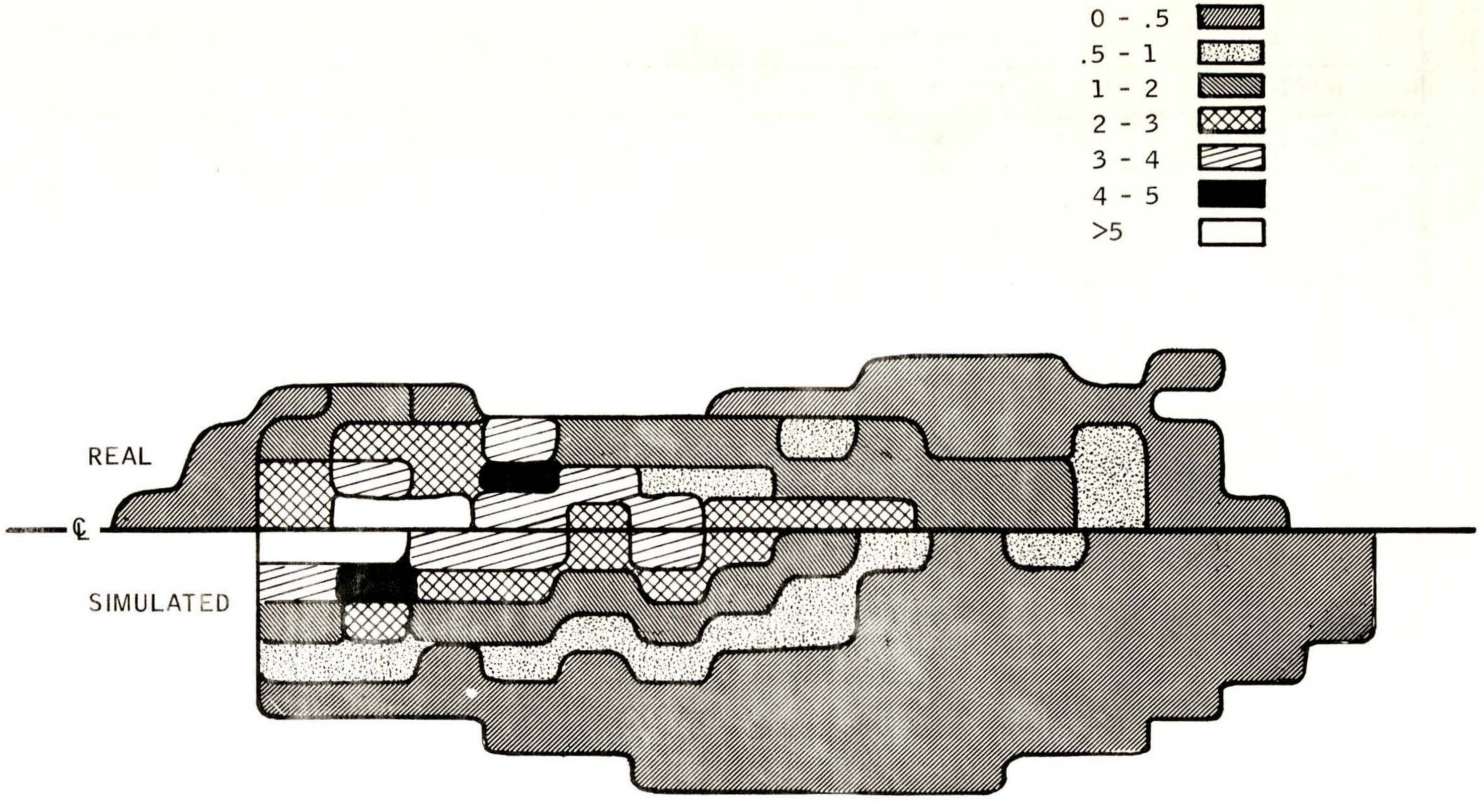

Figure 45. Comparison of Simulated and Real Patterns Using Approximate Measured Flow Rate

Table 3. Comparison of Match with Original Simulated and Measured Flow Data

Test Conditions		Simulation Conditions	
Aircraft	CL-215	Semi-Crossrange (ft)	105
Drop Number	4	λ	0.15
Altitude (feet)	315	σ (ft)	24
Speed (knots)	107	Percent Recovered	89
Gallons	700	K_1	3.97
		K_2	12.00

Comparison of Results

Interval (gal/100 ft^2)	Gallons			Area (ft^2)		
	Test	Simulation 1[a]	Simulation 2[b]	Test	Simulation 1	Simulation 2
0 - 0.2	99.8	47.8	52.7	142087	45900	51300
0.3 - 1.0	99.0	100.0	91.6	19688	23400	20200
1.1 - 2.0	138.8	125.2	107.9	9675	9000	7200
2.1 - 3.0	88.9	135.7	107.5	3600	5400	4500
3.1 - 4.0	84.1	93.2	125.7	2475	2700	3600
4.1 - 5.0	24.9	123.4	37.0	563	2700	900
5.1 - 6.0	30.5		102.7	563		1800
6.1 - 7.0	28.1			450		
7.1 - 8.0	17.2			225		
8.1 - 9.0						
9.1 - 10.						
>10	11.8			113		
Total	623.8	625.3	625.1	179437	89100	90000

	Test Data	Simulation 1	Simulation 2
Average (1)	2.4	2.4	2.7
Average (2)	0.3	0.7	0.7
Difference Data (Test-Simulated) Mean		-0.0980	-0.0952
Difference Data (Test-Simulated) Variance		0.4860	0.4959

a - Original

b - With measured flow data

The question remained: "What was the implication of this discovery on the model." A radical change in the flow-rate should produce, according to previous thinking, a radical change in the pattern. This was the case when the flow-rate distribution predicted from actual door-opening rate was used. The answer to this resides in the operation of the simulation. Consider for example the i th packet Q_i. Its mass is distributed in space from the time it emerges to the time its breakup is complete. The rate of mass loss is an inverse function of Q. Thus, the higher the flow rate, the larger the incremental quantity Q_i, and the farther it will travel to extinction. The total distance from point of release to extinction for a given Q_i will be the distance traveled by the aircraft before Q_i was released, plus the distance traveled prior to breakup. Under these conditions there are equivalent solutions to the time-allocation problem. This emphasizes, however, the importance of the flow-rate distribution as opposed to the simpler view of gross flow rate in determining pattern performance.

IV. TASK 2 - CROSSRANGE DEVELOPMENT

The Task 2 objective was to continue development of the MacPherson simulation to derive a crossrange development from the marginal distribution that would provide pattern isopleths showing lengths, widths, and areas at selected coverage levels over an altitude range: This effort included the following subtasks:

2.1 Working with selected pattern card data (to be furnished by the Forest Service), evaluate the nature of pattern crossrange distributions and their changes with altitude.

2.2 Analyze selected films, as may be necessary at the discretion of the contractor, to assist in developing the rules for complete pattern simulation over the altitude range.

2.3 Demonstrate the predictive technique for one aircraft (CL-215) over the altitude range. Determine the ability of the resulting simulation to predict pattern performance with at least one high-flow-rate tank and one trail-mode tank from the Marana test series.

BACKGROUND

In the initial High-Altitude Retardant Delivery Study (Ref. 1) the significance of volume flow rate from the tank was identified as the primary determinant of pattern formation on the ground. This critical value is determined by tank geometry, quantity of retardant, door area, and door-opening rate. These tank characteristics, in association with aircraft velocity, determined a

marginal distribution of the retardant on the range leg (or length) of the pattern expressed as percent retardant per linear foot. This distribution was little affected by altitude.

Although the range marginal distribution was adequate for qualitative assessment of the effect of various tank design solutions compared to flow-rate management, it was desirable to incorporate in the simulation the ability to spread the retardant out into true area representations for three reasons:

- Improved ability to visualize the effect of design options on pattern areas and lengths in terms of gallons-per-hundred-square-foot coverage units.

- Determine the effect of altitude considering this crossrange development, since the range marginal itself was little affected.

- Enable more precise specifications of new tanks by establishing, through iterative operation of the computer simulation, desired coverage levels, areas, or lengths in terms of flight envelopes, etc.

An additional benefit, having derived the crossrange development rules, is the ability to conduct detailed evaluation of existing air tankers in a computer simulation similar to a thorough Marana-like test series, with the potential of generating user guidelines on the predicted capabilities for various retardant delivery missions.

SUMMARY

The USFS RETARD computer program, used to construct ground pattern data from cup samples of recovered retardant on a grid, was modified by Honeywell to provide a wide range of statistics of pattern characteristics. Using card

data on actual patterns for a large number of drops from the CL-215, P2V and DC6B, pattern statistics were evaluated to establish a conceptual model for crossrange expansion. The pattern was represented by two concepts: (1) a pattern fringe area, typically of low coverage density (0.1 to 0.2 gpc) and (2) a major section containing the signficant coverage quantities. The former, presumably emanating from conventional stripping, has the appearance of a plateau or table that shows evidence of wind offset or diffusion. The latter has the appearance, when graphed three-dimensionally, of a mountain range that erodes or spreads out as it descends in altitude. Consequently, a two-part expansion was selected as the appropriate model.

The program was developed to extract an elliptical uniform retardant distribution from the range marginal distribution after adjustement for percent lost to represent the pattern fringe. The remainder of the retardant is expanded as a normal distribution, simulating the major portion of the retardant pattern.

The computer program was modified to utilize the above concept in terms of three empirically derived values which were assumed to be a function of altitude and, to a lesser extent, aircraft velocity: (1) λ percent in the uniform, (2) semi-crossrange (defining the extent of the quanity λ distributed uniformly), and (3) σ, the statistical value relating the normal distribution to an adjusted marginal distribution. This program, MIX 2, was then used to feed predicted pattern data into a further modification of the RETARD program to allow various statistical comparisons of the real and predicted pattern.

By exercising the simulation, successive runs were made to determine the best-fit values for the emperical quantities for each actual pattern. The process was repeated until the variance between actual and real patterns was minimized. This process was conducted on CL-215, DC6B, and P2V single-tank drops (using Phoschek XA). The relationships of the calibrated values were estimated, and the simulation was applied to a number of other aircraft

drops. Good fits were obtained to Aero Union B-17, Intermountain B-17, Aero Union C-119, and Aero Union B-17 trail drops for gross data (USFS) area, gallons, etc. Only one of the aircraft, the PB4Y2, did not yield a good fit. (The problem may be related to imprecision in the input data.)

CONCLUSIONS

The conceptual model of retardant delivery provides a good estimation of pattern performance, particularly where actual flow rates are known from static-test data. In addition, the analytic capability in the MIX 2 and modified RETARD programs provides the basic tool for evaluating such variables as retardant type and tank separation. The ability to directly compare two patterns also enables us to evaluate more subtle properties of similar drops and will considerably aid in evaluating the results of the recommended tests on the Experimental Tank and Gating System.

DISCUSSION

Conceptual Model

To establish a conceptual model for crossrange development, the Forest Service RETARD Model (which accepts cup-grid data and converts it to pattern plotts) was adopted to incorporate increased statistical analysis capabilities. Card data on actual drops from five CL-215 tests were then used to explore various statistical aspects of the pattern. The drops employed were:

CL-215 Drop Number	Altitude (ft)
51	178
4	300
36	500
53	750
45	1000

In each case, a full B Array (distributed quantity in each cup area) was generated in addition to a full set of conditional and marginal distributions for the pattern. One convenience introduced in the RETARD program was the adaption of the mid-grid cell size for all cell areas. All distributions were displayed using a calcomp plotter. These efforts led to a concept of viewing the pattern as the sum of two distributions -- one uniform, and one with a normal (bell-shaped) crossrange development. It further led to the three-dimensional representation of the patterns (Figure 46) in which the intercept of each graphic segment can be viewed as analagous to the quantity of retardant captured in a cup located at that segment. Note that Drop 53 (750 feet) was again eliminated from the study. This drop appeared anomolous in prior study, but it had not been possible to tell whether this drop or drop 45 (1000 feet) represented abnormal performance. The representations, both statistically and visually, suggest that the 750-foot drop does not perform in the same manner as the others. The reason for this is not clear. It is significant, however, in showing that most of the drops are related and orderly and thus refutes an intuitive supposition that the behavior is substantially random.

The figures show several interesting features:

- The uniform distribution that represents the fine particulate breakup. This is windblown in drop 4 in crossrange.

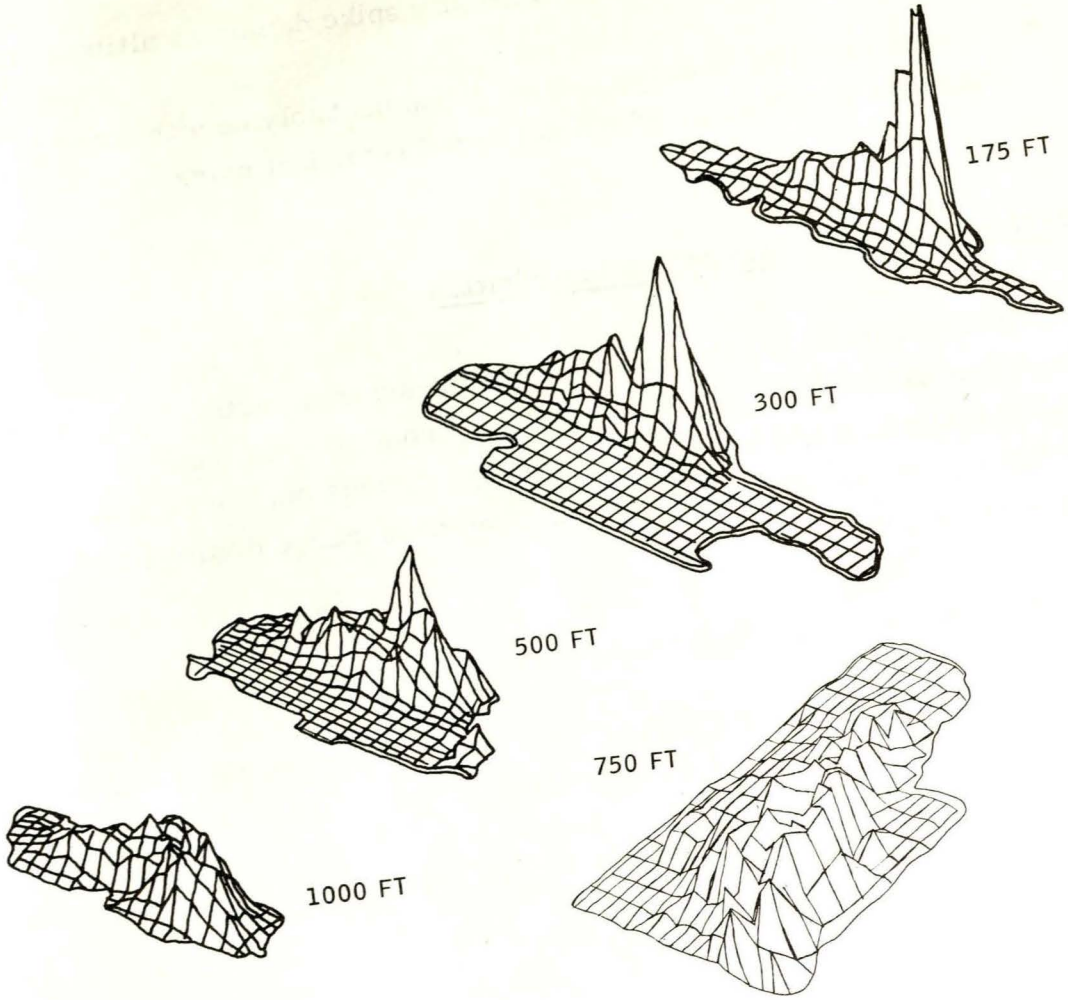

Figure 46. Pattern Forms

- The changes in the pattern densities occur at the top of the "mountain".
- The amplitude of the pattern density spike damps as altitude increases.
- The variability in pattern density can probably be attributed to the surface instabilities of the delivered retardant mass.

Development of the Simulation Distribution

The MIX2 program was modified for the crossrange distribution by adding a subroutine called MIXUN. The MIXUN subroutine uses the basic MacPherson range distribution and adds the crossrange dimension, which is composed of a uniform and a normal distribution. The crossrange distribution is based on four parameters:

- Semi-crossrange on uniform distribution (SEMX)
- λ – Mixing parameter, i.e. fraction of the recovered retardant in the uniform distribution (LAMDA)
- σ – Standard deviation of the normal crossrange distribution (SIGMA)
- Recovery percentage (PCTR)

The MIXUN subroutine develops the distribution and writes the output on magnetic tape for input into the RETARD program. Printed output is also generated.

The communication between the main program MIX-2 and MIXUN is through a labelled common block:

```
COMMON/MIX/DST (1075), GAL, RAT
```

where

DST (1075) = the MacPherson marginal range distribution from MIX-2

GAL = number of gallons dropped

RAT = Factor for converting marginal range to gallons

Additional input is read from an input card by the subroutine. This input contains the four crossrange distribution parameters, SEMX, LAMDA, SIGMA, and PCTR, that were defined above.

The final output of the simulated range and crossrange distribution from MIX-2 is an array identical to the B array used in RETARD. This array contains 28 cells in the crossrange direction and 56 cells in the range direction. The crossrange and range cell dimensions are 15 and 30 feet, respectively. The process used to develop this array is:

- The MacPherson marginal range distribution is redefined with cell size equal to 30 feet (range direction).

- An elliptical uniform ground distribution and marginal distribution is computed. An ellipse is formed whose major axis is equal to the extent in range of the MacPherson marginal range distribution. The semi-minor axis (crossrange axis) of the ellipse is input. Each B array cell within this ellipse is assigned an amount of retardant:

$$\text{Amount per cell} = \frac{\text{LAMDA} \times \text{GAL} \times \text{PCTR}}{100 \times (\text{No. of cells in ellipse})}$$

  The marginal range distribution of the uniform distribution is then computed.

- The uniform marginal range distribution is subtracted cell by cell from the MacPherson marginal range distribution.

- The difference from the above step is distributed normally in cross-range for each range increment. The standard deviation for the normal crossrange distribution is input to the MIXUN subroutine.

- The uniform and normal distributions are added.

Pattern Simulation

The combined and modified RETARD and MIX2 programs were applied to simulate the CL-215 data obtained at a 175-foot altitude. From the recovered data at Marana, the recovery percentage of 78 was applied uniformly to the MacPherson marginal distribution. This uniform assumption can be supported by assuming that the losses occur from the peripheral stripping of the fluid mass and that these particles go through subsequent breakup processes which produce very small particles.

Figure 47 is the program output of the MIX2 which shows how the marginal distribution is apportioned. The column headed MACPHERSON is the simulated marginal distribution for the original tank quantity, and the adjacent column MAC (ADJ) represents the uniform adjustment of the simulation to account for the losses. The column labeled UNIFORM represents the marginal distribution of the uniform elliptical pattern. This uniform distribution is subtracted from the MAC (ADJ) to produce the column labeled NORMAL. When the difference is negative, artifically the value is defined to be zero in the NORMAL column. The combined distribution is the sum of the UNIFORM and the NORMAL. (Figures 48 through 52.)

Figure 53 is a three-dimensional view of the simulation output. This simulation is similar to the actual pattern except that the surface irregularities

RANGE INTERVAL		MACPHERSON	MAC(ADJ)	UNIFORM	NORMAL	COMBINED
0.	3.000000E+01	4.234744E-01	2.667574E-01	9.000000E-01	0.	9.000000E-01
3.000000E+01	6.000000E+01	2.552766E+00	1.608241E+00	1.800000E+00	0.	1.800000E+00
6.000000E+01	9.000000E+01	2.702532E+00	1.702280E+00	2.700000E+00	0.	2.700000E+00
9.000000E+01	1.200000E+02	3.620122E+00	2.280677E+00	2.700000E+00	0.	2.700000E+00
1.200000E+02	1.500000E+02	4.585491E+00	2.888796E+00	3.600000E+00	0.	3.600000E+00
1.500000E+02	1.800000E+02	5.724504E+00	3.606630E+00	3.600000E+00	6.629764E-03	3.606630E+00
1.800000E+02	2.100000E+02	7.237227E+00	4.559831E+00	3.600000E+00	9.598308E-01	4.559831E+00
2.100000E+02	2.400000E+02	9.046547E+00	5.699199E+00	3.600000E+00	2.099199E+00	5.699199E+00
2.400000E+02	2.700000E+02	1.176411E+01	7.423988E+00	3.600000E+00	3.823988E+00	7.423988E+00
2.700000E+02	3.000000E+02	1.490124E+01	9.387161E+00	3.600000E+00	5.787161E+00	9.387161E+00
3.000000E+02	3.300000E+02	1.843726E+01	1.161611E+01	3.600000E+00	8.016107E+00	1.161611E+01
3.300000E+02	3.600000E+02	2.304687E+01	1.451701E+01	3.600000E+00	1.091701E+01	1.451701E+01
3.600000E+02	3.900000E+02	2.887760E+01	1.819352E+01	3.600000E+00	1.459352E+01	1.819352E+01
3.900000E+02	4.200000E+02	3.595454E+01	2.265136E+01	3.600000E+00	1.905136E+01	2.265136E+01
4.200000E+02	4.500000E+02	4.433792E+01	2.793289E+01	3.600000E+00	2.433289E+01	2.793289E+01
4.500000E+02	4.800000E+02	5.343798E+01	3.366655E+01	3.600000E+00	3.006655E+01	3.366655E+01
4.800000E+02	5.100000E+02	6.264192E+01	3.946630E+01	3.600000E+00	3.586630E+01	3.946630E+01
5.100000E+02	5.400000E+02	6.999516E+01	4.409476E+01	2.700000E+00	4.139476E+01	4.409476E+01
5.400000E+02	5.700000E+02	7.073851E+01	4.456514E+01	2.700000E+00	4.186514E+01	4.456514E+01
5.700000E+02	6.000000E+02	2.987218E+01	1.882135E+01	1.800000E+00	1.702135E+01	1.882135E+01
6.000000E+02	6.300000E+02	8.146387E-02	5.144824E-02	9.000000E-01	0.	9.000000E-01
6.300000E+02	6.600000E+02	0.	0.	0.	0.	0.
6.600000E+02	6.900000E+02	0.	0.	0.	0.	0.
6.900000E+02	7.200000E+02	0.	0.	0.	0.	0.
7.200000E+02	7.500000E+02	0.	0.	0.	0.	0.
7.500000E+02	7.800000E+02	0.	0.	0.	0.	0.
7.800000E+02	8.100000E+02	0.	0.	0.	0.	0.
8.100000E+02	8.400000E+02	0.	0.	0.	0.	0.
8.400000E+02	8.700000E+02	0.	0.	0.	0.	0.
8.700000E+02	9.000000E+02	0.	0.	0.	0.	0.
9.000000E+02	9.300000E+02	0.	0.	0.	0.	0.
9.300000E+02	9.600000E+02	0.	0.	0.	0.	0.
9.600000E+02	9.900000E+02	0.	0.	0.	0.	0.
9.900000E+02	1.020000E+03	0.	0.	0.	0.	0.
1.020000E+03	1.050000E+03	0.	0.	0.	0.	0.
1.050000E+03	1.080000E+03	0.	0.	0.	0.	0.
1.080000E+03	1.110000E+03	0.	0.	0.	0.	0.
1.110000E+03	1.140000E+03	0.	0.	0.	0.	0.
1.140000E+03	1.170000E+03	0.	0.	0.	0.	0.
1.170000E+03	1.200000E+03	0.	0.	0.	0.	0.
1.200000E+03	1.230000E+03	0.	0.	0.	0.	0.
1.230000E+03	1.260000E+03	0.	0.	0.	0.	0.
1.260000E+03	1.290000E+03	0.	0.	0.	0.	0.
1.290000E+03	1.320000E+03	0.	0.	0.	0.	0.
1.320000E+03	1.350000E+03	0.	0.	0.	0.	0.
1.350000E+03	1.380000E+03	0.	0.	0.	0.	0.
1.380000E+03	1.410000E+03	0.	0.	0.	0.	0.
1.410000E+03	1.440000E+03	0.	0.	0.	0.	0.
1.440000E+03	1.470000E+03	0.	0.	0.	0.	0.
1.470000E+03	1.500000E+03	0.	0.	0.	0.	0.
1.500000E+03	1.530000E+03	0.	0.	0.	0.	0.
1.530000E+03	1.560000E+03	0.	0.	0.	0.	0.
1.560000E+03	1.590000E+03	0.	0.	0.	0.	0.
1.590000E+03	1.620000E+03	0.	0.	0.	0.	0.
1.620000E+03	1.650000E+03	0.	0.	0.	0.	0.
1.650000E+03	1.680000E+03	0.	0.	0.	0.	0.
NUMBER OF GALLONS FOR EACH		5.000000E+02	3.150000E+02	6.300000E+01	2.558018E+02	3.188018E+02

Figure 47. Typical MIX-2 Program Output

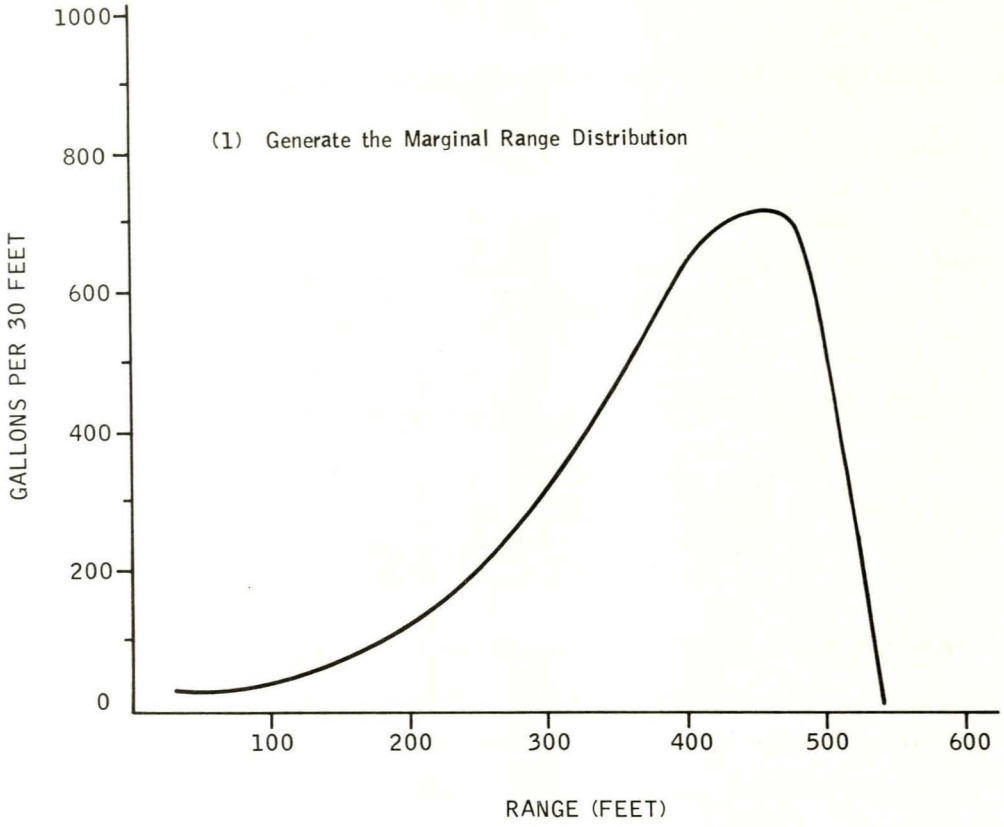

Figure 48. Simulated Marginal Range Distribution – 100% Recovery

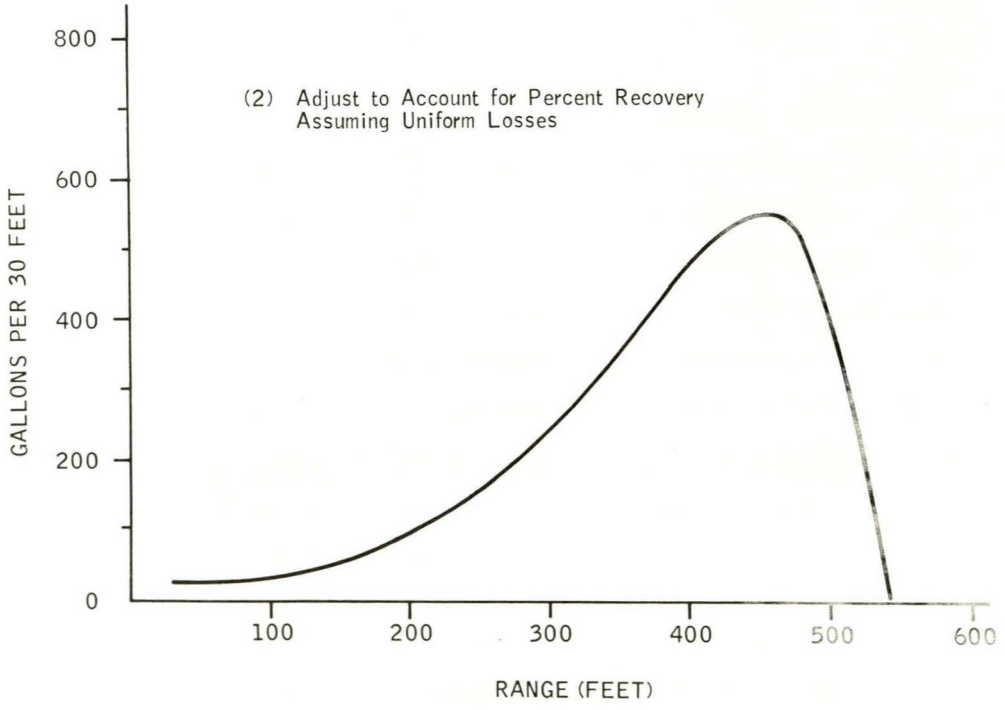

Figure 49. Simulated Marginal Range Distribution – 78% Recovery

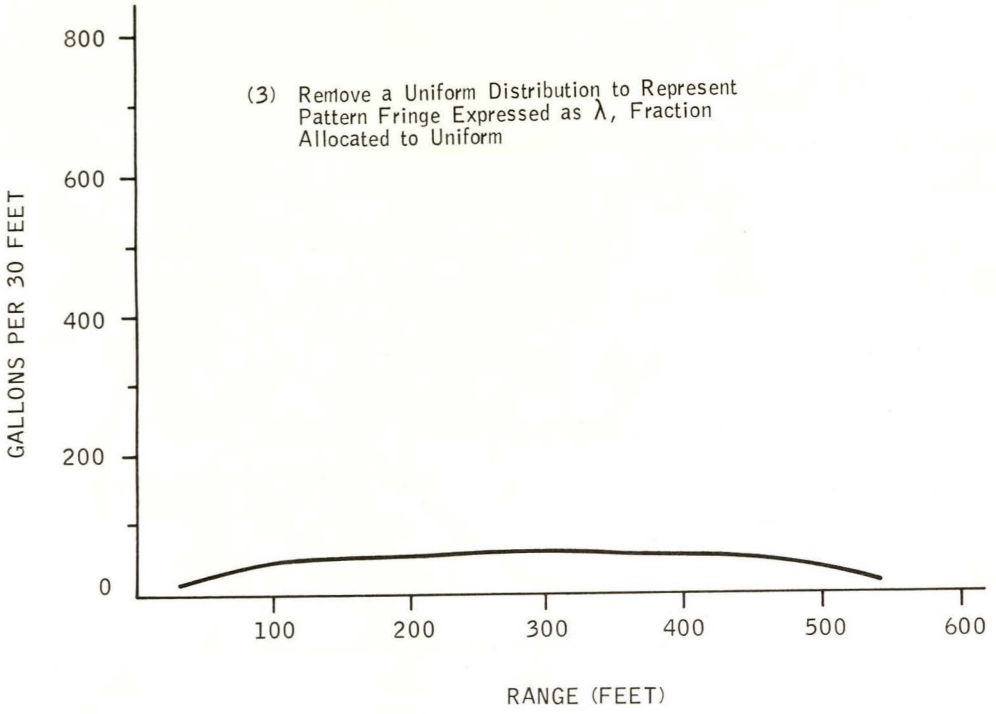

Figure 50. Simulated Uniform Range Distribution – $\lambda = 0.2$

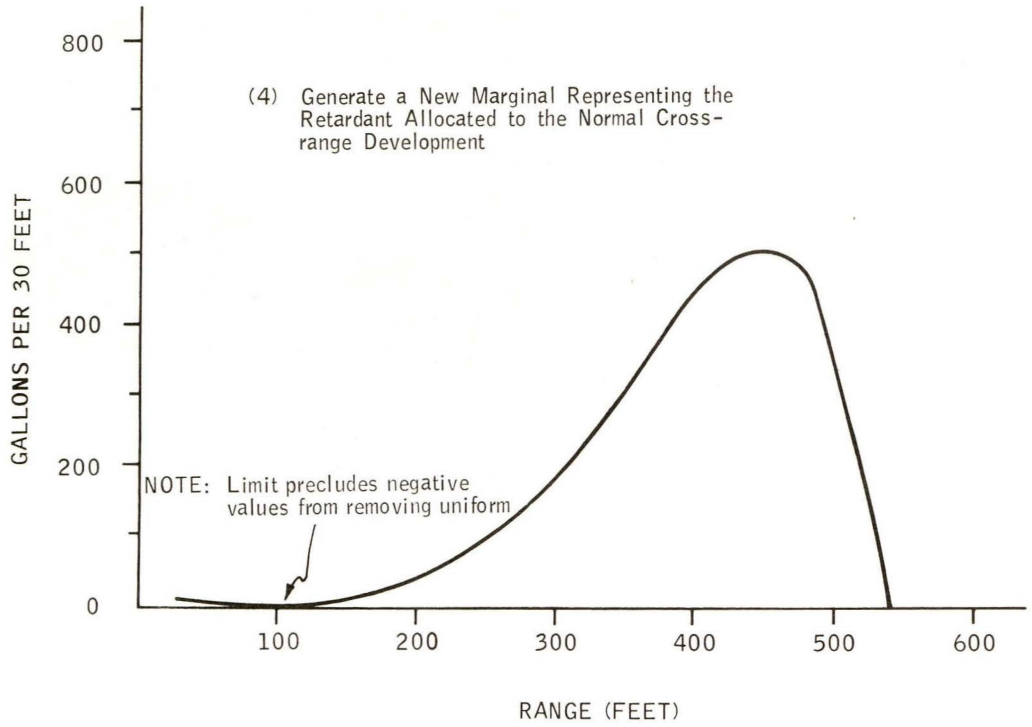

Figure 51. Simulated "Normal" Range Distribution – $(1 - \lambda) = 0.8$

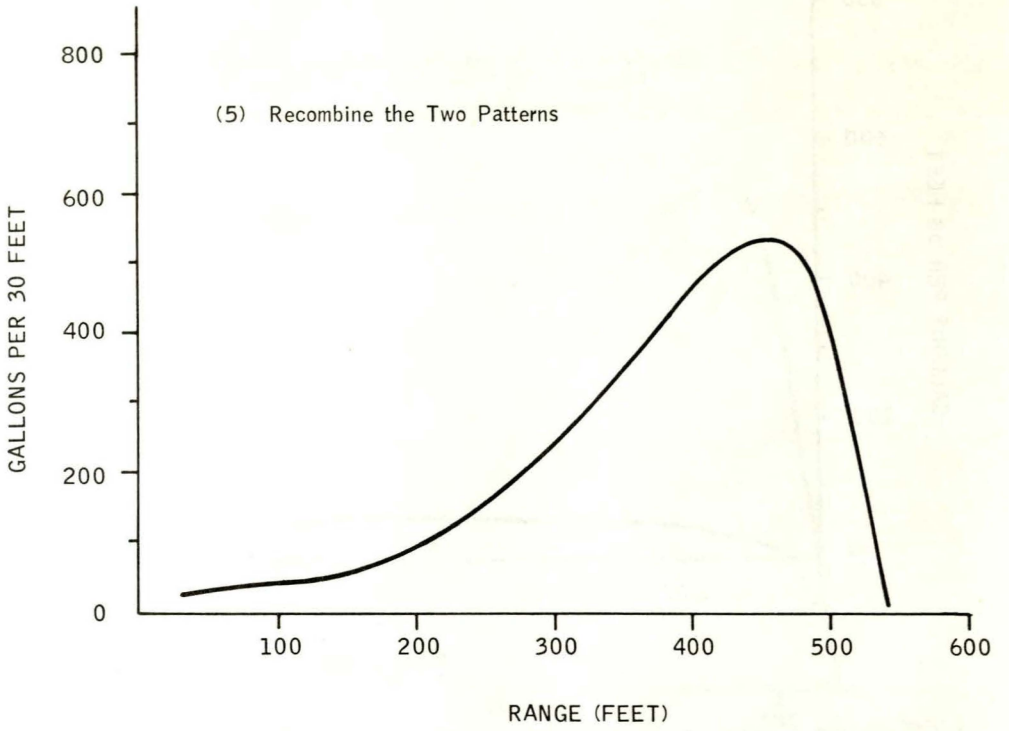

Figure 52. Combined Uniform and Normal Range Distribution

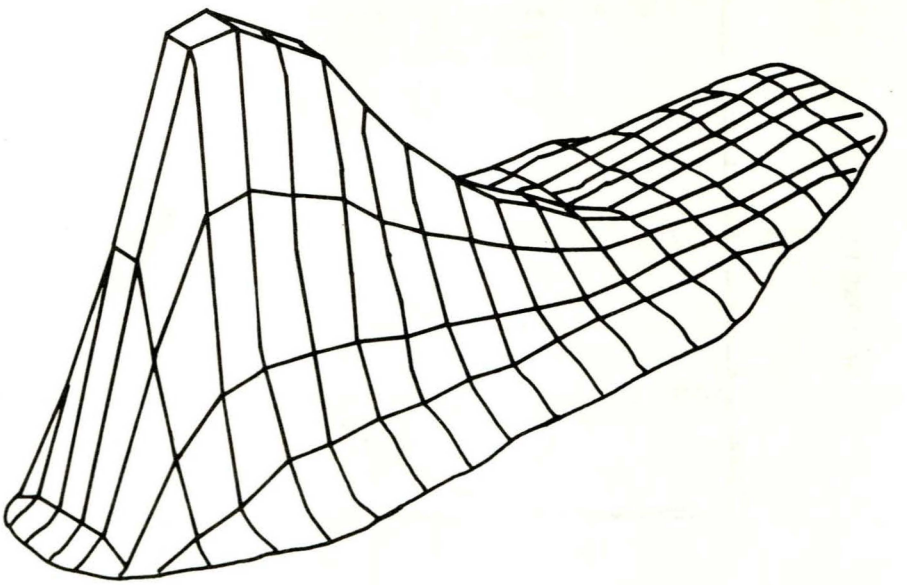

Figure 53. Three-Dimensional Pattern Simulation

are not present. The pattern is a smooth version of the recovered drop. This difference between real pattern and simulated patterns is important in trying to match the simulation to a particular altitude. Although the availability of actual flow data from the CL-215 suggested a partial correction to this problem, evidence in other simulation data suggest the smooth versus irregular appearance will persist.

The criteria of equivalent patterns was investigated, and there are at least four ways of comparing two patterns:

- Equivalent Weibull representations -- same value of η and β in simulated and actual patterns
- Equivalent area density levels between patterns; simulated patterns should cover similar pattern areas as test data patterns
- Equivalent length at 1 gpc, 2 gpc, and 4 gpc for simulated and test patterns
- Minimum variance of the difference between simulated and test patterns.

To investigate these criteria several pattern simulations were conducted, and the four criteria were examined. It was concluded that the best method for assigning the four parameters was the minimum variance of the distribution of the difference between the real and simulated pattern values.

As a criteria for determining the best fit, the difference distribution is evaluated for test data and pattern parameters. The variance of this distribution will be minimized at the point of best fit.

To illustrate, a single run (No. 51) was evaluated (Figures 54 through 57).

.0	0.0	.0	.1	.0	.0	.0	0.0	0.0	0.0
.0	.0	.1	.1	.1	.1	.1	.0	0.0	0.0
.1	.1	.1	.1	.1	.1	.1	.1	.0	0.0
.0	.0	.1	.1	.2	.1	.1	.1	0.0	0.0
.0	.0	.1	.2	.3	.3	.2	.1	.0	.0
.1	.1	.1	.2	.5	.5	.6	.1	.1	.0
.0	.0	.0	.2	.3	.4	.4	.3	.2	.1
.1	.1	.1	.2	.4	.7	1.4	1.0	.3	.1
.1	.1	.1	.1	.6	1.4	1.6	1.1	.3	.1
.0	0.0	.1	.3	.7	1.6	1.6	1.0	.6	.2
.0	0.0	.1	.3	.5	1.2	1.8	1.4	.7	.4
.1	.1	.1	.1	.4	1.2	2.3	2.5	1.6	.5
.0	.1	.1	.3	.5	1.5	2.6	2.0	1.3	.2
.0	0.0	.1	.3	.8	1.6	2.4	3.7	3.3	.9
.0	.1	.1	.4	.7	1.7	3.0	5.9	3.5	1.1
.1	.1	.1	.3	.6	1.5	3.7	6.0	8.2	1.9
.1	.1	.1	.2	.4	1.5	4.0	8.8	5.9	.9
.1	0.0	.2	.1	.6	1.2	1.7	.5	.1	.6
.0	0.0	.1	.3	.5	.8	.8	.1	.1	0.0
.0	0.0	.1	0.0	.1	.2	.1	0.0	0.0	0.0
.0	0.0	.1	.1	.1	.1	.1	0.0	0.0	0.0
.0	0.0	0.0	0.0	.1	.1	.1	0.0	0.0	0.0
.0	0.0	0.0	0.0	.1	.1	0.0	0.0	0.0	0.0
.0	0.0	0.0	.1	.1	.1	0.0	0.0	0.0	0.0
.0	0.0	0.0	0.0	.1	.1	0.0	0.0	0.0	0.0

Figure 54. Run 51 Test Data

.0	.1	.2	.1	0.0	0.0	0.0	0.0
.0	.2	.3	.3	.2	0.0	0.0	0.0
.1	.2	.5	.5	.3	.1	.1	0.0
.0	.2	.3	.4	.4	.3	.2	.1
.0	.2	.4	.7	1.4	1.0	.3	0.0
.0	.1	.6	1.4	1.6	1.1	.3	0.0
.0	.3	.7	1.6	1.6	1.0	.6	.2
.1	.3	.5	1.2	1.8	1.4	.7	.4
.1	.1	.4	1.2	2.3	2.5	1.6	.5
.0	.3	.5	1.5	2.6	2.0	1.3	.2
.0	.3	.8	1.6	2.4	3.7	3.3	.9
.1	.4	.7	1.7	3.0	5.9	3.5	1.1
.0	.3	.6	1.5	3.7	6.0	8.2	1.9
.0	.2	.4	1.5	4.0	8.8	5.9	.9
.2	.1	.6	1.2	1.7	.5	0.0	.6
.0	.3	.5	.8	.8	0.0	0.0	0.0
.0	0.0	0.0	.2	0.0	0.0	0.0	0.0
.0	0.0	0.0	.1	0.0	0.0	0.0	0.0

Figure 55. Run 51 Test Data with Densities ≤ 0.1 gpc Removed

.0	.0	.0	.2	.2	.2	.2	.0	.0	.0
.0	0.0	.2	.2	.2	.2	.2	.2	0.0	0.0
.0	0.0	.2	.2	.2	.2	.2	.2	0.0	0.0
.0	.2	.2	.2	.2	.2	.2	.2	.2	0.0
.0	.2	.2	.2	.3	.3	.2	.2	.2	.0
.2	.2	.2	.3	.3	.3	.3	.2	.2	.2
.2	.2	.2	.4	.6	.6	.4	.2	.2	.2
.2	.2	.3	.6	.9	.9	.6	.3	.2	.2
.2	.2	.4	.8	1.2	1.2	.8	.4	.2	.2
.2	.2	.5	1.1	1.7	1.7	1.1	.5	.2	.2
.2	.3	.6	1.4	2.3	2.3	1.4	.6	.3	.2
.2	.3	.7	1.7	2.8	2.8	1.7	.7	.3	.2
.2	.3	.9	2.2	3.6	3.6	2.2	.9	.3	.2
.0	.3	.9	2.4	4.0	4.0	2.4	.9	.3	.0
.0	.3	1.0	2.6	4.4	4.4	2.6	1.0	.3	.0
.0	.2	1.0	2.5	4.4	4.4	2.6	1.0	.2	.0
.0	.1	.6	1.6	2.5	2.5	1.6	.6	.1	.0
.0	0.0	0.0	.2	.2	.2	.2	0.0	0.0	0.0

Figure 56. Simulated Data (semi crossrange = 75 ft; λ = 0.2; σ = 20 ft; recovery = 78%)

-.0	-.0	-.0	-.0	-.2	-.2	-.2	-.2	-.0	-.0	-.0
0.0	0.0	.1	-.0	-.1	-.2	-.2	-.2	-.2	0.0	0.0
0.0	0.0	.2	.1	.2	-.0	-.2	-.2	-.2	0.0	0.0
0.0	.1	.0	.4	.4	.2	-.0	-.0	-.2	-.2	0.0
-.0	-.0	-.0	.2	.2	.1	-.0	-.0	-.1	-.2	-.0
-.0	-.2	-.0	.2	.5	1.0	.6	.1	-.2	-.2	-.2
-.0	-.2	-.0	.3	1.0	1.1	.5	-.1	-.2	-.2	-.2
-.0	-.2	.1	.4	1.0	.7	.1	-.0	-.2	-.2	-.2
-.0	-.0	.0	.1	.4	.5	.2	-.1	-.0	-.2	-.2
-.0	-.1	-.1	-.1	.2	.6	.8	.5	.1	-.2	-.2
-.0	-.2	.0	-.1	.1	.3	-.2	-.1	-.4	-.3	-.2
-.0	-.2	.1	.1	-.2	-.4	.8	1.6	.2	-.3	-.2
-.0	-.1	.1	-.2	-.5	-.6	2.3	1.3	.2	-.3	-.2
-.0	-.0	-.0	-.3	-.9	-.5	2.0	5.8	1.0	-.3	-.0
-.0	-.0	-.1	-.6	-1.1	-.5	4.4	3.3	-.1	-.3	-.0
-.0	.1	-.0	-.4	-1.4	-2.7	-3.9	-2.6	-.4	-.2	-.0
-.0	-.0	.2	-.1	-.8	-1.8	-2.5	-1.6	-.6	-.1	-.0
0.0	0.0	0.0	0.0	.1	-.2	-.2	-.2	0.0	0.0	0.0

Figure 57. Differenced Data (simulated data translated so the simulated and actual means coincide)

The optimization method consists of varying the semi-crossrange, mixing parameter and the standard deviation of the normal crossrange, and also observing the change in the computed variance of the difference distribution. A local minimum of this variance will be used to determine the best fit. To produce this minimum a steepest-descent statistical design was employed (Ref. 4).

For a semi-crossrange of 72.5, $\lambda = .19$, and 19 feet for σ, the local minimum are:

Mean Difference	.01268 gpc
Variance	.7106 $(gpc)^2$
Standard Deviation	.843 gpc

Comparing Simulated and Test Patterns

The RETARD program was further modified to provide for comparing simulated patterns with test patterns using both the MIX2 and RETARD programs (Figure 58). The methods incorporated into RETARD are described in the steps below:

1. The test pattern data for one drop is read from cards, and statistics are computed in the previous manner. The B array for this drop is stored in an array called TD (test data).

2. The simulated pattern data for one set of parameters (SEMX, LAMDA, SIGMA, PCTR) generated by MIX2 is read from magnetic tape. The data is processed and statistics are computed. A special subroutine called UNCOM is used to calculate the contour intervals on the simulated data B array. The B array is stored in an array called SD (simulated data).

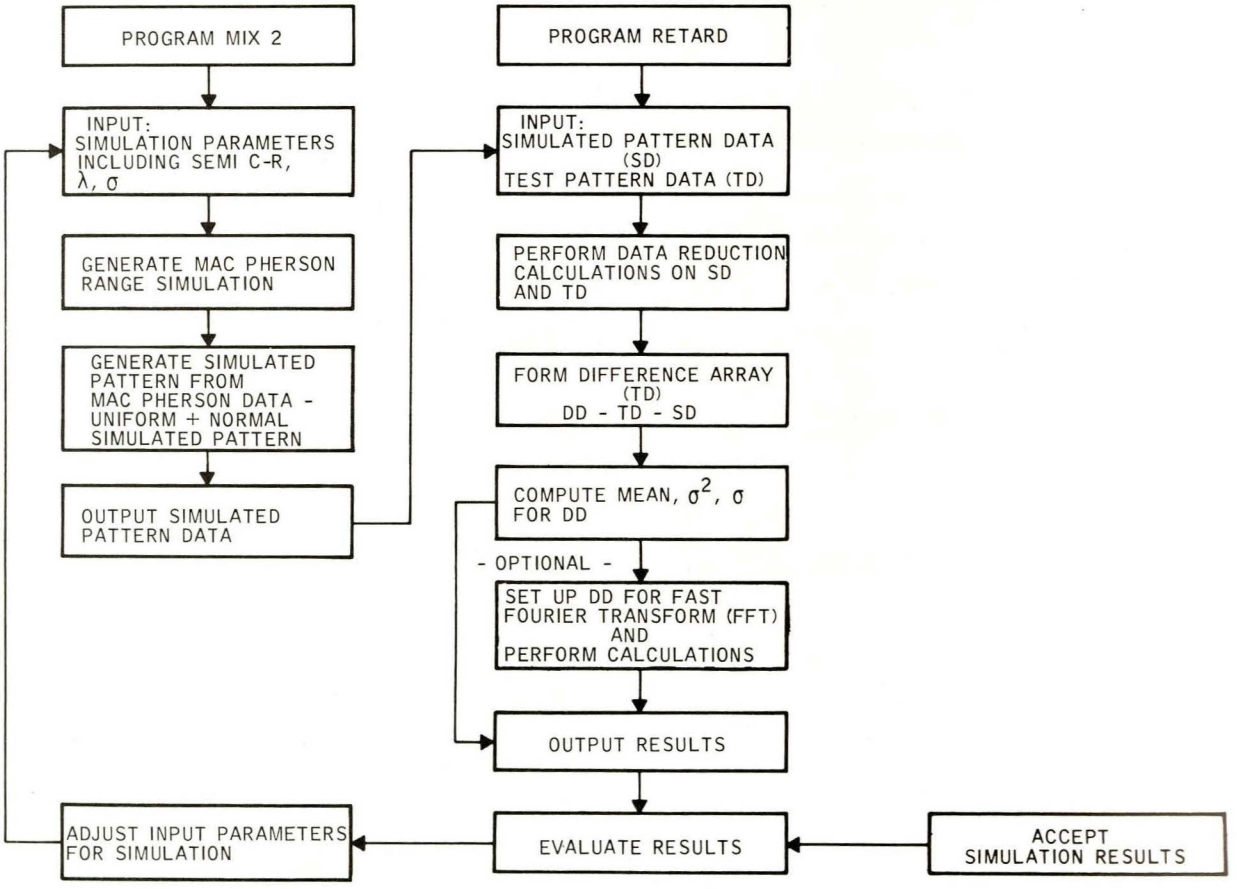

Figure 58. Flow Chart of MIX 2/RETARD Comparison Process

3. A subroutine called COMPARE is used to compute comparison statistics on the test and simulated pattern data. The TD (test data) is modified to delete all cells with retardant density of less than 0.1 gallon per 100 square feet. This was done to remove the effect of wind drift. A differenced data array, DD, is computed by subtracting the simulated data from the test data cell by cell. The mean, variance, and standard deviation of the differenced data array are computed.

4. At this point an option is available to compute the Fourier Transforms* of the differenced data. This option can be exercised on the marginal distributions in range and crossrange, or on the entire distribution row by row, or column by column. The subroutines used for the Fourier Transforms are PREKO, FTIME, TIMEF, and FFT.

5. The results are printed. If more than one simulated pattern is to be compared to the test pattern, as might be the case in a parametric study, the procedure returns to Step 2 for the next simulated pattern. When this process is completed, Step 6 is performed.

6. The results are evaluated. If further adjustment of parameters is desired, the entire process is repeated. This may be desirable to make the simulation better agree with the test data.

---

* See Section V for a discussion of the Fourier methods.

The subroutines and calling sequences that have been developed at this time are:

- SUBROUTINE UNCOM (AA, BTOT, ITOT, SUM). This subroutine performs retardant contour interval calculations on simulated pattern data in B array format:

  AA = simulated pattern data - Dimension (28, 56)

  BTOT - Dimension (12)
  ITOT - Dimension (12)
  } Variables used to compute contour intervals

  SUM

- SUBROUTINE COMPARE (B, F10, IDP, NAME, ICASE, NCASE, AVGCR, AVGR, SIGCR, SIGR). This subroutine computes comparison data for the recovery test and simulated patterns:

  B = B array of retardant recovery or simulated pattern data - Dimension (28, 56)

  F10 = Flags for selecting output - Dimension (10)

  If F10(1) = 0, no CalComp plots are generated

  F10(1) = 1, both conditional and marginal distributions are plotted

  F10(1) = 2, only marginal distributions are plotted

  If F10(2) = 0, both conditional and marginal distributions are printed

  F10(2) > 0, only marginal distributions are printed

IDP = Drop number

NAME = Retardant name - Dimension (4) } Used on CalComp plot label

ICASE = If ICASE = 0, indicates recovery test pattern data is bein processed

If ICASE > 0, the pattern data is simulated and is the ICASEth pattern of the batch

NCASE = No. of simulated patterns per test pattern

AVGCR = Mean of the cross range distribution, ft

AVGR = Mean of the range distribution, ft

SIGCR = Standard deviation of the crossrange distribution, ft

SIGR = Standard deviation of the range distribution, ft.

} For the test pattern data

Once the simulation was operable, a range of expected results to be achieved by varying parameters was investigated. This variability due to parameter variation was examined with the experimental arrangement shown in Figure 59.

The data recorded from the simulation consisted of the number of gallons and the area at the prescribed densities used in RETARD. By comparing the results with actual data, five tentative pattern parameters sets were selected (Table 4).

	75° Semi-Crossrange			100° Semi-Crossrange			125° Semi-Crossrange		
	$\lambda = 0.1$	$\lambda = 0.2$	$\lambda = 0.3$	$\lambda = 0.1$	$\lambda = 0.2$	$\lambda = 0.3$	$\lambda = 0.1$	$\lambda = 0.2$	$\lambda = 0.3$
$\delta = 15°$									
$\delta = 20°$									
$\delta = 25°$									

78% RECOVERY
RUNS AT $\lambda = 0.2$, $\delta = 20, 25, 30, 100°$ Semi-Crossrange
75% and 71% were also made.

Figure 59. Factorial Computer Experiment Setup

Table 4. Selected Parameter Sets

Parameter	Altitude (feet)				
	175	300	500	750	1000
Recovery (percent)	78	76	75	75	82
λ	0.2	0.2	0.2	0.2	0.2
σ	20	20	25	30	30
Semi-Crossrange	75	100	100	100	100

Figures 60 through 63 show the best fits available for CL-215 drops at each of our altitudes. Although this effort was completed prior to the availability of measured flow data, the results remain (as evidenced by the Task 1

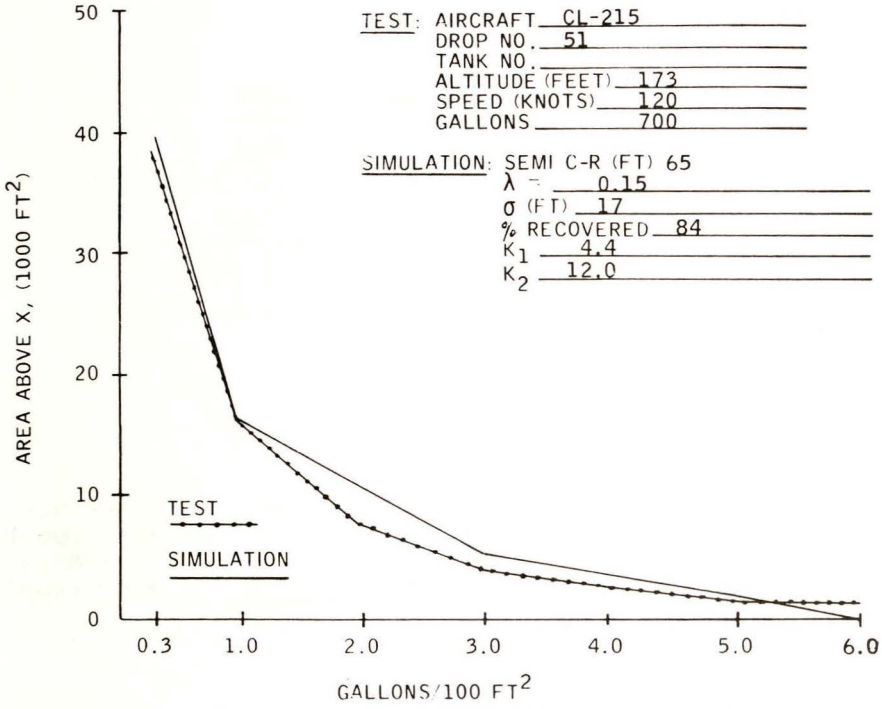

INTERVAL (GAL/100 FT^2)	GALLONS		AREA (FT^2)	
	TEST	SIMULATION	TEST	SIMULATION
0 - 0.2	34.5	24.3	41,962	29,700
0.3 - 1.0	102.3	95.2	21,600	22,500
1.1 - 2.0	122.7	79.7	8,550	5,400
2.1 - 3.0	91.5	136.2	3,712	5,400
3.1 - 4.0	33.7	66.3	1,012	1,800
4.1 - 5.0	61.2	84.8	1,350	1,800
5.1 - 6.0	18.7	99.1	338	1,800
6.1 - 7.0	52.7		788	
7.1 - 8.0	25.4		338	
8.1 - 9.0	9.2		113	
> to g	33.6			
TOTAL	585.5	585.6	79,987	68,400

	TEST DATA	SIMULATION DATA
AVERAGE (1)	3.3	2.9
AVERAGE (2)	0.7	0.9

DIFFERENCE DATA: MEAN = -0.0336
VARIANCE = 1.0000

Figure 60. Comparison of Test and Simulation Data - CL-215 Drop at 173 Feet

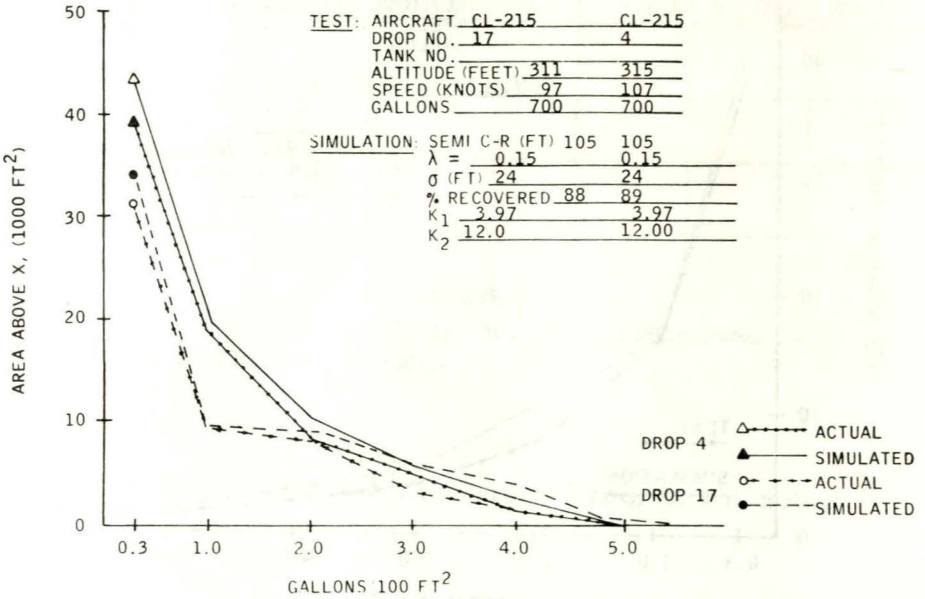

INTERVAL (GAL/100 FT^2)	DROP 4				DROP 17			
	GALLONS		AREA (FT^2)		GALLONS		AREA (FT^2)	
	TEST	SIMULATION	TEST	SIMULATION	TEST	SIMULATION	TEST	SIMULATION
0 - 0.2	99.8	47.8	142,087	45,900	49.6	43.1	63,112	43,200
0.3 - 1.0	99.0	100.0	19,688	23,400	107.0	98.7	21,150	23,400
1.1 - 2.0	138.8	125.2	9,675	9,000	180.3	117.4	1,237	810
2.1 - 3.0	88.9	135.7	3,600	5,400	120.8	68.7	4,725	2,700
3.1 - 4.0	84.1	93.2	2,475	2,700	75.8	120.2	2,250	3,600
4.1 - 5.0	24.9	123.4	563	2,700	33.8	120.6	783	2,700
5.1 - 6.0	30.5		563		32.1	48.5	563	900
6.1 - 7.0	28.1		450		7.1		113	
7.1 - 8.0	17.2		225		0			
> to g	11.8		113		0			
TOTAL	623.2	625.3	179,437	89,100	616.2	617.1	105,187	84,600

	TEST DATA	SIMULATION DATA
AVERAGE (1)	2.4	2.4
AVERAGE (2)	0.3	0.7
AVERAGE (1)	2.2	2.7
AVERAGE (2)	0.6	0.7

	DROP 4	DROP 17
DIFFERENCED DATA:	-0.0980	-0.0448
TEST-SIMULATED:	0.4860	0.5730

Figure 61. Comparison of Test and Simulation Data – CL-215 Drops at 311 and 315 Feet

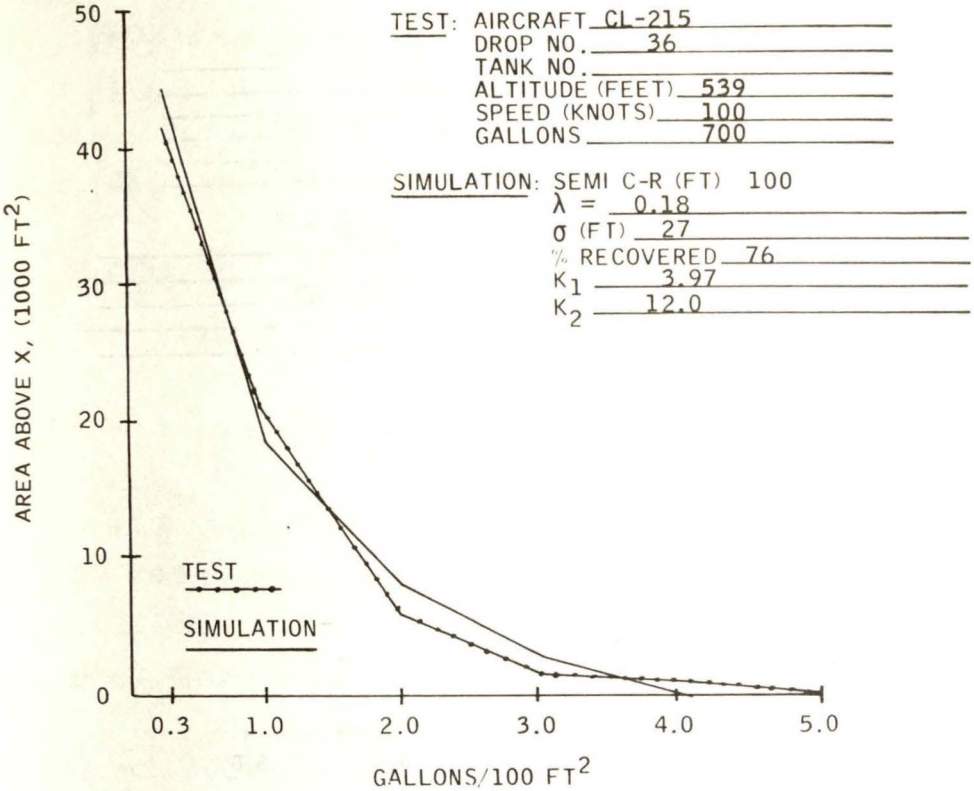

INTERVAL (GAL/100 FT^2)	GALLONS/		AREA (FT^2)	
	TEST	SIMULATION	TEST	SIMULATION
0 - 0.2	49.2	43.5	64800	51300
0.3 - 1.0	96.5	117.9	20475	25200
1.1 - 2.0	222.5	129.1	14400	9000
2.1 - 3.0	98.9	141.5	4387	5400
3.1 - 4.0	35.5	100.1	1125	2700
4.1 - 5.0	18.2		450	
5.1 - 6.0	22.9		450	
TOTAL	543.6	532.2	106087	93600

	TEST DATA	SIMULATION DATA	
AVERAGE (1)	1.8	1.8	DIFFERENCED DATA: MEAN = -0.0312
AVERAGE (2)	0.5	0.6	(TEST-SIMULATED) - VARIANCE = 0.2820

Figure 62. Comparison of Test and Simulation Data - CL-125 Drop at 539 Feet

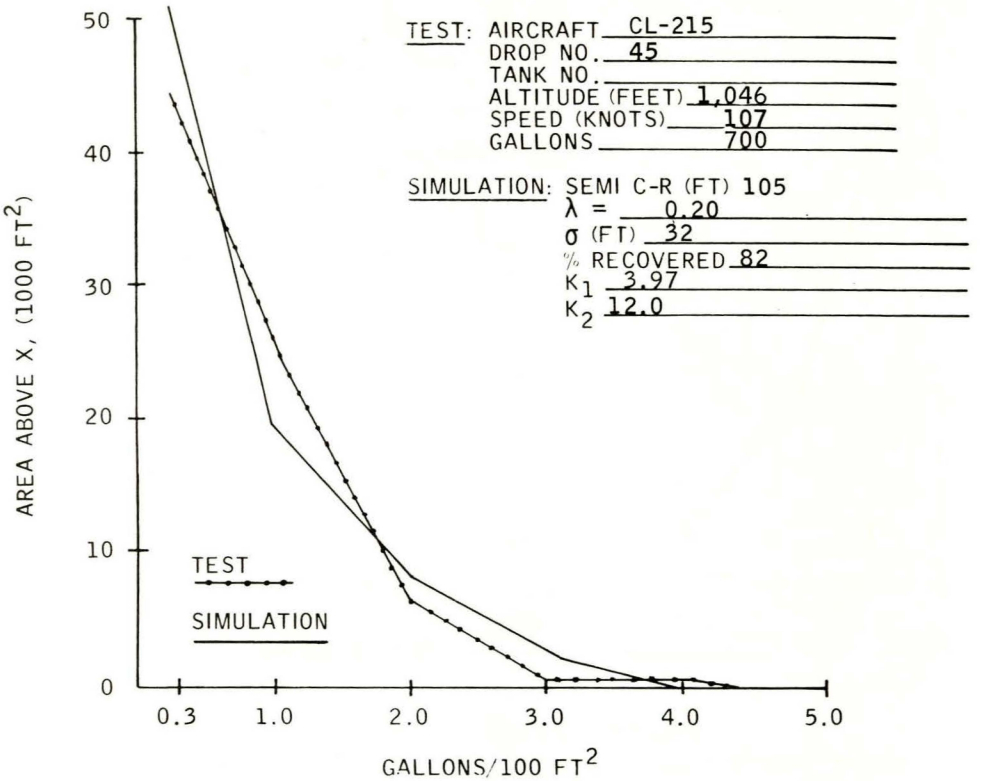

INTERVAL (GAL/100 FT^2)	GALLONS		AREA (FT^2)	
	TEST	SIMULATION	TEST	SIMULATION
0 - 0.2	20.8	49.2	24,412	58,500
0.3 - 1.0	105.9	143.5	18,112	30,600
1.1 - 2.0	292.8	165.9	19,237	11,700
2.1 - 3.0	140.4	133.7	6,075	5,400
3.1 - 4.0	17.3	87.3	563	2,700
TOTAL	577.3	579.6	68,400	108,900

	TEST DATA	SIMULATION DATA
AVERAGE (1)	1.6	1.7
AVERAGE (2)	0.8	0.5

DIFFERENCED DATA: MEAN = -0.0137
(TEST-SIMULATED) VARIANCE = 0.2390

Figure 63. Comparison of Test and Simulation Data - CL-215 Drop at 1046 Feet

discussion) approximately valid. More importantly, better variance matches were actually obtained for DC6B and P2V where good flow rates were known prior to the simulation. It is probable that better matches can be achieved with a direct input of the real flow rate. Within these limitations, good matches were actually obtained. Note that:

- Percent recovered was taken from actual data available from the drop being simulated.

- Semi-crossrange, λ and σ increased with altitude.

- Although the data show variance in the simulation value K_1 for the low-altitude drop, this is relatively minor. This change reduces the first harmonic error in the simulation, but has little effect on the pattern prediction. Thus the value K_1 = four remains substantially valid.

A significant predictive capability finding was the ability of the simulation to follow small velocity changes introduced by the aircraft. This is shown in Figure 61 where two drops at approximately 300 feet were available.

DC6 and P2V Studies

Based on the CL-215 study, a similar process was applied to single-tank drops from the DC6B and P2V for which both measured flow data and pattern data cards were available. Using values of crossrange variables established for similar drops of the CL-215 provided reasonable first guesses for the iterative program; matches were obtained after only a few iterations. Figures 64 through 67 show the results of the best-fit patterns. Note, only single-tank drops were used to avoid the potential errors due to unknown mixing values in multiple-tank drops. Variances were, in general, lower for these tanks, probably because the flow rates were more accurate than for the CL-215 study.

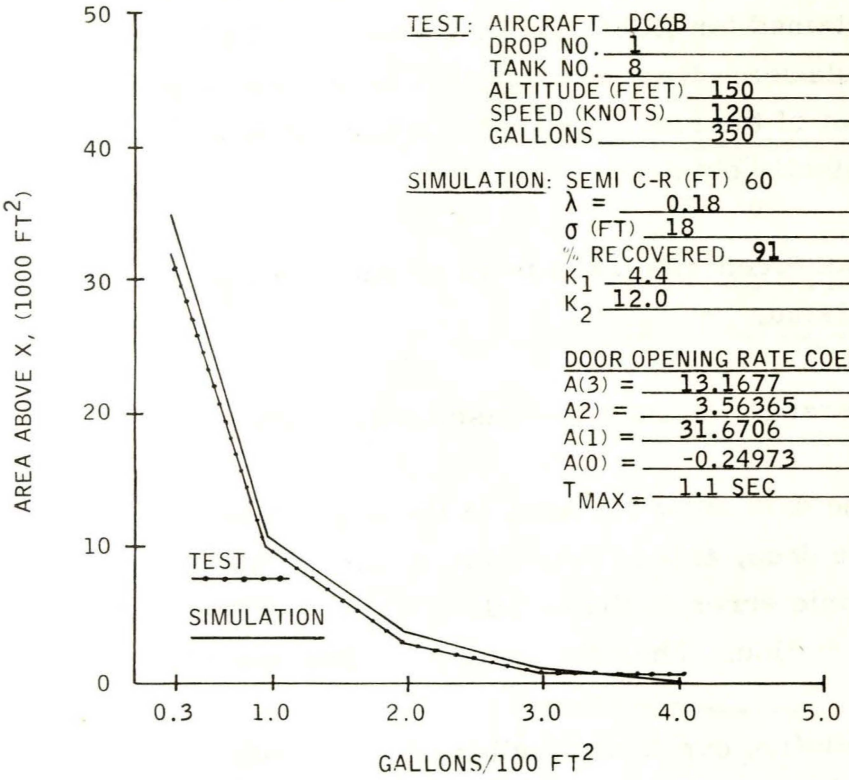

INTERVAL (GAL/100 FT^2)	GALLONS		AREA (FT^2)	
	TEST	SIMULATION	TEST	SIMULATION
0 - 0.2	25.6	21.2	31,162	31,500
0.3 - 1.0	111.1	102.9	21,375	22,500
1.1 - 2.0	95.0	102.8	6,750	7,200
2.1 - 3.0	53.6	65.0	2,250	2,700
3.1 - 4.0	10.5	27.9	338	900
4.1 - 5.0	9.5		225	
5.1 - 6.0	12.5		225	
TOTAL	317.8	319.9	62,325	64,800

	TEST DATA	SIMULATION DATA
AVERAGE (1)	1.6	1.5
AVERAGE (2)	0.5	0.5

DIFFERENCED DATA: MEAN = -0.0300
(TEST-SIMULATED) VARIANCE = 0.1440

Figure 64. Comparison of Test and Simulation Data – DC6B Drop at 150 Feet

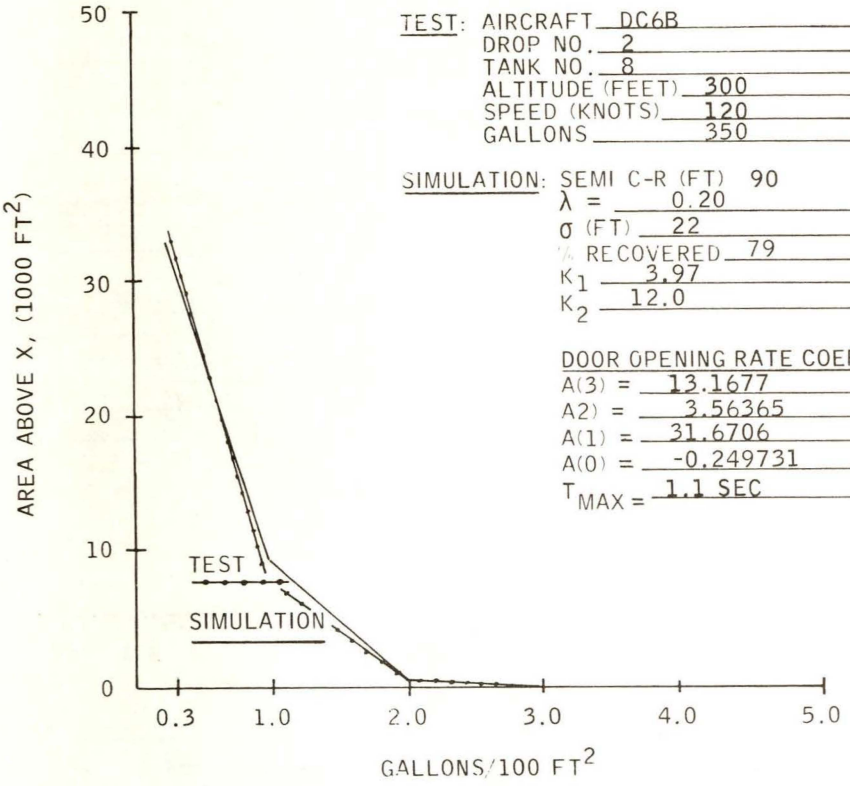

TEST: AIRCRAFT DC6B
DROP NO. 2
TANK NO. 8
ALTITUDE (FEET) 300
SPEED (KNOTS) 120
GALLONS 350

SIMULATION: SEMI C-R (FT) 90
λ = 0.20
σ (FT) 22
% RECOVERED 79
K_1 3.97
K_2 12.0

DOOR OPENING RATE COEFFICIENTS:
A(3) = 13.1677
A2) = 3.56365
A(1) = 31.6706
A(0) = -0.249731
T_{MAX} = 1.1 SEC θ_{MAX} = 57

INTERVAL (GAL/100 FT^2)	GALLONS		AREA (FT^2)	
	TEST	SIMULATION	TEST	SIMULATION
0 - 0.2	31.7	41.7	36,787	50,400
0.3 - 1.0	130.5	101.9	25,087	23,400
1.1 - 2.0	99.3	115.2	7,437	8,100
2.1 - 3.0	13.6	18.5	563	900
TOTAL	275.1	277.2	69,975	82,800

	TEST DATA	SIMULATION DATA
AVERAGE (1)	1.0	1.0
AVERAGE (2)	0.4	0.3

DIFFERENCED DATA: MEAN = -0.0287
(TEST-SIMULATED) VARIANCE = 0.111

Figure 65. Comparison of Test and Simulation Data – DC6B Drop at 300 Feet

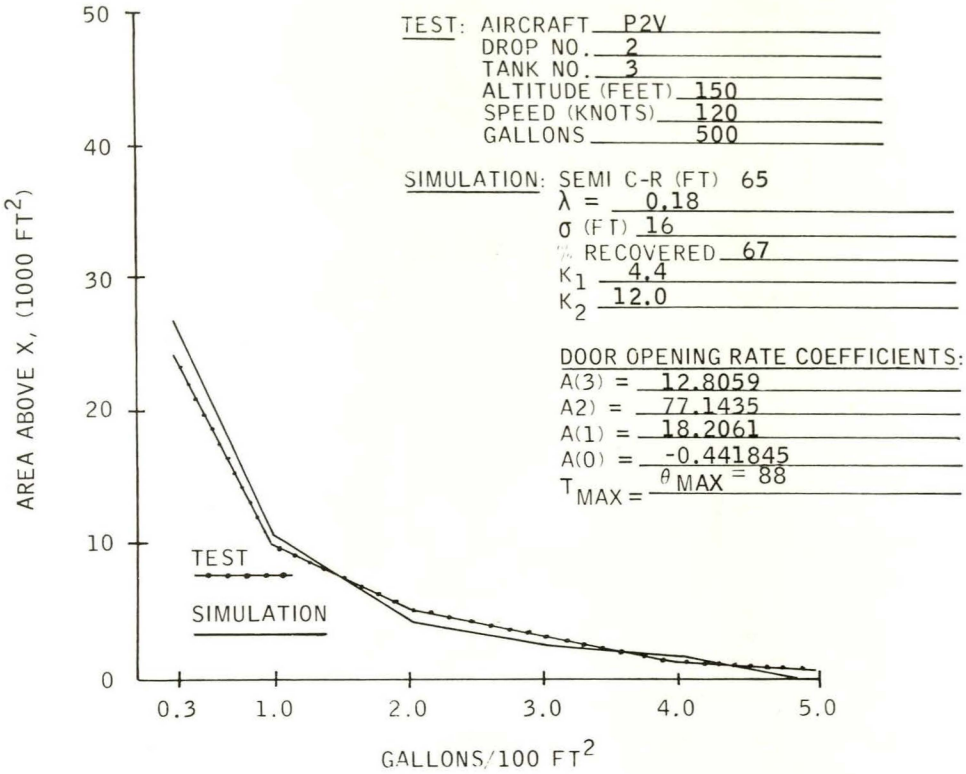

INTERVAL (GAL/100 FT^2)	GALLONS		AREA (FT^2)	
	TEST	SIMULATION	TEST	SIMULATION
0 - 0.2	23.2	33.9	28,462	39,600
0.3 - 1.0	62.0	72.4	13,837	15,300
1.1 - 2.0	72.8	83.8	5,063	5,400
2.1 - 3.0	45.1	41.3	1,912	1,800
3.1 - 4.0	60.8	30.1	1,800	900
4.1 - 5.0	48.8	77.7	1,125	1,800
5.1 - 6.0	24.1		450	
TOTAL	336.7	339.2	52,650	64,800

	TEST DATA	SIMULATION DATA
AVERAGE (1)	2.5	2.2
AVERAGE (2)	0.6	0.5

DIFFERENCED DATA: MEAN = -0.0282
(TEST-SIMULATED) VARIANCE = 0.187

Figure 66. Comparison of Test and Simulation Data - P2V Drop at 150 Feet

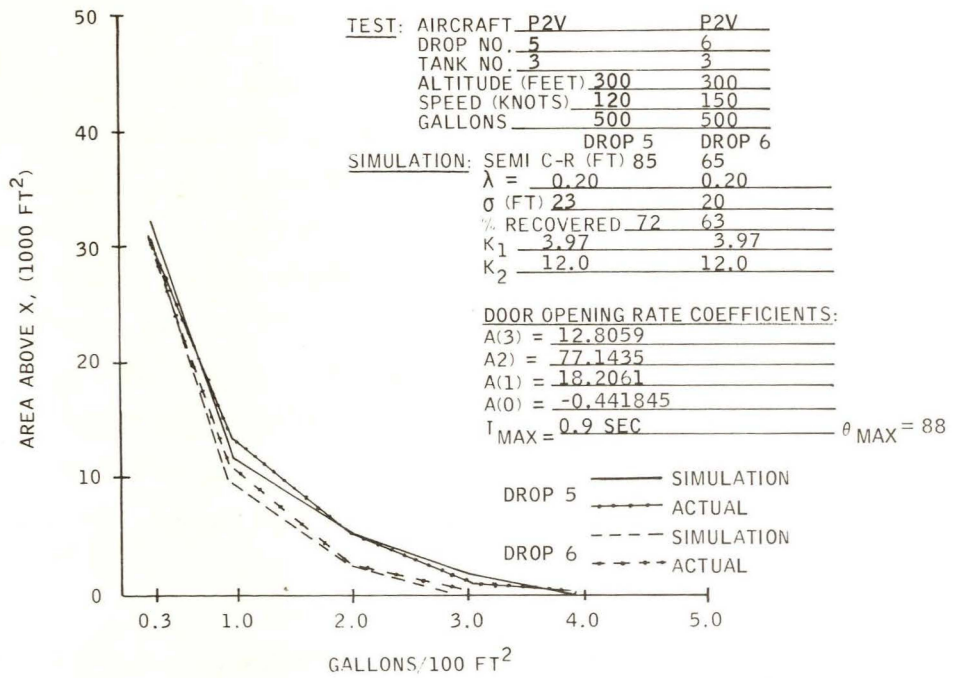

INTERVAL (GAL/100 FT^2)	DROP 5				DROP 6			
	GALLONS		AREA (FT^2)		GALLONS		AREA (FT^2)	
	TEST	SIMULATION	TEST	SIMULATION	TEST	SIMULATION	TEST	SIMULATION
0 - 0.2	24.1	46.5	28,575	56,700	26.1	43.3	29,587	63,000
0.3 - 1.0	84.4	90.0	16,200	19,800	100.2	103.3	19,688	20,700
1.1 - 2.0	108.9	83.4	7,762	6,300	116.9	104.4	8,325	7,200
2.1 - 3.0	98.4	83.1	4,162	3,600	55.7	67.8	2,250	2,700
3.1 - 4.0	38.7	58.5	1,125	1,800	15.4		450	
4.1 - 5.0	4.5		113					
TOTAL	358.9	362.6	57,937	88,200	314.3	318.8	60,300	93,600

	TEST DATA	SIMULATION DATA	TEST DATA	SIMULATION DATA
AVERAGE (1)	1.7	1.6	1.4	1.2
AVERAGE (2)	0.6	0.4	0.5	0.3

DIFFERENCED DATA: MEAN = -0.0216 MEAN = -0.022
(TEST-SIMULATED) VARIANCE = 0.256 VARIANCE = 0.136

Figure 67. Comparison of Test and Simulation Data - P2V Drops at 300 Feet

Extension to Other Aircraft

The results of the CL-215, DC6B, and P2V studies were scattergraphed to infer rules for manipulating the simulation variables (Figure 68). Using values selected from the scattergraph, a number of runs were conducted to assess the match achieved for other aircraft. These results were compared with USFS summary data, using the RETARD program rather than actual pattern runs. They are shown in Figures 69 through 73 for the Intermountain B-17, Aero Union B-17's, and the Aero Union C-119. Note that, for the Aero Union B-17, two runs are presented. The first uses the rules directly as inferred; the second reduces the λ value from 0.20 to 0.15. This departure is shown to provide a slightly better match. In all other cases, the rules as inferred were adhered to.

Achieving a good match to the PB4Y2 was difficult, although a number of variations were attempted in the adjustment parameters (Table 5). This aircraft was also the least well fit to the marginal range distributions reported in Reference 1, Volume 1. The difficulty may be traceable to lack of precision in the flow-rate parameters.

Application to Trail Drops

The Aero Union B-17 trail was selected to assess the general applicability of the model for low-flow-rate tanks. The first simulation followed rules inferred, as above, and produced a good fit to the area statistics. It did not, however, produce a look-alike pattern; the pattern was too short and wide. The second simulation was run using a semi-crossrange inferred from the actual pattern. This simulation preserved the area match, while correcting the proportions of the pattern (Figure 74).

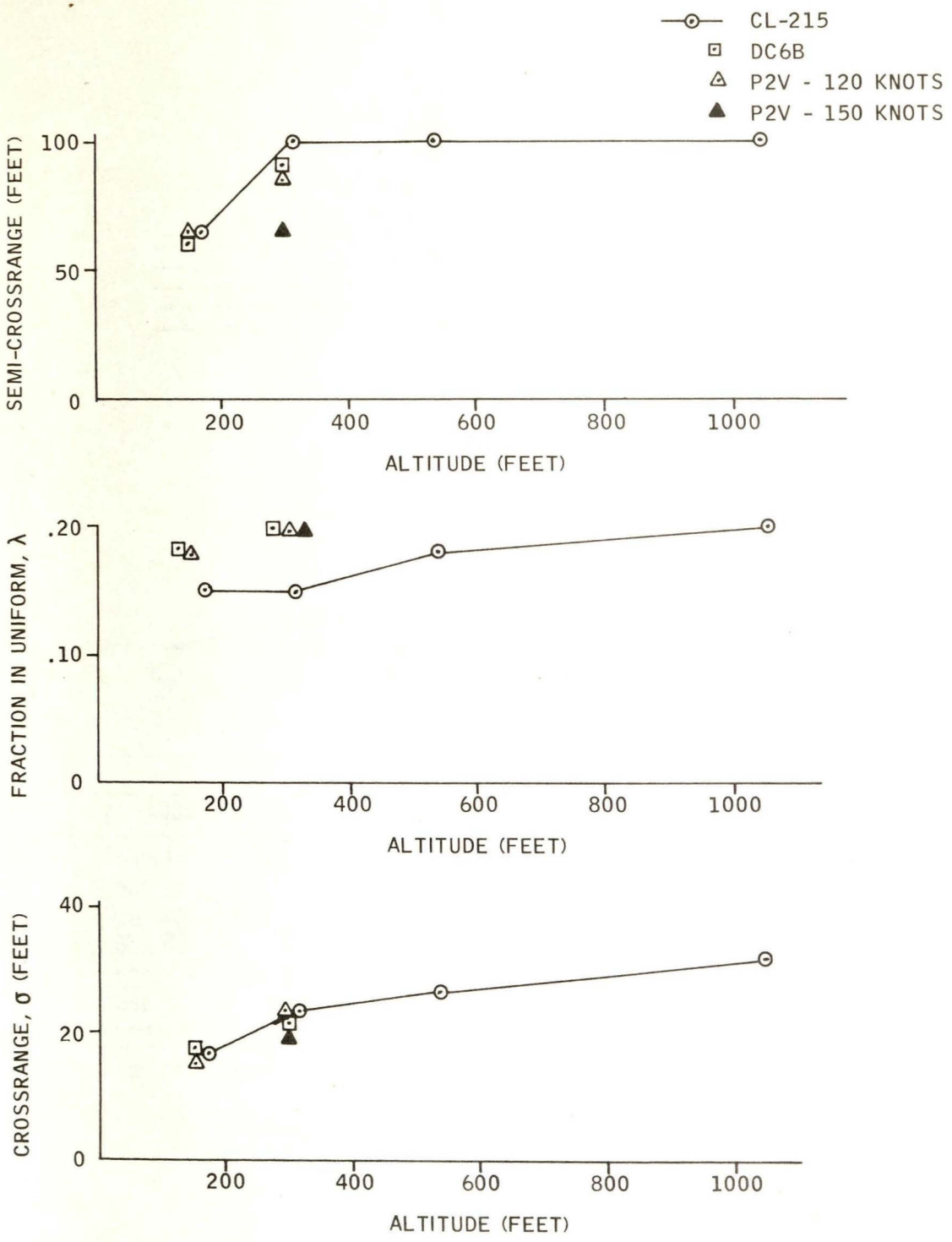

Figure 68. Simulation Results Scattergraph

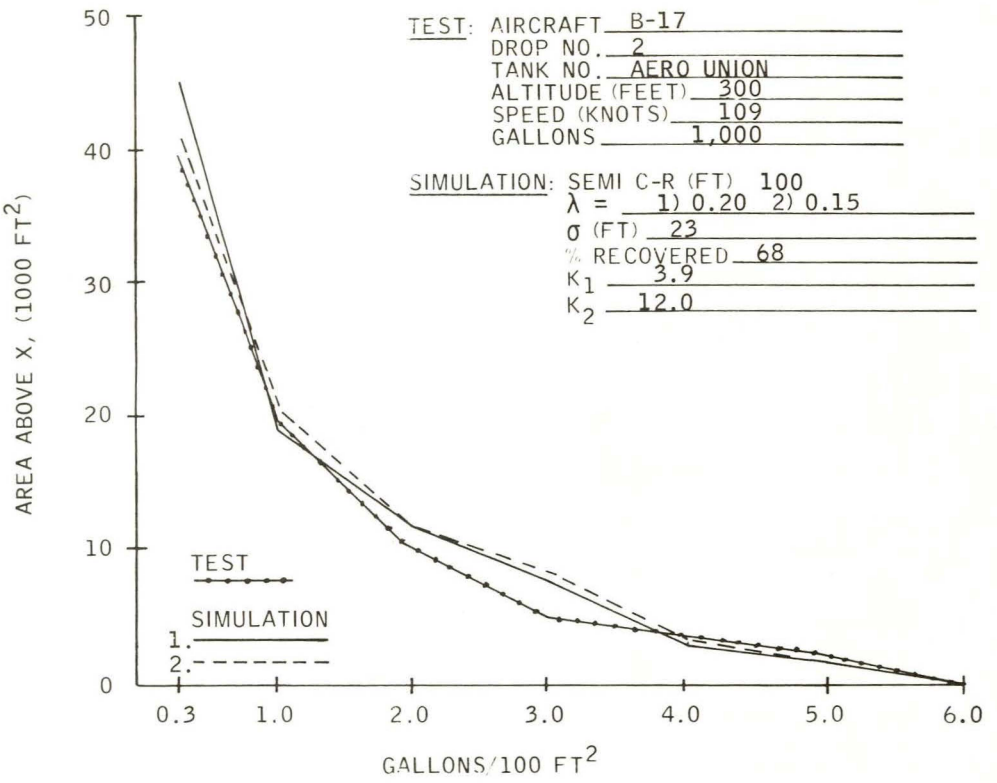

INTERVAL (GAL/100 FT^2)	GALLONS			AREA (FT^2)		
	TEST	SIMULATION 1	SIMULATION 2	TEST	SIMULATION 1	SIMULATION 2
0 - 0.2	44.6	62.9	55.3	57,825	46,800	51,300
0.3 - 1.0	93.5	109.5	92.1	19,283	25,200	20,700
1.1 - 2.0	135.7	103.1	113.8	9,338	7,200	8,100
2.1 - 3.0	121.2	109.3	84.7	5,063	4,500	3,600
3.1 - 4.0	57.6	166.1	159.0	1,688	4,500	4,500
4.1 - 5.0	45.0	42.6	79.4	1,013	900	1,800
5.1 - 6.0	183.4	103.6	104.7	2,251	1,800	1,800
TOTAL	681.0	697.0	689.0	96,461	90,900	91,800

	TEST DATA	SIMULATION DATA	
		λ = 0.20	λ = 0.15
AVERAGE (1)	2.9	2.8	2.6
AVERAGE (2)		0.8	0.8

Figure 69. Comparison of Test and Simulation Data - Aero Union B-17 Drop at 300 Feet

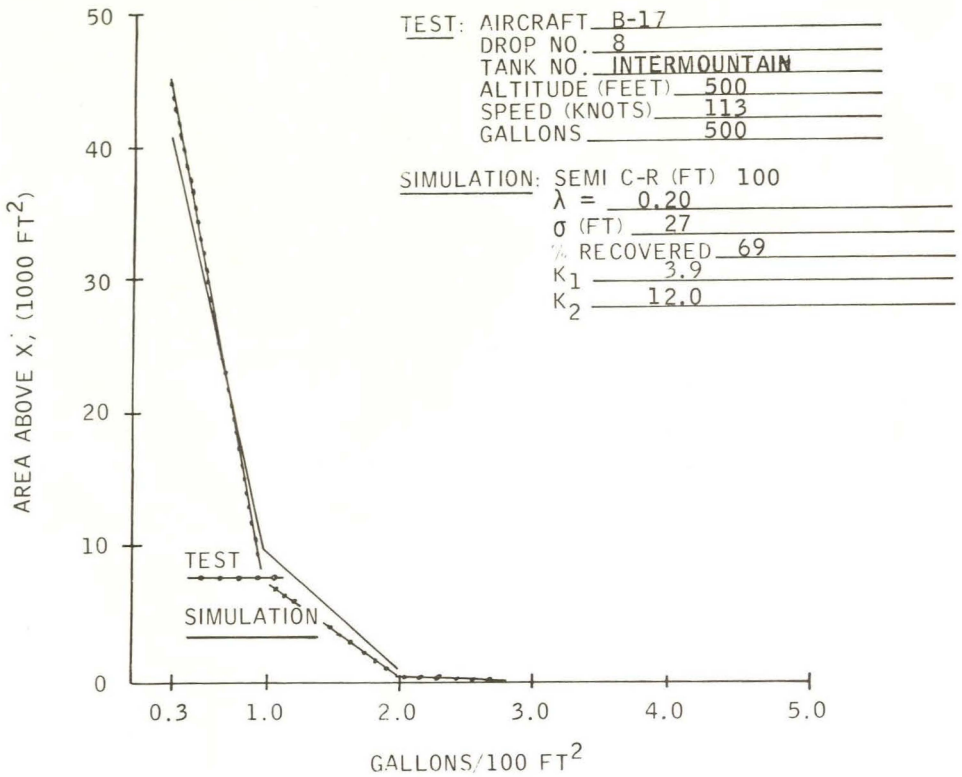

INTERVAL (GAL/100 FT^2)	GALLONS		AREA (FT^2)	
	TEST	SIMULATION	TEST	SIMULATION
0 - 0.2	61.4	50.4	73128	72000
0.3 - 1.0	174.0	146.0	36226	29700
1.1 - 2.0	99.1	135.6	7313	9000
2.1 - 3.0	14.2	18.8	674	900
TOTAL	349.0	350.8	117342	111600

	TEST DATA	SIMULATION DATA
AVERAGE (1)	0.85	1.0
AVERAGE (2)		0.2

Figure 70. Comparison of Test and Simulation Data - Intermountain B-17 Drop at 500 Feet

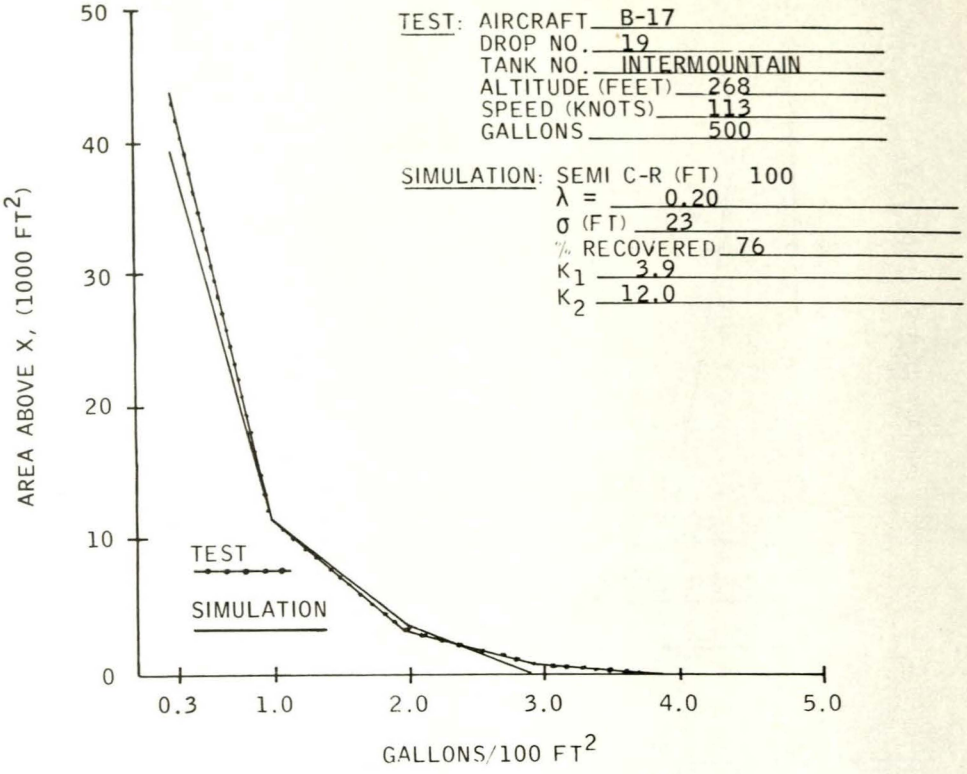

INTERVAL (GAL/100 FT^2)	GALLONS		AREA (FT^2)	
	TEST	SIMULATION	TEST	SIMULATION
0 - 0.2	33.0	49.5	37,913	59,400
0.3 - 1.0	148.6	127.6	31,163	27,000
1.1 - 2.0	124.3	119.0	8,663	8,100
2.1 - 3.0	60.9	85.8	2,588	3,600
3.1 - 4.0	15.4		450	
TOTAL	382.0	318.9	80,777	98,100

	TEST DATA	SIMULATION DATA
AVERAGE (1)	1.3	1.2
AVERAGE (2)		0.4

Figure 71. Comparison of Test and Simulation Data – Intermountain B-17 Drop at 268 Feet

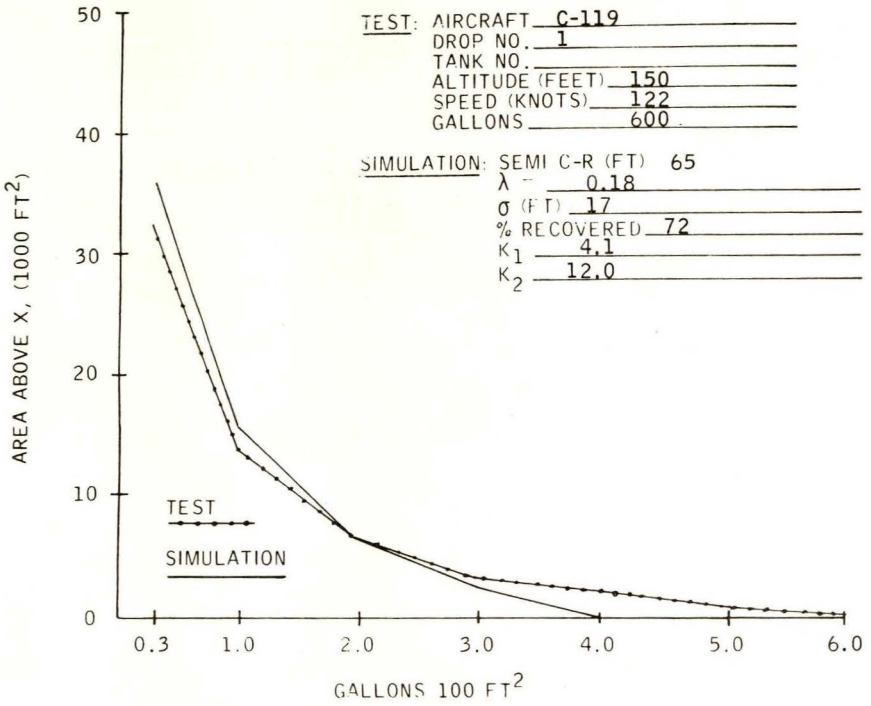

INTERVAL (GAL/100 FT^2)	GALLONS		AREA (FT^2)	
	TEST	SIMULATION	TEST	SIMULATION
0 - 0.2	28.0	31.2	31,838	42,300
0.3 - 1.0	77.0	93.3	18,000	20,700
1.1 - 2.0	101.0	122.8	7,313	8,100
2.1 - 3.0	72.0	90.6	3,038	3,600
3.1 - 4.0	36.0	98.5	1,126	2,700
4.1 - 5.0	50.0		1,125	
5.1 - 6.0	72.0		1,125	
TOTAL	436.0	436.3	65,566	77,400

	TEST DATA	SIMULATION DATA
AVERAGE (1)	2.6	1.9
AVERAGE (2)		0.6

Figure 72. Comparison of Test and Simulation Data - Aero Union C-119 Drop at 150 Feet

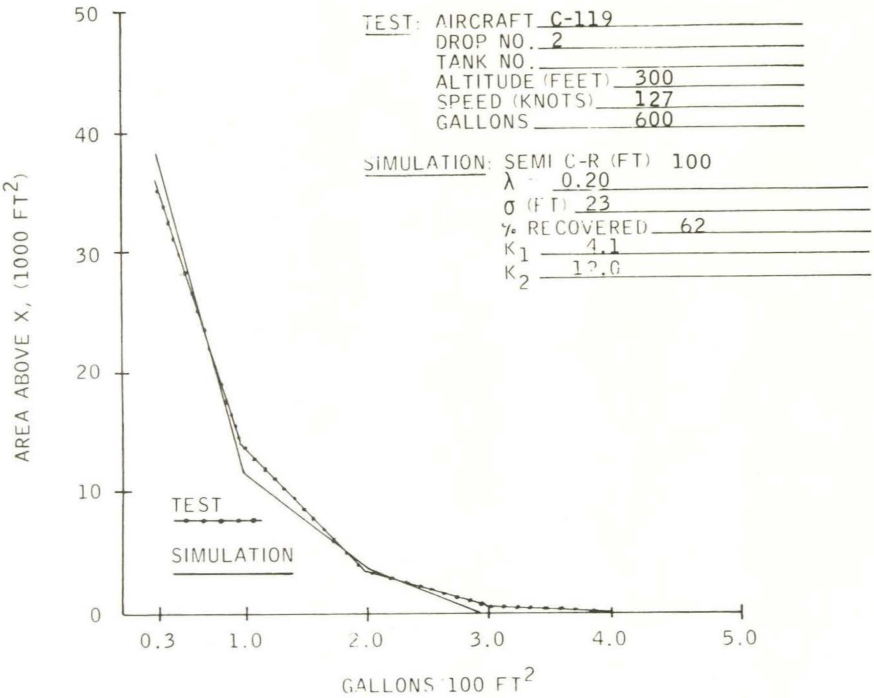

INTERVAL (GAL/100 FT^2)	GALLONS		AREA (FT^2)	
	TEST	SIMULATION	TEST	SIMULATION
0 - 0.2	37.0	55.8	41625	68400
0.3 - 1.0	114.0	127.3	21938	26100
1.1 - 2.0	138.0	114.2	10013	8100
2.1 - 3.0	59.0	81.5	2588	3600
3.1 - 4.0	18.0		563	
4.1 - 5.0	10.0		225	
TOTAL	376.0	378.9	76952	106200

	TEST DATA	SIMULATION DATA
AVERAGE (1)	1.4	1.2
AVERAGE (2)		0.4

Figure 73. Comparison of Test and Simulation Data – Aero Union Drop at 300 Feet

Table 5. Comparison of PB4Y2 Simulation with Test Results

Test Conditions		Simulation	1	2	3	4	5
Aircraft	PB4Y2	Semi-Crossrange (ft)	100	65	40	35	35
Drop Number	4	λ	0.20	0.20	0.20	0.20	0.15
Altitude (feet)	300	σ (ft)	23	20	15	10	10
Speed (knots)	149	Percent Recovered	75.2	75.2	75.2	75.2	75.2
Gallons	300	K_1	4.0	4.0	4.0	4.0	4.0
		K_2	12.0	12.0	12.0	12.0	12.0

Comparison of Results

Interval (gal/100 ft^2)	Gallons, Test	Gallons, Simulation 1	2	3	4	5
0 - 0.2	57.3	69.1	59.8	33.1	21.2	19.1
0.3 - 1.0	73.0	157.5	166.6	156.1	106.9	88.9
1.1 - 2.0	60.1			37.5	99.1	118.6
2.1 - 3.0	35.3					
Total	226.0	226.6	226.6	226.6	227.2	226.6

Interval (gal/100 ft^2)	Area (ft^2) Test	Area (ft^2), Simulation 1	2	3	4	5
0 - 0.2						
0.3 - 1.0	76387	138600	114300	88200	42300	44100
1.1 - 2.0	14513	37800	35100	32400	25200	23400
2.1 - 3.0	4613			3600	8100	9900
3.1 - 4.0	1575					
Total	97088	176400	149400	124200	75600	77400

	Test Data	Sim 1	Sim 2	Sim 3	Sim 4	Sim 5
Average (1)	1.0	0.4	0.5	0.7	0.9	1.0
Average (2)	N.A.	0.1	0.2	0.1	0.3	0.3

TEST:		SIMULATION 1	SIMULATION 2
AIRCRAFT	B-17	SEMI-CR (FT)	65	30
DROP NO.	5	λ =		0.2
TANK NO.	AERO UNION TRAIL	σ (FT)	16	8
ALTITUDE (FEET)	150			
SPEED (KNOTS)	122	% RECOVERED	69	
GALLONS	1,000	K_1	3.9	
		K_2	12.0	

INTERVAL (GALLONS)	GALLONS			AREA (FT^2)		
	TEST	SIMULATION 1	SIMULATION 2	TEST	SIMULATION 1	SIMULATION 2
0 - 0.2	38.7	54.3	3.1	39,925	79,200	42,300
0.3 - 1.0	129.2	201.8	141.1	22,613	43,200	29,700
1.1 - 2.0	212.3	220.7	79.4	14,851	16,200	5,400
2.1 - 3.0	117.7	219.2	179.9	4,500	9,000	7,200
3.1 - 4.0	59.8		291.9	1,801		8,100
4.1 - 5.0	74.3			1,800		
5.1 - 6.0	67.9			1,126		
TOTAL	694.0	696.1	695.4	86,616	147,600	92,700

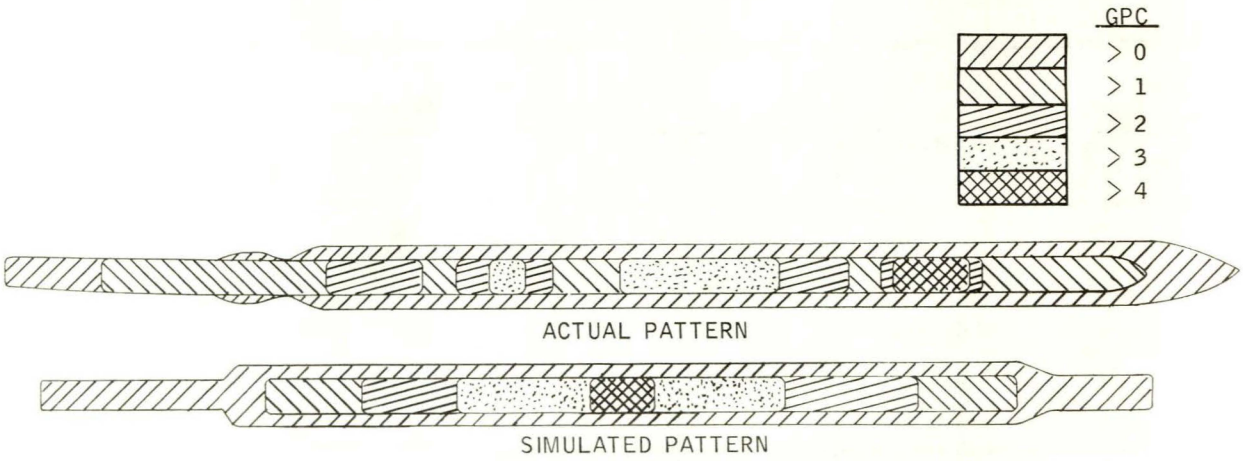

Figure 74. Comparison of Test and Simulation Data – Aero Union B-17 Trail Drop

Multiple-Tank Drop

One run was made to determine the general applicability of the single-tank simulation when applied to the multiple-tank condition. This run used a CL-215 drop of 1400 gallons. Although the data (Table 6) show a reasonable approximation, the variance is high. Figure 75 shows a three-dimensional representation of the actual pattern compared with that of a similar one-tank pattern. This suggests that multiple-tank drops are better simulated as the sum of two overlapping patterns than by the pattern generated from a functionally similar tank of larger size.

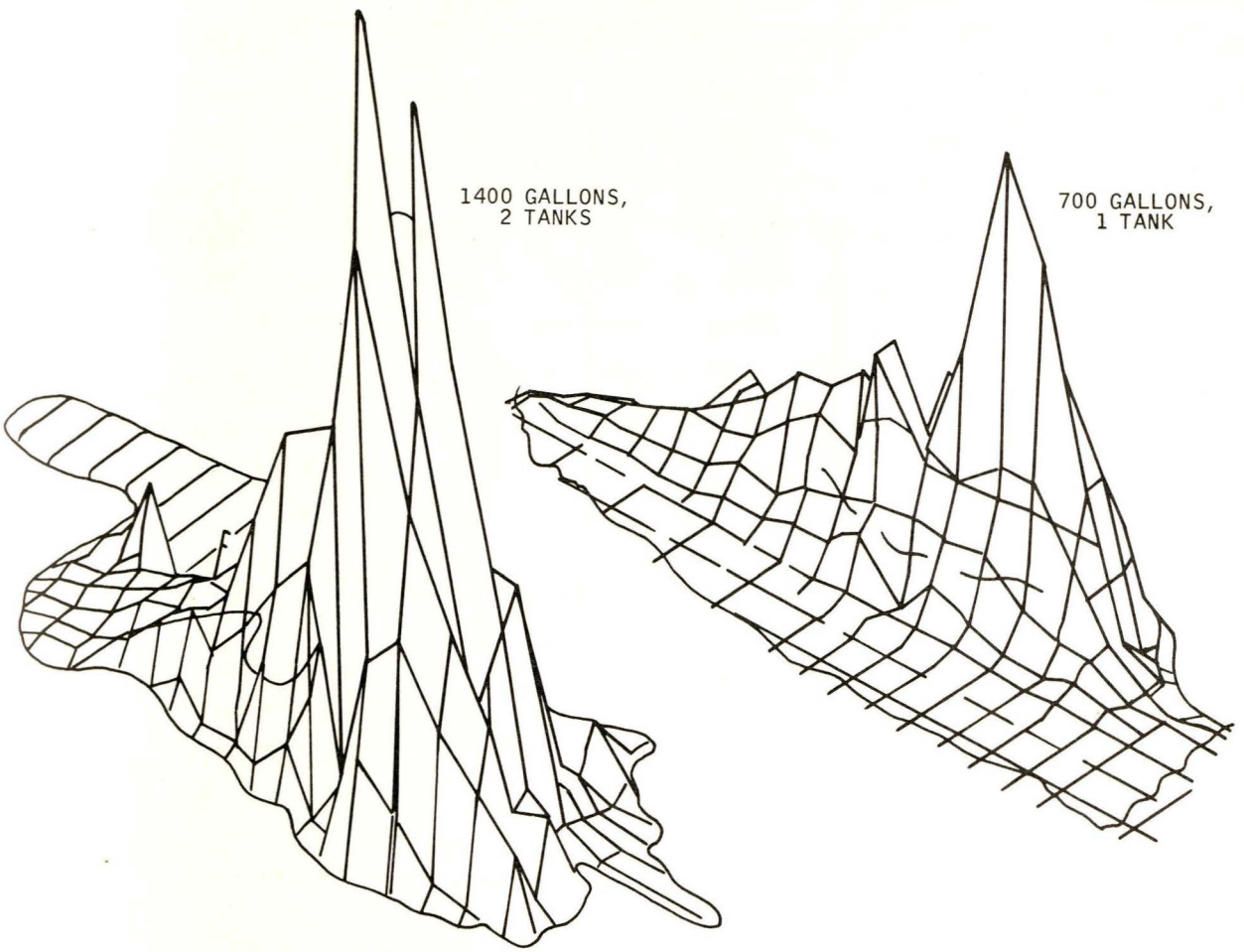

Figure 75. Three-Dimensional Patterns of One- and Two-Tank Drops

Table 6. Simulation Applied to Multiple-Tank Drop

Test Conditions		Simulation Conditions	
Aircraft	CL-215	Semi-Crossrange (feet)	105
Drop Number	21	λ	0.15
Altitude (feet)	296	σ (feet)	24
Speed (knots	92	Percent Recovered	91
Gallons	1400	K_1	3.97
		K_2	12.0

Comparison of Results

Interval (gal/100 ft^2)	Gallons		Area (ft^2)	
	Test	Simulation	Test	Simulation
0 - 0.2	34.1	2.5	41400	9900
0.3 - 1.0	113.3	168.7	21487	48600
1.1 - 2.0	221.9	134.4	1518	990
2.1 - 3.0	177.9	92.1	7087	3600
3.1 - 4.0	151.9	124.7	4275	3600
4.1 - 5.0	129.8	80.0	2925	1800
5.1 - 6.0	96.9	0.0	1800	0
6.1 - 7.0	50.0	111.3	788	1800
7.1 - 8.0	24.9	197.7	338	2700
8.1 - 9.0	38.6	78.2	450	900
9.1 - 10.	42.7	0.0	450	0
>10	179.1	285.4	1350	2700
Total	1260.9	1274.9	97537	85500

	Test Data	Simulation Data
Average (1)	4.5	5.6
Average (2)	1.2	1.5

Differenced Data (Test-Simulation)	Mean	-0.0395
	Variance	1.7770

V. TASK 3 - BOND NUMBER STUDIES

Task 3 considered the science of breakup physics as it applied to an explanation of retardant phenomena for the simulation effort and in its potential for refining drop-test data.

BACKGROUND

Work under the original High-Altitude Retardant Delivery program produced a better understanding of the complex hydrodynamic events that determine how a pattern develops. Essentially, the process is an acceleration-dominated phenomenon in which the most significant portions of the pattern result from unstable breakup of the liquid mass rather than classical stripping as previously suspected. This instability can be characterized through the use of a non-dimensional Bond Number relationship. This number is an inertial-forces-to-surface-tension ratio. This theory accounts for observed phenomenon, and, through its use, the time to instability can be predicted.

Although there is no directly quantitative relationship between the physical processes and the simulation, the qualitative influence provided through better understanding of the physical basis of breakup exerted a profound effect both on the model and the interpretation of simulation results. The purpose of this task was to develop continued resolution of breakup physics for the possible benefits of more detailed understanding.

SUMMARY

Film analyses of several tanker drops confirmed the ability to approximate the time of onset of Taylor Instabilities and the time of breakup through use

of Bond Number. This was particularly evident in the post-analysis of the CL-215 drop after the actual flow-rate information became available. Specifically, several anomalous conditions were corrected when the evacuation times from static tests were used. These analyses further suggest a three-phased process governing buildup to unstable breakup. First, the release phase during which fluid is added from the tank. It is followed by a period during which the liquid mass deforms. The deformation process is interrupted by the onset and subsequent amplification of the frontal instabilities. This explanation potentially accounts for the apparent reduction in pattern width resulting from higher aircraft velocities and lower (trail-like) flow-rates suggested by exercising the simulation model. Specifically, higher velocities and smaller instantaneous quantities (Q) tend to increase Bond Number, thus reducing the time to instability. Consequently, the width-generating deformation phase is terminated earlier, contributing to narrower patterns.

A second part of the task study evolved from the observation that actual pattern data contained a frequency component that was not directly accounted for in the flow-rate distribution. This frequency information is potentially related to the dominant modes of surface instability. To explore this possibility, a Fourier transform routine was added to the RETARD evaluation program. This is essentially a technique of extracting frequency data, identifying it, and interpreting the result. Although the effort did not achieve a point where definitive conclusions on the premise would result, its application is of sufficient benefit that some additional exploration of the technique might be warranted in further studies.

CONCLUSIONS

The Task 3 study results led to the following conclusions:

- The Bond Number as a characterization of the breakup mechanism appears valid in accounting for observed phenomenon. It further suggests that the ultimate computer simulation will relate the current values of σ and semi-crossrange to aircraft velocity and flow rate in a more precise fashion than those of the current empirical rules.

- The potential of the Fourier transform for deriving quantitative data on the dimensions of the instabilities from ground patterns cannot be confirmed at this stage of investigation. The technique however, as embodied in the Modified Retard Program, is useful in analyzing different data between similar patterns.

DISCUSSION

Bond Number Analysis of CL-215

Film studies of the CL-215 illustrated early onset of instabilities. It is characteristic that the break begins slightly after 2 seconds in the airstream. This approximate value has been identified with the release time out of the tank. Characteristic breakup times estimated from the Bond Number are 2.25 seconds for the 700-gallon release and 2.6 seconds for the 1400-gallon drop. This led to an estimate of the combined event in excess of 4 seconds, which was markedly different than the B-17 and PB-4Y2 experience.

Once the impulsive character of the CL-215 release was recognized, a review of the films was made. In examining the films on other PB4Y and

P2V drops, it became clear that a release over a long time period could not be represented by a single Bond Number. The instabilities start, and are followed by additional flow which modifies the instability pattern. The CL-215 impulsive discharge is an ideal release to characterize the Bond Number of the event. Calibration similar to that developed for the water drop can be made. Simpkins and Bales (Reference 5) showed that the onset of instabilities for the water drop was

$$t^* = \frac{65}{(B_o)^{1/4}}$$

where

$$t^* = \frac{\Sigma\, 1/2\, \mu}{r_o} \quad t$$

$$\Sigma\, 1/2 = \frac{P_g}{P_a}$$

P_g = density of air

P_a = density of liquid

μ = velocity of fluid mass

r_o = radius of undeformed fluid mass

B_o = Bond Number

To estimate the Bond Number, the Weber number is first estimated. The Weber number is the ratio of the aerodynamic stress to surface tension.

Once the Weber number is known, the Bond number is given by

$$B_o = 3/8\, C_D\, W_\Sigma$$

where C_D is the drag coefficient, and W_Σ is the Weber number.

For the water drop, the drag is estimated to be 2. 5 to account for the loss due to peripheral stripping. The drag coefficient of a rigid sphere is known to be 1. 0 for the range of Reynolds numbers applicable. The combination of the drag coefficient and the proportionality constant might be incorrect for the large retardant mass.

The CL-215 does allow us to estimate this proportionality constant, assuming the validity of the drag coefficient to accommodate the mass loss and distortion. Two films were studied with this technique: Drop 17, 700 gallons at 311 feet, and Drop 21, 1400 gallons at 296 feet.

Figures 76 and 77 are the tracing obtained from viewing the film sequences of drops 17 and 21. Figure 76 is the complete tracing every six frames which corresponds to 0. 125-second increments. Figure 77 has been simplified to show the onset of instability, followed by the breakup phase. The tank releas was completed in 0. 75 second.

When the delivery numbers are inserted into the formulas for breakup time and the proportionality constant is estimated, the following result is obtained:

K = 36. 2 for 700-gallon drop

K = 38. 9 for 1400-gallon drop

and the average is 37. 6.

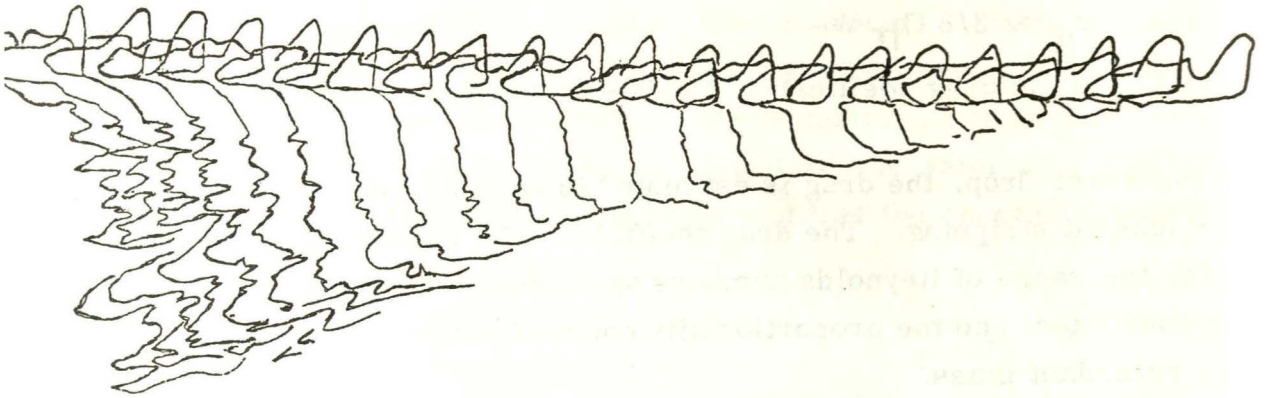

Figure 76. Film Tracing of 1400-Gallon Drop

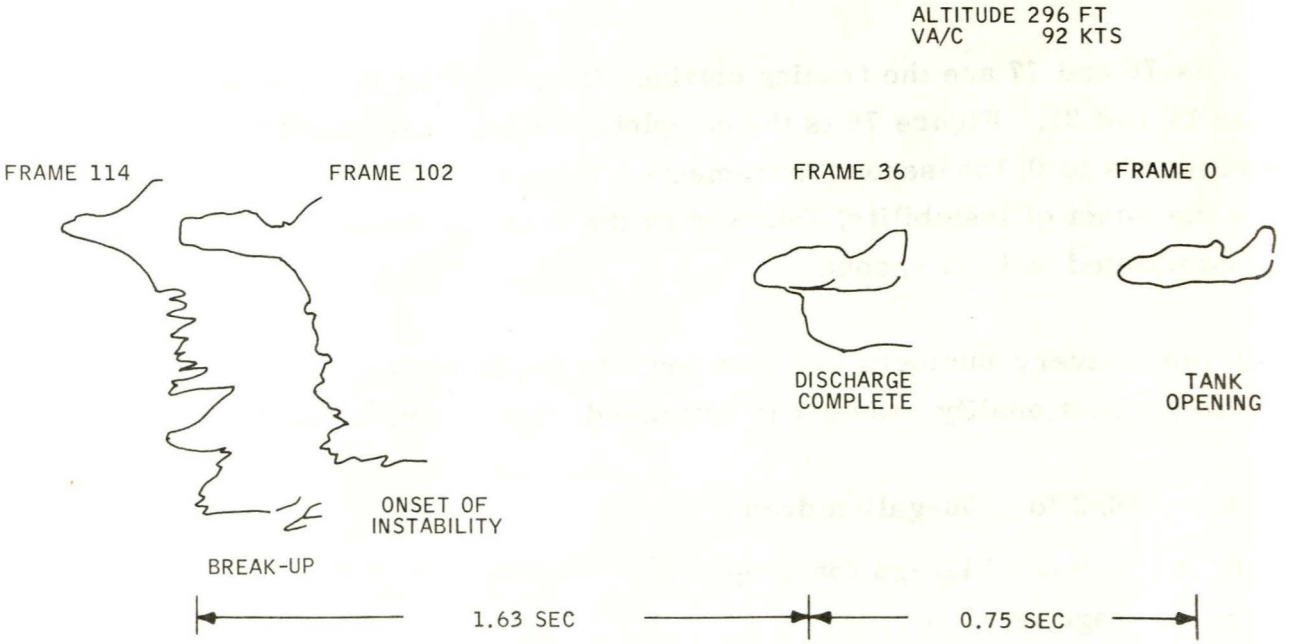

Figure 77. Frame Detail of Film Tracing

Fourier Analysis

Initial attempts at the simulation of true area patterns showed the computer's inability to generate smooth curves (marginal) to duplicate the peak and valley contours of the actual pattern. The averaging process for eliminating high peaks did not preserve the Weibul distribution characteristics that had been found to directly represent patterns. (Part of this problem apparent in the CL-215 effort was reduced when actual flow rate data became available.)

In exploring this apparent difficulty, a new hypothesis was introduced that depends on understanding the breakup phenomena. The convolution of the volume flow rate into the marginal distribution accounts for the basic (average) performance of the pattern. The frontal instabilities causing breakup result in a frequency-related phenomena that modulates the flow-rate-determined values. The analog may be characterized by an alternating electrical signal with a carrier wave (flow rate) and a signal (frequency component) superimposed. If the analogy holds, the recovered pattern would contain frequency and possibly amplitude information on the zonal harmonics associated with breakup. The analytic methods for handling this kind of information are found in Fourier Analysis and the particular concept of the Fourier Transform.

In principle, this approach asserts, that a complex signal can be approximated as the sum of a series of sine waves with clearly defined phase and amplitude characteristics.

If this signal is amplified and attenuated, the series will be modified, retaining its relative coherence. If two series arrive from different processing of the same signal, they can be related by a transform function, H, so $S_1 = (H) S_2$; and this condition is theoretically reversible.

Consider this relationship in terms of the retardant drop condition:

- A flow-rate distribution is convoluted through the computer program to a marginal distribution. Both distributions can be described by a Fourier Series, and, in theory, a transform function could be written that would relate the two distributions.

- The actual pattern distribution differs from the transformed flow-rate distribution becuase of (1) a frequency component imposed by the breakup phenomena which is assumed to be functional rather than random and (2) noise.

- The difference data between the flow-rate-determined marginal and the actual marginal can be described by a new Fourier Series.

- If the new series is processed by the reverse of the transform convoluting the flow-rate to the marginal, a transformed series describing the frontal instabilities might be derived.

- The results of such findings potentially could be related to perturbation analysis or normal modes analysis of the instability functions.

- In addition, the concept offers the possiblity of yielding a reversible formula for the simulation study. Given the desired marginal, calculate the flow rate distribution. This can only be done by iteration on the current computer program.

The test of the Fourier methods usefulness is to apply them to the range and crossrange marginal distributions to see if these techniques add any new insight into the pattern analysis or the breakup process. These one-dimensional curves in range and crossrange, can be analyzed with existing programs

based on the difference array in the RETARD program. The output of such an analysis will be the sinusoidal variation of the difference marginal distributions. A finite series of harmonic functions will represent the residual data, i. e., the RMS amplitude and phase of sinusoids and their harmonics.

Fourier Methods

The Fourier integral can be used to represent an arbitrary function f (t) valid for every t:

$$f(t) = \frac{1}{2\pi} \int_{-\infty}^{\infty} F(\omega)\, e^{i\omega t}\, dt.$$

The quantity $F(\omega)$ given by

$$F(\omega) = \int_{-\infty}^{\infty} f(t)\, e^{-i\omega t}\, dt$$ is known as the Fourier integral or the Fourier transform of f (t). The function $F(\omega)$ is complex.

$$F(\omega) = R(\omega) + iX(\omega) = A(\omega)\, e^{iQ(\omega)}$$

where

$A(\omega)$ is the Fourier spectrum of f (t)

$A^2(\omega)$ is its energy spectrum

$Q(\omega)$ is its phase angle (Ref. 6)

To compute the Fourier representation of a finite set of data points, the favored computational tool is the Fast Fourier Transform (FFT). (Ref. 7). FFT is a highly efficient method of calculating Discrete Fourier Transform of a time series. For retardant, this is not a time series; rather it is a spatial variable.

The Honeywell program to analyze time-series data developed in the vibration laboratory has been modified to apply the retardant patterns (Figure 78). The input signal is normally a time record, and, in the pattern analysis, this input is the difference between the summed cup data across a row and the corresponding MacPherson simulation. TIMEF is a program to organize the time series into two separate series which are applied to the FFT program. FFT produces the real and imaginary components for pairs of data points.

The Discrete Fourier Transform is given by this representation of the data as real and imaginary components, aj + bj, j = 0, 1, - - - N/2. These data are the ingredients for the frequency representation of the time series magnitude

$$| F(n) | = 1/2 \sqrt{a_n^2 + b_n^2},$$

and the phase

$$\theta_n = \tan^{-1} \left(- \frac{b_n}{a_n} \right).$$

Each frequency component has an amplitude and a phase.

The output of FFT program is transformed into phase and magnitudes for the frequency domain. These data are further processed to produce the analogus electrical power spectrum of the data. It is at this point that some interpretation is required. In communication problems, this power spectrum represents the amount of power that the waveform contains at a given frequency. If a known frequency source is available to combine with the data record through a narrowband filter, the amount of power can be measured (Figure 79). A tape record is continuously compared with the signal through all of the frequency bands of interest.

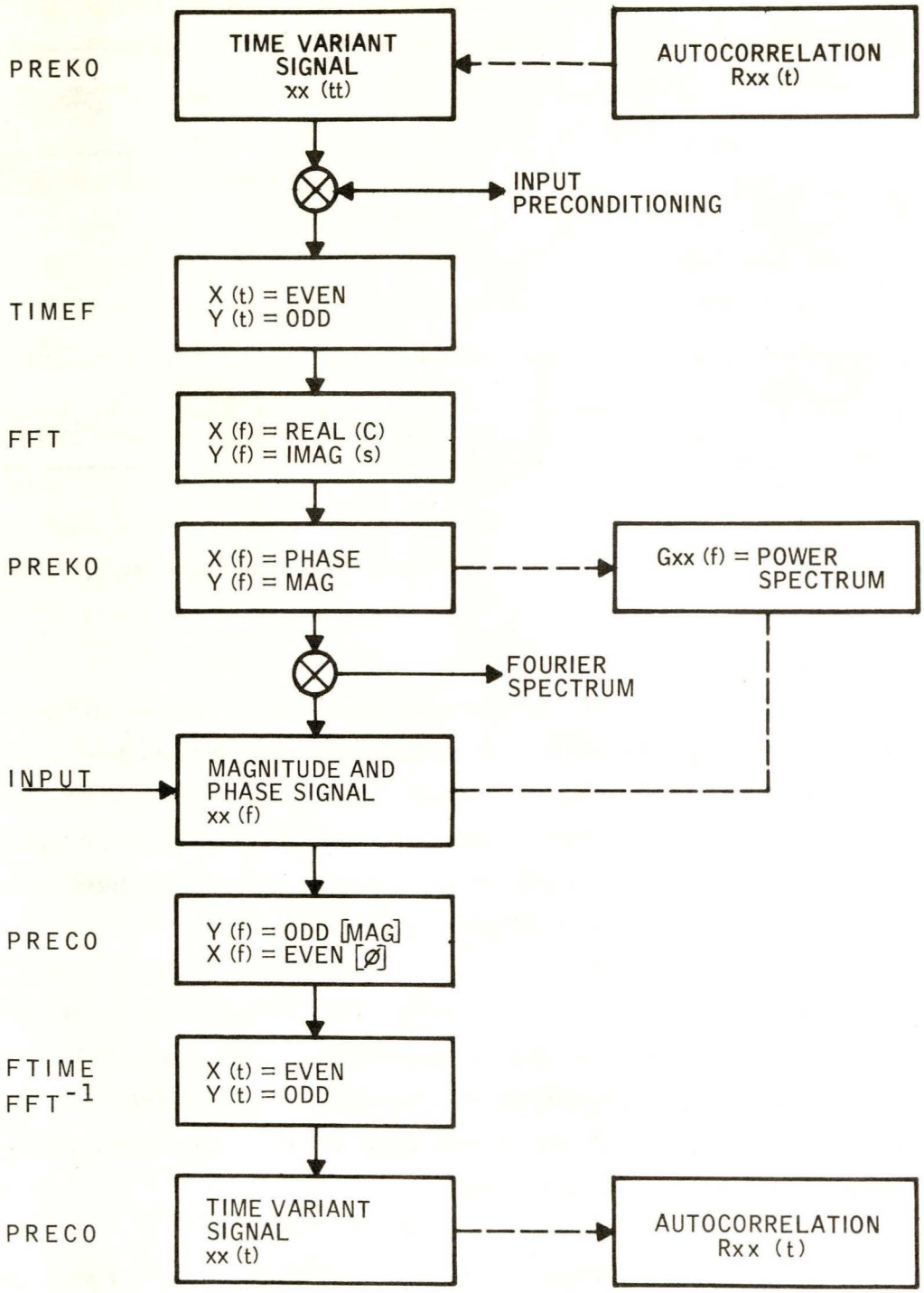

Figure 78. Time-Series Analysis Program

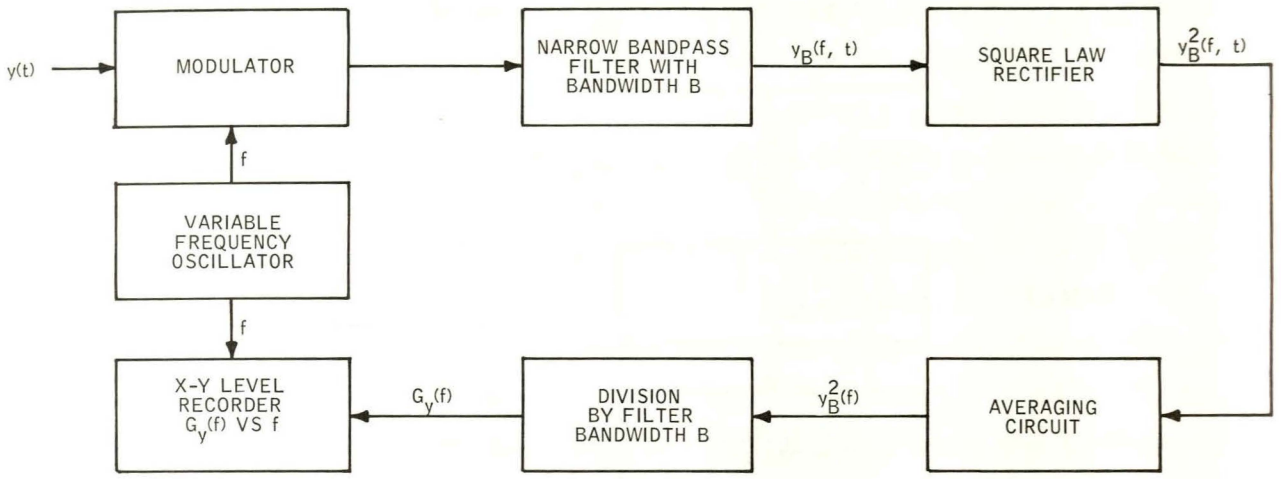

Figure 79. Single-Filter Type Power Spectral Density Analyzer

For retardant, the power spectrum corresponds to a sine wave whose frequency is determined by the distance of two consecutive cup stations--for the Honeywell program, this is 30 x 15 feet. Thus, the highest frequency that can be resolved is the record length in feet divided by N/2 -1. For example, a record of 32 range stations is 960 feet in length, and the highest frequency that can be resolved is a sine wave whose period is 64 feet.

The analogous interpretation to the communication problem exists with the retardant case. The power in the record can be determined for the highest frequency and the possible multiples. For the record of 960 feet, the lowest frequency is the fundamental which is a sine wave of a period equal to 960 feet. Thus, 15 harmonics can be measured.

The units of these (power density) data are (gal^2/ft^3) which is an unnatural set of units.

The positive square root will give the RMS amplitude of the appropriate sine wave. This amplitude represents the magnitude of that component of the record.

One feature of this analysis is that the inverse transform will produce the time or spatial variant signal. This has particular importance in the retardant case. If the Fourier representations of tanks could be characterized, the expected ground pattern with its expected variation could be reproduced by adding the Fourier inverse transform to the extended MacPherson simulation.

To explore this hypothesis the existing Honeywell program for harmonic analysis and difference data generated by the Modified RETARD program were utilized. Specifically, a simulated pattern is subtracted from a real pattern (Figure 80). This yields another pattern matrix representing the difference data. The results are shown in terms of the range marginal distribution (or two P2V and two DC6B drops) in Figures 81 through 84. A similar study on the CL-215 was conducted prior to the availability of measured flow data. As a result, the material was meaningful only in terms of exploring the technique. This factor was substantially responsible for our inability to carry the frequency analysis to a logical conclusion.

By use of the Fourier Analysis program, the power spectrum (the amount of difference) contained in each harmonic of the pattern length can be ascertained. This is shown on a relative scale for three P2V drops in Figure 85. It is difficulty to produce a proper power scale with the existing program, which is designed primarily for more conventional vibration analysis. Nonetheless, a relative scale is appropriate for the current state of analysis.

Analysis has shown that errors in the low harmonics (960-, 400-, 316-foot periods) are attributable to errors in the simulation, i. e., smooth-curve simulated marginal to best fit smooth-curve actual pattern. The remaining difference data would be expected to contain the breakup induced data transformed over altitude.

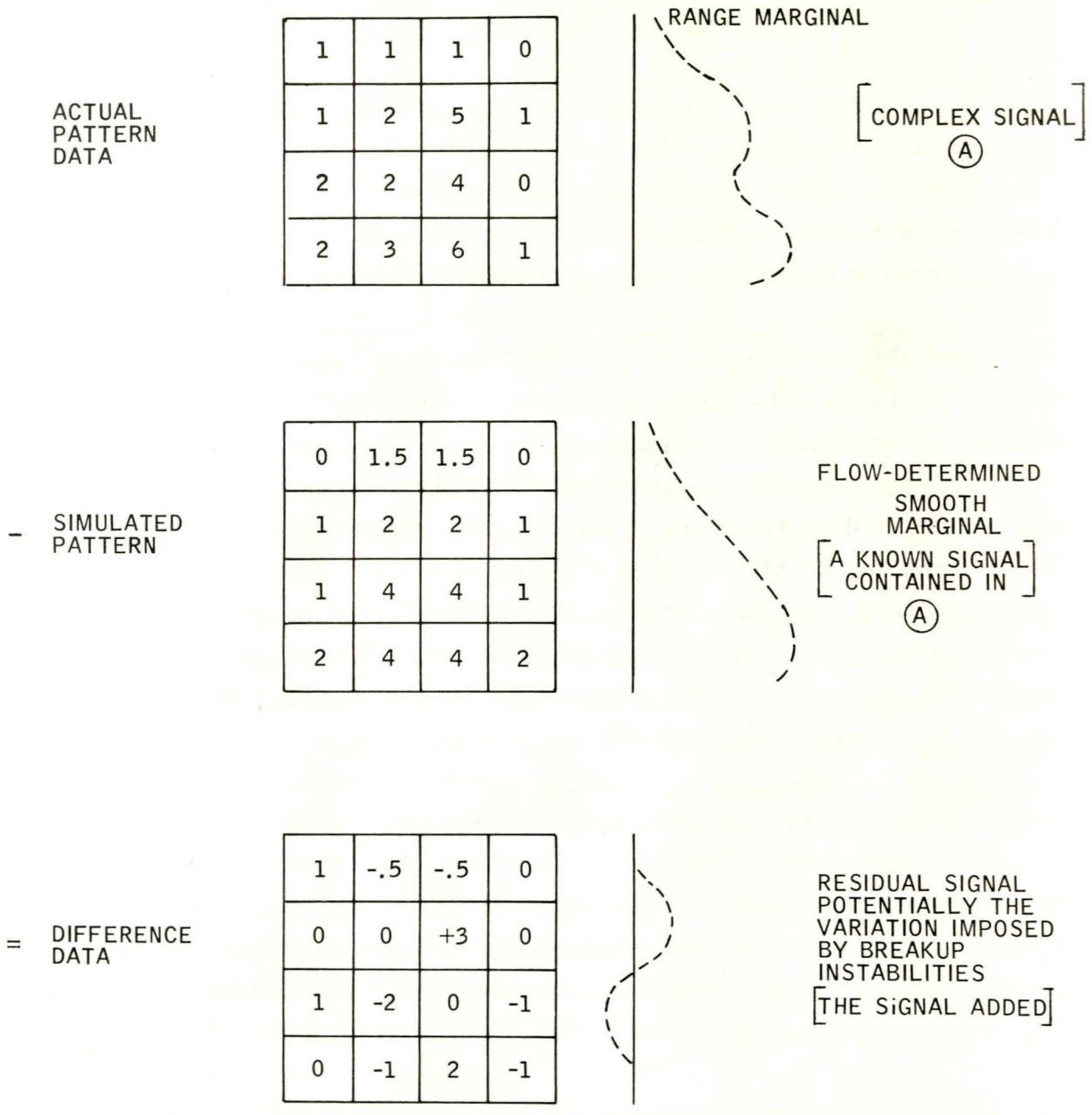

Figure 80. Simplified Example of the Hypothetical Interpretation of Pattern Frequency Data with Respect to Unstable Breakup

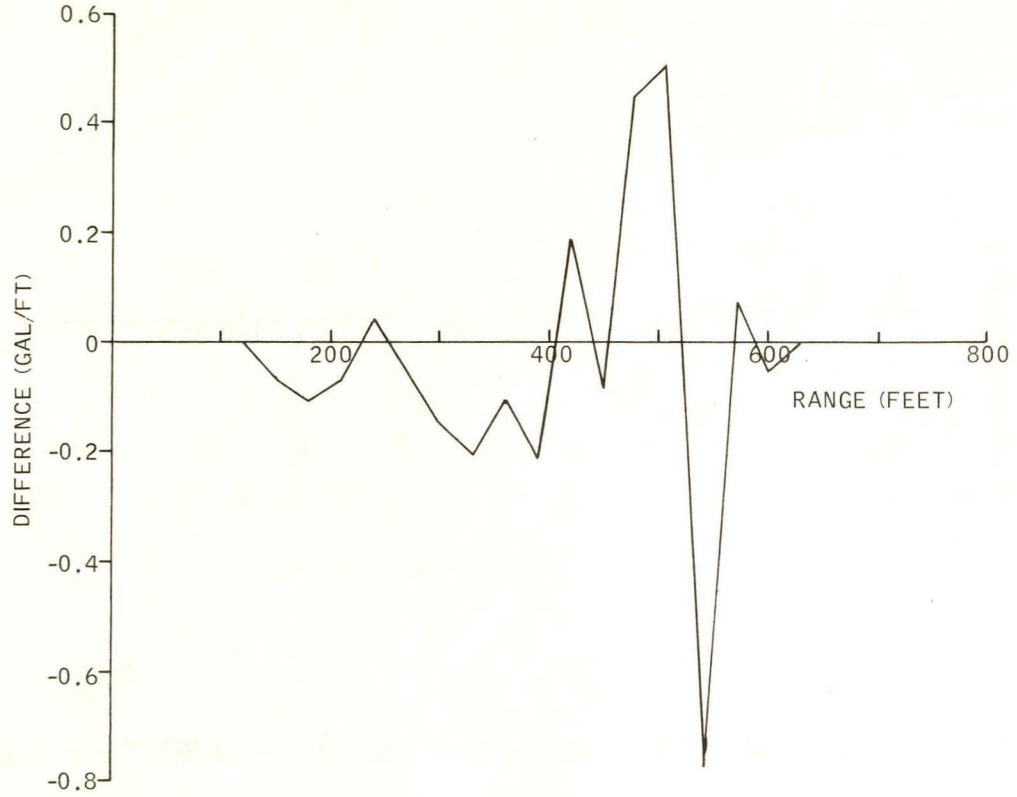

Figure 81. Marginal Difference Series (Range) – P2V Drop No. 2

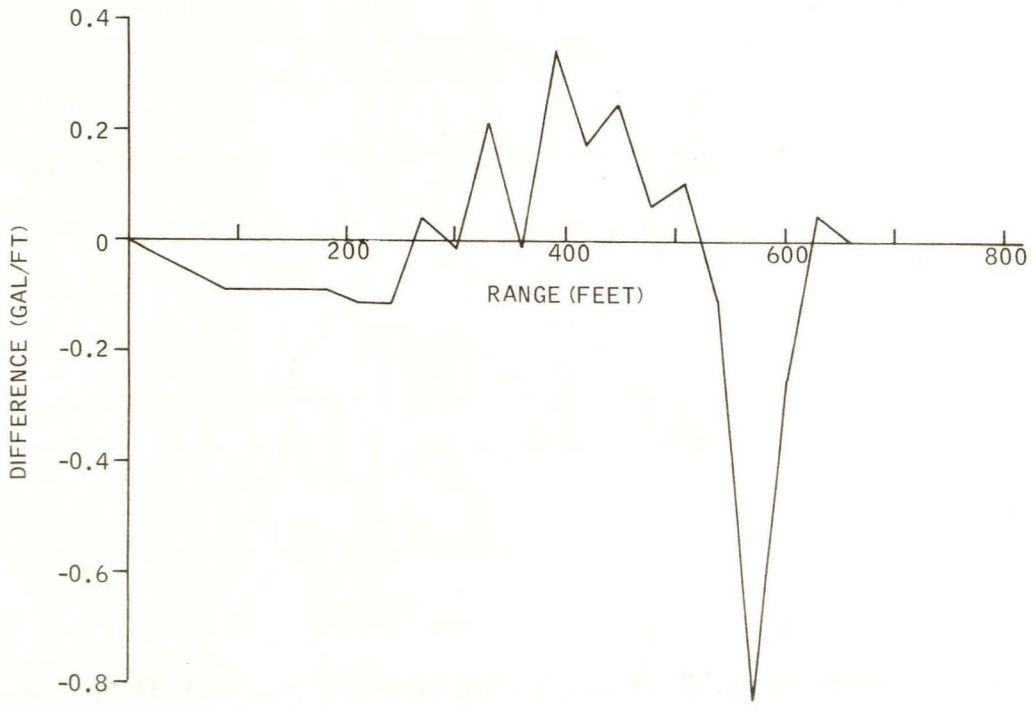

Figure 82. Marginal Difference Series (Range) – P2V Drop No. 6

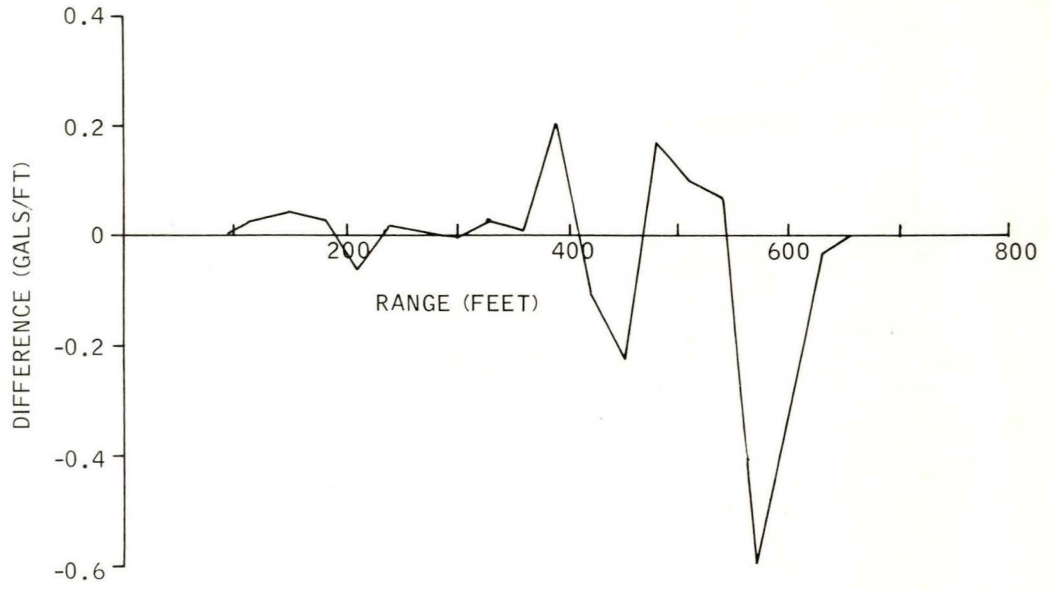

Figure 83. Marginal Difference Series (Range) - DC6B Drop No. 1

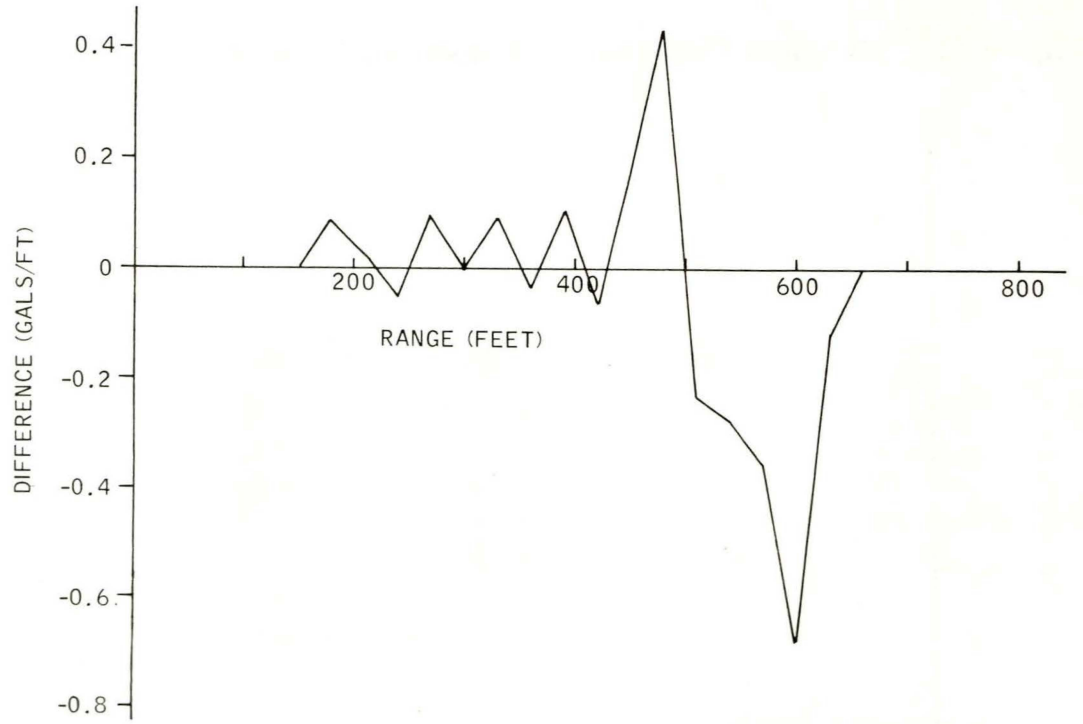

Figure 84. Marginal Difference Series (Range) - DC6B Drop No. 2

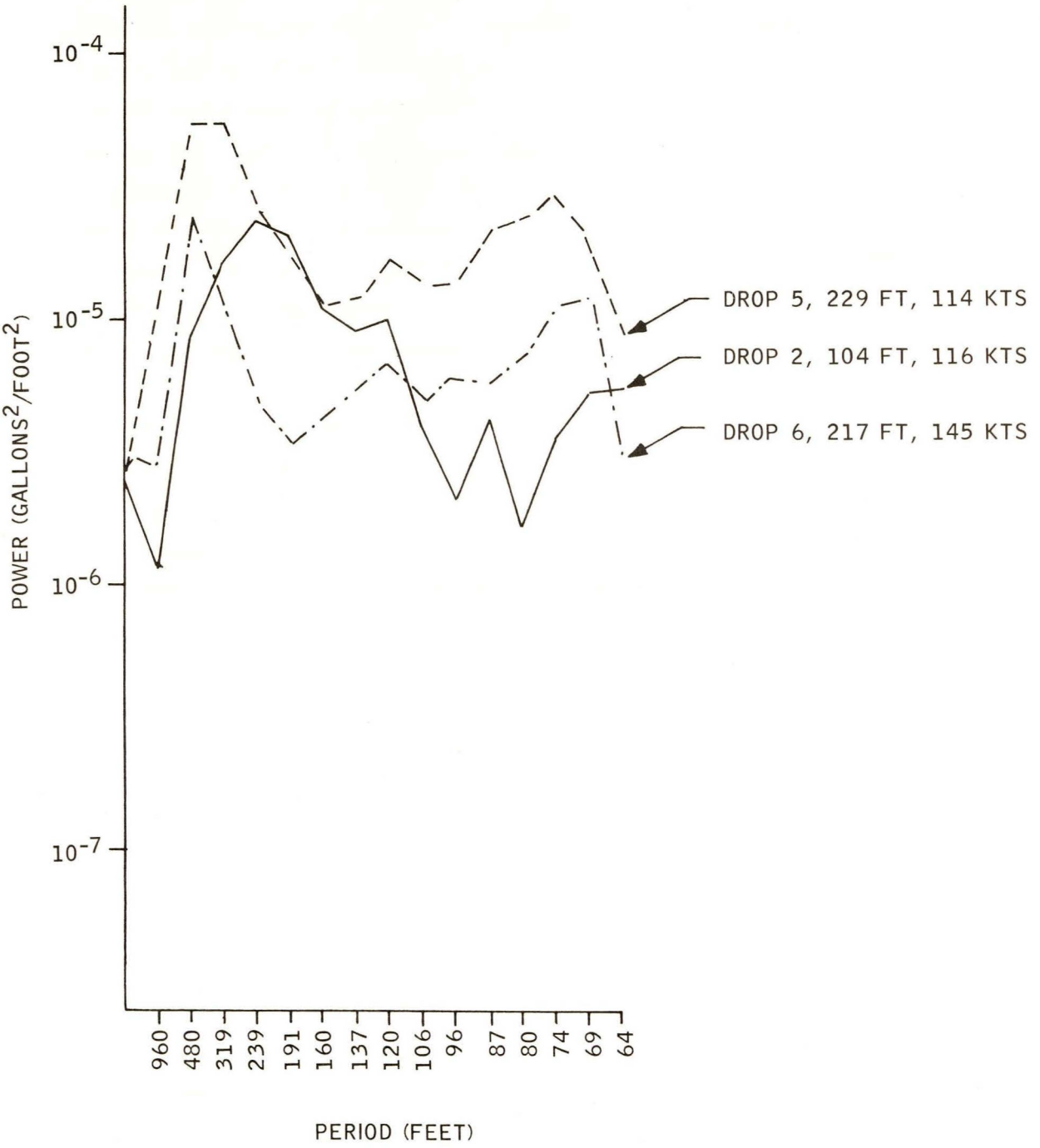

Figure 85. Power Spectrum for Three P2V Drops

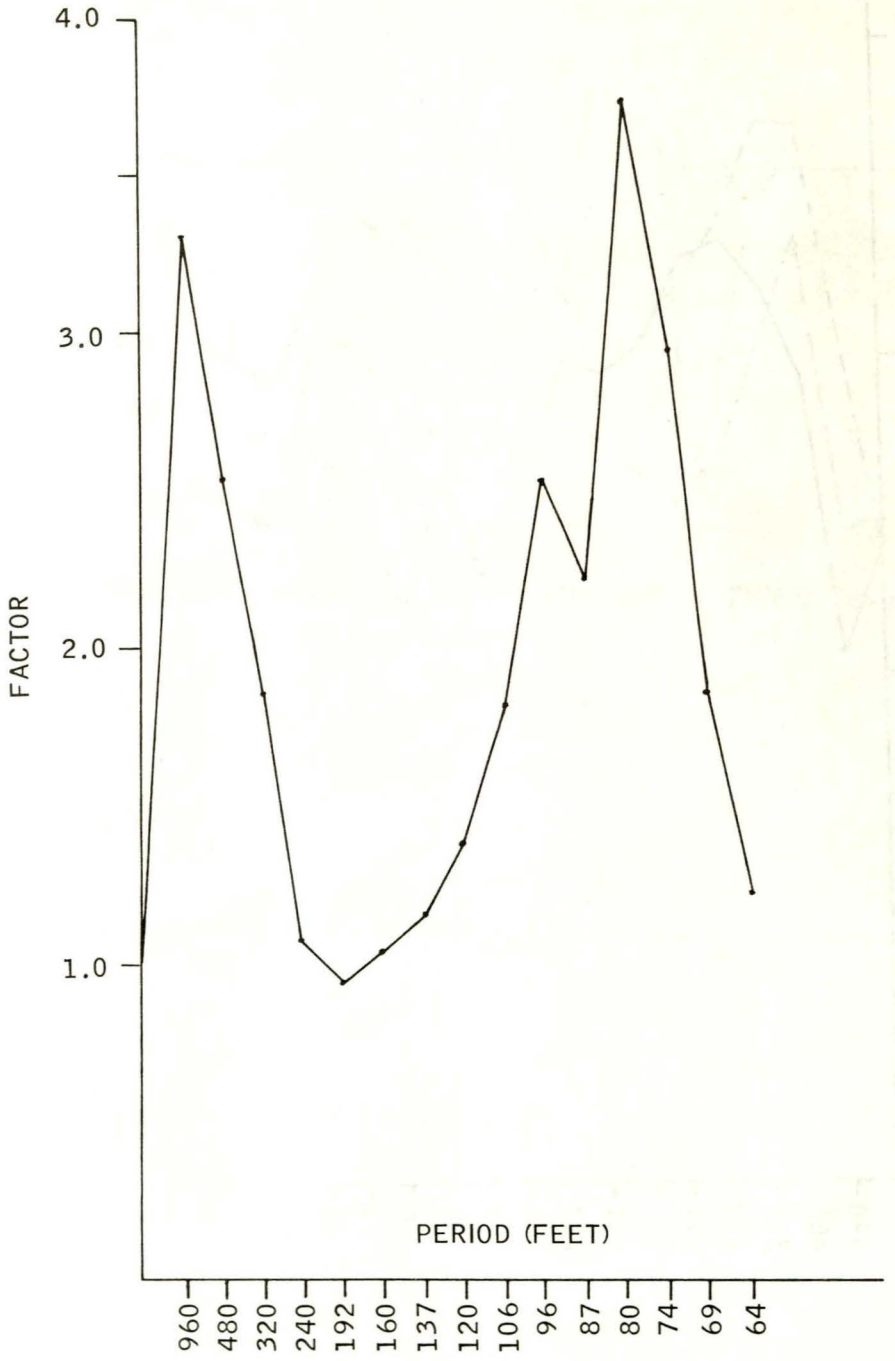

Figure 86. Power Spectrum Gain Factor Associated with 125-Foot Altitude Increase

Since only a qualitative assessment is possible at the state to which the analysis was carried, let us examine the power spectrum comparison as an indicator the technique's merit. The two drops at like altitudes (5 and 6) have similar spectral components despite a considerable difference in velocity. This supports the assumption that imposed frequency data was more coherent than random and, therefore, potentially recoverable. The difference in altitude is more pronounced (drop 2 to drop 5). Figure 86 plots the gain factor of the power spectrum associated with an increase in altitude of 125 feet. This would suggest a significant shift in the data toward higher frequencies, which might be indicative of incomplete breakup (low frequency) at the low altitude.

Although the Fourier Transform approach to inferring characteristics of the breakup physics cannot be conclusively demonstrated, it appears to offer some promise for inferring performance that might otherwise be beyond tractability on a first-principles basis. The technique of evaluating difference data, essentially without imposing normalizing restraints, does provide a useful tool for resolving subtle differences in pattern that might otherwise be ignored. The technique should be considered for further investigation as the need for more precise information on breakup phenomenon or more subtle refinements of the performance models is required.

APPENDIX A
MIX2 PROGRAM

This computer program incorporates the technique found in "An Improved Theoretical Model for the Ground Distribution of Water Released from a Fire-Bomber" by J. I. MacPherson, Aeronautical Report LR-488. A revised stripping equation was included. The general flow chart for the program is shown in Figure A-1.

The program uses equations based on aircraft speed, tank geometry, and the erosion process; and produces time histories and ground-range distributions for the liquid released from fire retardant tanker. A crossrange development based on a combination of a uniform and a normal distribution is included in the program. The result is a simulated retardant drop pattern. Figure A-2 provides references to the tank geometry input values.

Program input is listed in Table A-1; Table A-2 is a glossary; Table A-3 lists the arrays, and Table A-4 the program output.

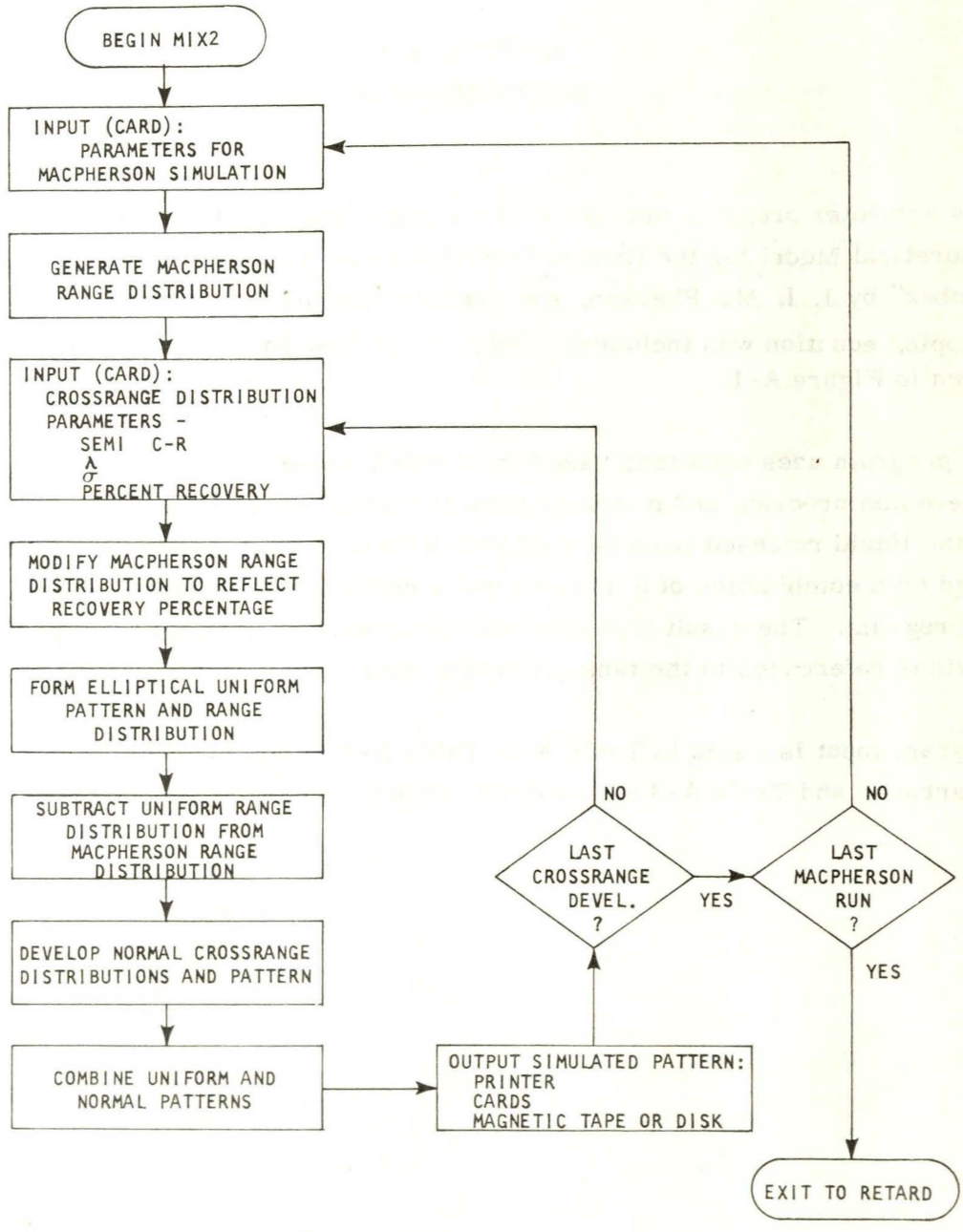

Figure A-1. MIX2 MacPherson Program with Pattern Simulation

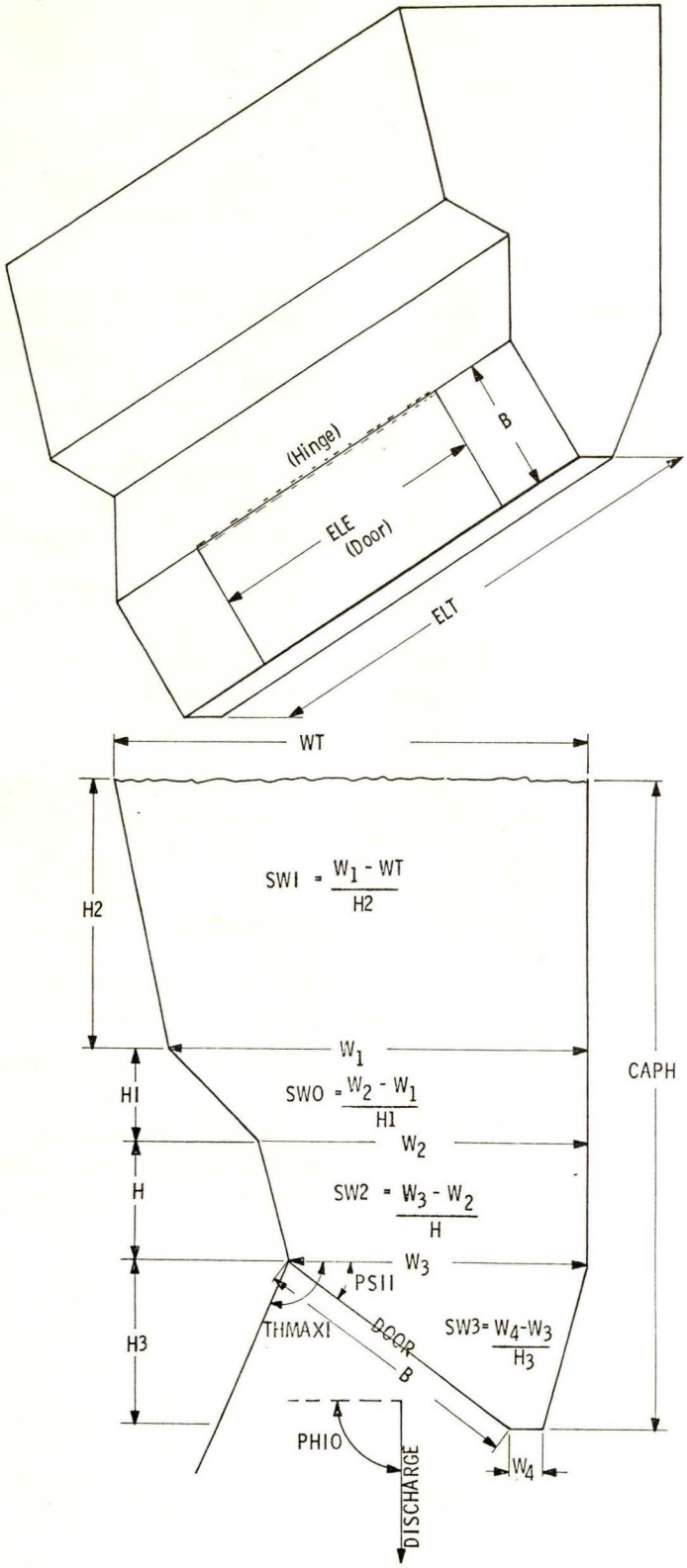

Figure A-2. Aircraft Tank Variables

Table A-1. MIX2 Program Input

Format: 8F10.5

Card	Fortran Symbol	Description	Units
1	AFLAG	AFLAG = 1., print ejection data = 0., do not print ejection data	-
	BFLAG	BFLAG = 1., print bulk increment data = 0., do not print print bulk increment data	-
	DFLAG	A print control - tells how many print lines to leave out.	-
	EFLAG	Reduced memory flag. EFLAG = 1. means reduced memory run. Use CM (central memory) = 120000 and Dimension DS (1, 1). EFLAG = 0. means regular memory requirement. Use CM = 3000000 and Dimension DS(60,1075)	-
	GFLAG	Flag for mixing uniform + normal CR distributions GFLAG = 0., no mixing, all output printed = 1., no mixing, suppress intermediate output = 2., mix uniform + normal dist.'s suppress intermediate output.	-
	HFLAG	Number of mix cases (cards #6) per MacPherson range distribution.	-
	ACFLAG	ACFLAG = 2., program uses CL-215 coding $\neq$ 2., program uses general tank coding	-

Table A-1. MIX2 Program Input (Continued)

Format: 8F10.5

Card	Fortran Symbol	Description	Units
2	ELT	Tank length	ft
	ELE	Door opening length	ft
	B	Door width	ft
	H	Vertical measurement between door hinge and tank discontinuity	ft
	Cap H	Initial head when tank is full	ft
	WT	Width of top of liquid when tank is full	ft
	ALF	Area reduction factor	–
	PHI0	Tank discharge angle measured from horizontal	degrees
3	SW1	Collective slope of tank sides, i.e.	–
	SW2	the increase in tank interior width	–
	SW3	per unit change in vertical dimension	–
	PSI	Angle of tank bottom with horizontal	degrees
	THEP	Door opening rate	rad/sec
	TR	Number of time intervals for bulk liquid breakdown	–
	THMAX	Maximum door angle from horizontal	degrees
	DELT	Integration time interval	sec
4	VAC	Aircraft speed	ft/sec
	RHO	Density of liquid	$Slugs/ft^3$
	K1	Erosion factor	–
	K2	Erosion factor	–
	PP	Pressure	lb/ft^2
	TX	Size of time interval for bulk breakdown	sec
	GAL	Total number of gallons in tank	gallons
	CFLAG	Number of compartments in the tank	–

Table A-1. MIX2 Program Input (Concluded)

Format: 8F10.5

Card	Fortran Symbol	Description	Units
5	SWO	Slope of first tank section } If required; otherwise	—
	HI	Height of first tank section } use zero.	ft
	TMAX	Door opening time if empirical data is used. For uniform rate use TMAX = 0.	sec
	COEF (1)	Coefficients for cubic equation fitted to empirical door opening data. $\Theta = f(t) = \bar{COEF}(1) * t^3 + \bar{COEF}(2) * t^2 + \bar{COEF}(3) * t + \bar{COEF}(4)$	
	COEF (2)		
	COEF (3)		
	COEF (4)		
6*	SEMX	Semi crossrange axis for the uniform distribution	ft
	LAMDA	Mixing parameter, the fraction of the recovered retardant in the uniform distribution	—
	SIGMA	Standard deviation of the normal crossrange distribution	ft
	PCTR	Percent of retardant recovered	%
		* This card is used only for runs where the crossrange distribution is to be developed. The number of these cards in the run is specified by HFLAG on the first input card.	

Table A-2. MIX2 Program Glossary

Fortran Symbol	Description	Input Units
ACFLAG	ACFLAG = 2., program uses CL215 coding $\neq$ 2., program uses general tank coding	—
AFLAG	1 = PRINT EJECTION DATA 0 = DO NOT PRINT	—
ALF	Area reduction factor	—
B	Door opening width	ft
BFLAG	1 = PRINT BULK INCREMENT DATA 0 = DO NOT PRINT	—
CAPH	Initial head of water in tank	ft
CFLAG	Number of compartments in the tank	—
DELT	Integration time interval	sec
DFLAG	A print control - tells how many print lines to leave out	—
DQD	Stripping rate	ft^3/sec
DT	Time interval for bulk analysis	sec
DTOR	Conversion factor-degrees to radians	—
EFLAG	Reduced memory flag EFLAG = 1. means reduced memory run Use CM(central memory) = 120000 and Dimension DS (1,1) EFLAG = 0. means regular memory requirement. Use CM = 300000 and Dimension DS (60,1075)	—
ELE	Length of tank opening	ft
ELT	Tank length	ft
G	Acceleration of gravity	ft/sec^2
GAL	Total number of gallons in tank	gal
GFLAG	Flag for mixing uniform + normal CR distributions GFLAG = 0., no mixing, all output printed = 1., no mixing, suppress intermediate output = 2., mix uniform + normal dist.'s, suppress intermediate output	—
H	Vertical height between opening and chine	ft

Table A-2. MIX2 Program Glossary (Continued)

Fortran Symbol	Description	Input Units
HFLAG	Number of mix cases (cards #6) per MacPherson range distribution	—
HI	Height of first tank section	ft
K1	Erosion factor	
K2	Erosion factor	
LAMDA	Mixing parameter, the fraction of the recovered retardant in the uniform distribution	—
PCTR	Percent of retardant recovered	%
PHI	Angle between bulk water velocity vector and horizontal	degrees
PHI0	Tank discharge angle measured from horizontal	degrees
PI	π	
PI2	$\pi / 2$	
PP	Pressure	lb/ft^2
PSI	Angle of tank bottom from horizontal	degrees
Q	Volume of liquid	cu. ft
Q DOT	Volume discharge rate from tank	ft^3/sec
RHO	Density of liquid	
RTOD	Conversion factor - radians to degrees	
SEMX	Semi crossrange axis for the uniform distribution	ft
SIGMA	Standard deviation of the normal crossrange distribution	ft
SWO	Slope of first tank section	—
SW1	Collective slope of tank sides, i. e.,	—
SW2	the increase in tank interior width	—
SW3	per unit change in vertical dimension	—
T	Time from door release	sec
THEP	Door opening rate	rad/sec
THETA	Door angle from horizontal	degrees

Table A-2. MIX2 Program Glossary (Concluded)

Fortran Symbol	Description	Input Units
THMAX	Maximum door angle from horizontal	degrees
TMAX	Door opening time if empirical data is used For uniform rate use TMAX = 0	sec
TR	Time interval for bulk liquid analysis	sec
V	Falling velocity of bulk liquid	ft/sec
VAC	Aircraft speed	knots
VE	Exit velocity from tank	ft/sec
VT	Vertical velocity of bulk liquid at Z_t	ft/sec
VZ	Velocity of top of water in tank	ft/sec
VZ1	Component of velocity of top of liquid due to discharge velocity	ft/sec
VZ2	Component of velocity of liquid due to area created by open door	ft/sec
WT	Width of top of liquid in tank when full	ft
WZ	Width of top of liquid in tank	ft
X	Distance measured along flight path from initial release	ft
Z	Depth of liquid in tank	ft
ZT	Vertical distance below tank exit plane	ft

Table A-3. MIX2 Program Arrays

TIM (300) Time by intervals of TX (sec)
VEX (300) Ejection velocity by intervals of TX (ft/sec)
QDOTX (300) $\dot{\bar{Q}}$ by intervals of TX (cu ft/sec)
Q $\bar{o}$ (2500) No. cu. ft of Retardant by time interval DT (cu ft)
QDOT $\bar{o}$ (2500) $\dot{\bar{Q}}$ per interval DT (cu ft/sec)
Z $\bar{o}$ (2580) Height of water (ft)
VE $\bar{o}$ (2500) Ejection velocity (ft/sec)
VZ $\bar{o}$ (2500) Velocity of top of water (ft/sec)
WZZ $\bar{o}$ (2500) Width of top of water at any Z (ft)
DS (60, 1075) Density - cell occupancy
DST (1075) Marginal distribution
DSS (200) Marginal distribution by 25 foot increments
$\bar{COEF}$ (4) + $\bar{COEF}$ (3) *t + $\bar{COEF}$ (4)

Table A-4. MIX2 Program Output

1. Initial Conditions	
2. Exit velocity data:	
a. Time after release of door	sec
b. Liquid depth	ft
c. Exit velocity	ft/sec
d. Velocity at top of liquid	ft/sec
e. Width at top of liquid	ft
f. Volume rate of flow	ft^3/sec
g. Cumulative volume	ft^3
h. Angle of door	degrees
3. Bulk by increments of .02 sec.	
a. Time after release	sec
b. Ejection velocity	ft/sec
c. Volume flow rate	ft^3/sec
d. Volume per increment	cu. ft
e. Cumulative volume	cu. ft
4. The marginal and cumulative distributions for each 25 foot increment in range. The remainder of the output is obtained only when simulating the cross-range distribution. This output is obtained for each crossrange development.	

Table A-4. MIX2 Program Output (Concluded)

5. The marginal range distributions for: a) MacPherson - The normal MacPherson simulation b) Mac(Adj) - The MacPherson simulation adjusted to reflect the recovery percentage c) Uniform - The portion in the uniform distribution d) Normal - The portion in the normal distribution e) Combined - The combined uniform and normal distributions. All of these distributions are in units of gallons.
6. The cumulative marginal range probability distributions for the same a, b, c, d, & e in 5 above.
7. The uniform portion of the pattern in B-Array format (cross range across the page and range down the page, cell size 15' by 30').
8. The normal portion of the pattern in B-Array format. 9. The combined uniform and normal distribution pattern in B-Array format. This item #9 output data is also written on magnetic tape file or disk file for input to the RETARD program.

APPENDIX B
MODIFIED RETARD PROGRAM

The Forest Service computer RETARD program was modified to run with test and/or simulated retardant pattern data. The program can compute various comparisons between test and simulated data. The MIX2 and RETARD programs are run sequentially so that the simulated pattern output from MIX2 (on magnetic tape or disk file) is input to RETARD (Figure B-1).

The program can be run basically in one of three modes:

- Test pattern data only. The test pattern data is read from cards (no magnetic tape option)
- Simulated pattern data only. This is output from MIX2
- Test pattern data and simulated pattern data in combination.

When simulated pattern data is used, a card number 2 must be prepared for each simulated pattern.

Figure B-2 shows an example data deck setup for a case where four simulated patterns are to be compared to one test pattern. The simulated pattern data is generated by MIX2 and stored sequentially on a temporary disk file. The simulated patterns are read from disk by RETARD at the places indicated on Figure B-2.

The modified program input format is described in Table B-1.

The output from RETARD for a program run such as shown in Figure B-2 is listed in Table B-2.

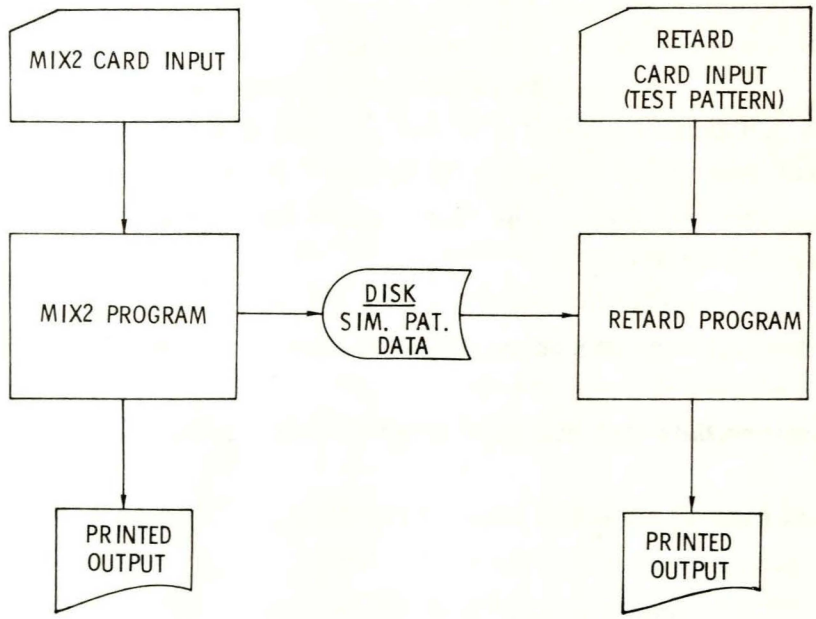

Figure B-1. MIX2 and RETARD Program Sequential Runs

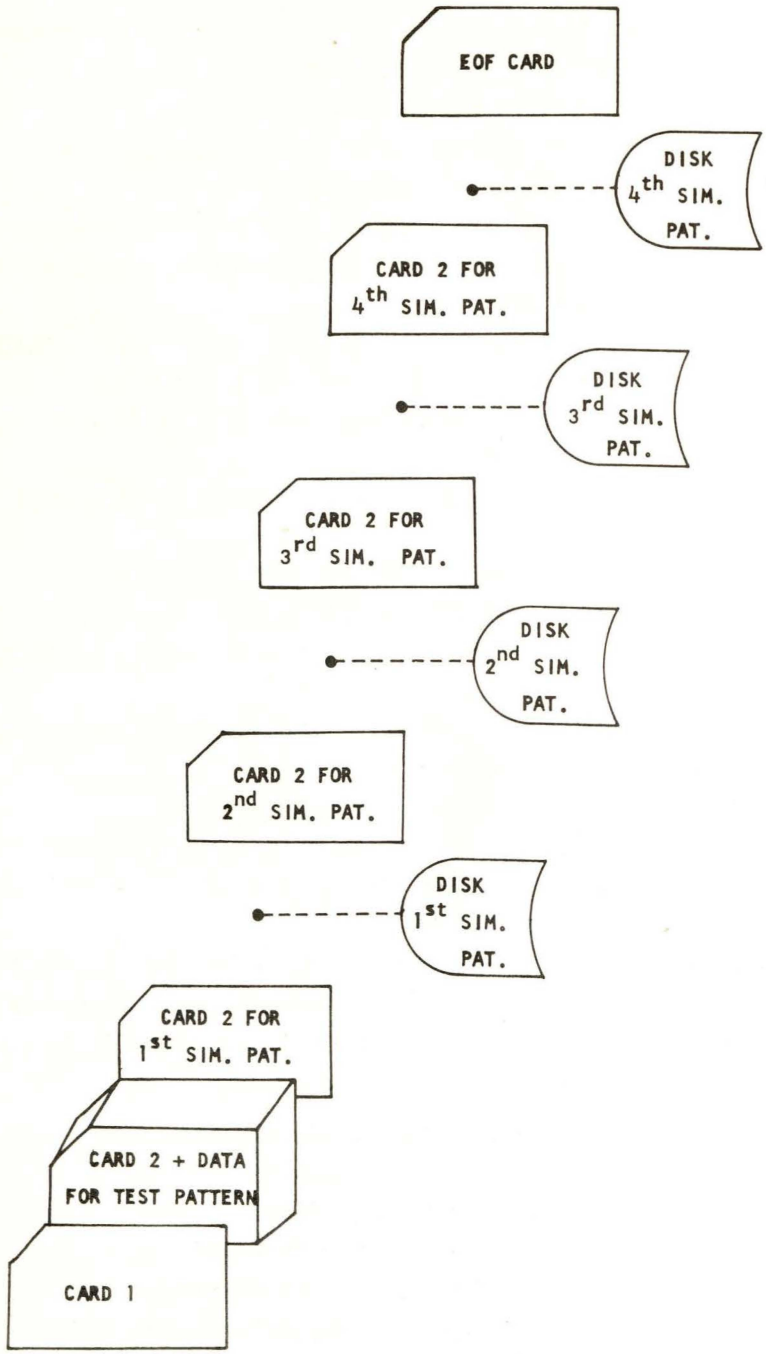

Figure B-2. RETARD Example Data Deck

Table B-1. Modified RETARD Program Input

```
CARD  1    : CONTAINS THIRTEEN FIELDS
  COL  1- 8  : 8-DIGIT ACCOUNT NUMBER
  COL  9-16  : PROGRAM NAME  *RETARD*          OPTIONAL
  COL 17-28  : PROJECT NAME  *FIRE MGMT.*
  COL 29     : 1 - IF NO CONVERSION OF DATA IS NEEDED
             : 2 - IF CONVERSION NEEDED
  COL 30     : NOT USED
  COL 31     : 0 OR BLANK IF NO HISTOGRAM CALCOMP PLOTS WANTED
               1 IF HISTOGRAM CALCOMP PLOTS ARE WANTED
  COL 32     : 1 - IF DISPERSION PATTERN IS TO BE PRINTED
             : 2 - IF NOT
  COL 33     : 1 - IF CONTOUR INTERVALS ARE TO BE CALCULATED
             : 2 - IF NOT
  COL 34     : 0 CR BLANK TO RUN WITH TEST PATTERN DATA
               1 IF SIMULATED PATTERN DATA IS USED THIS DATA COMES
                 FROM TAPE 2 IN BINARY FORMAT READ (2) (BBB(I,J),
                 I = 1, 28), J = 1, 56)
    THE FOLLOWING INPUT FLAG MAY BE USED TO DELETE CONDITIONAL CROSSRANGE
    PROBABILITY DISTRIBUTION PRINTING
  COL 35     : 0 CR BLANK TO PRINT DISTRIBUTIONS
               1 TO DELETE PRINTING OF THESE DISTRIBUTIONS
    THE FOLLOWING INPUT FLAGS WERE ADDED TO SELECT OPTIONS COMPARING
    TEST AND SIMULATED PATTERN DATA
  COL 36-37  : 0 OR BLANK - NORMAL RUN, EITHER TEST OR SIMULATED DATA
               GREATER THAN 0 - A COMPARISON RUN.  THE NUMBER PUNCHED IN
               36-37 (RIGHT JUSTIFIED) IS THE NUMBER OF SIMULATED PATTERNS
               COMPARED WITH ONE TEST PATTERN.

               THE ORDER OF THE DATA IS AS FOLLOWS - -
                   CARD 1
                   CARD 2 FOR TEST PATTERN
                   CARDS WITH TEST PATTERN DATA
                   CARD 2 FOR 1ST SIMULATED PATTERN
                   CARDS (OR MAG TAPE) WITH 1ST SIM. PATTERN
                   CARD 2 FOR 2ND SIMULATED PATTERN
                   CARDS (OR MAG TAPE) WITH 2ND SIM. PATTERN
                            ETC., REPEATING SIM. PATTERN DATA
```

Table B-1. Modified RETARD Program Input (Concluded)

```
   COL  38      : 0 CR BLANK TO READ SIM. PATTERN DATA FROM MAG TAPE
                  1 TO READ SIM. PATTERN DATA FROM CARDS
   COL  39      : 0 CR BLANK MEANS NO FOURIER ANALYSIS
                  1 MEANS DO FOURIER ANALYSIS
   COL  40-43   : NOT USED
   COL  44-45   : CONTAINS NUMBER OF END-OF-FILES ON MASTER TAPE
CARD 1 WILL BE USED ONCE EACH TIME THE PROGRAM IS USED.
CARD 2          : CONTAINS FIFTEEN FIELDS
   COL  1- 2    : 2-DIGIT NUMBER CORRESPONDING TO DROP NUMBER
   COL  3- 6    : 4-DIGIT NUMBER CORRESPONDING TO MONTH AND DAY
  *COL  7-22    : NAME OF RETARDANT USED
   COL 23-25    : DROP HEIGHT IN FEET (NEAREST FOOT)
   COL 26-28    : AIRCRAFT SPEED (NEAREST MPH)
   COL 29-31    : CROSSWIND VELOCITY (NEAREST FOOT)
   COL 32-35    : AIRCRAFT DIRECTION (NEAREST DEGREE)
   COL 36-39    : RETARDANT DENSITY (NEAREST 0.001)
   COL 40-43    : VISCOSITY (NEAREST WHOLE NUMBER)
   COL 44-46    : SALT CONTENT (NEAREST 0.1)
   COL 47-48    : TEMPERATURE (NEAREST DEGREE)
   COL 49-50    : HUMIDITY (NEAREST DEGREE
   COL 51-53    : LID TARE WEIGHT (NEAREST 0.1 GM)
         +        CUP TARE WEIGHT (NEAREST 0.1 GM)
  *COL 54-57    : NUMBER OF GALLONS DROPPED
  *COL 58-60    : PSR, NO. OF SIGMAS, EXCESS OVER IS REMOVED FROM THE TEST
                  DATA ARRAY.  FOR FINAL COMPARISON
   *FOR SIMULATED PATTERNS ONLY THESE DATA ARE ENTERED
ALL NUMBERS MUST BE RIGHT JUSTIFIED WITHOUT DECIMAL POINTS
CARD  3-82      : CONTAINS RAW DATA FOR EACH DROP, TWENTY NUMBERS PER
                : CARD EACH TO THE NEAREST 0.1 GM RIGHT JUSTIFIED
   FIRST - A - ARRAY (CENTER)
               800 VALUES ON 40 CARDS
   SECOND  -   AA-AARAY (MIDDLE)
               600 VALUES ON 30 CARDS
   THIRD   -   AAA-ARRAY (OUTER)
               192 VALUES ON 10 CARDS
CARDS 2-82 WILL BE REPEATED FOR EACH DROP THAT IS RUN IN SUCCESSION.
A STANDARD EOF CARD AT THE END OF THE DATA WILL STOP THE PROGRAM.
```

Table B-2. Modified RETARD Program Output

A. Output For Test Pattern

1. Contour Intervals - Gallons/100 square feet
2. Contour Intervals - Square foot coverage
3. B-Array Dump of retardant pattern - gallons/100 square feet
4. Marginal Crossrange Distribution for 3
5. Marginal Range Distribution for 3
6. B-Array Dump of retardant pattern, only densities greater than 0.1 gallons/100 square feet
7. Marginal Crossrange distribution for 6
8. Marginal Range distribution for 6

B. Output For Simulated Pattern

1. Contour Intervals - Gallons/100 square feet
2. Contour Intervals - Square feet coverage
3. B-Array Dump of retardant pattern - Gallons/100 square feet
4. Marginal Crossrange distribution for 3
5. Marginal Range distribution for 3

C. Comparison of Test and Simulated Data

1. Mean of Range and Crossrange distributions for Test and Simulated Data
2. B-Array for Differenced Data (Test Data-Simulated Data)-gallons/100 square feet
3. Mean, variance, and standard deviation for differenced data array
4. Fourier Analysis for Range Marginal Distribution (optional)
5. Fourier Analysis for Crossrange Marginal Distribution (optional)

Parts B and C of the output are repeated for each simulated pattern that is compared to the test pattern.

There are other output options in addition to the output described in Table B-2. If running with test data alone, only Part A is obtained. When running with simulated data alone, only Part B is obtained. Additional printed output in the form of conditional crossrange distributions can also be obtained. There are options for obtaining plots on a Cal Comp plotter. The conditional crossrange and marginal range and crossrange distributions can be plotted this way. The control of these options is through the card 1 input.

APPENDIX C
PATSIM PROGRAM

PATSIM is a retardant ground pattern simulation program. The input and output were designed for ease of use. A small deck of input cards describe a particular aircraft tank and these cards need not be changed from run to run. The remaining variable input consists only of delivery speed and altitude. The output consists of graphic pattern representations, retardant contour quantities (gallons) and areas, and pattern length data. All output is on the printer.

The PATSIM input data consits of three types of data:

- Aircraft Tank Variables - Need to be set up only once for a given tank.
- Constants - This input is optional. Values are set in the program but can be changed by the input if necessary.
- Drop Delivery Variables - Aircraft speed and altitude.

All input variables and constants are stored in an A-array. The variable and constant names are equal to locations in this array. The array location numbers are used when preparing input.

The format on an input card is:

Col.	1-10	: 1st variable number	Col.	11-20	: 1st variable value
	21-30	: 2nd " "		31-40	: 2nd " "
	41-50	: 3rd " "		51-60	: 3rd " "
	61-70	: 4th " "		71-80	: 4th " "

All numbers are punched with decimal points.

From one to four variables or constants may be entered on one input card. A completely blank card signals the end of one set of data or run. The variables need not be entered in any particular numerical order.

Another type of input card is used for comments and begins with an asterisk(*) in column 1. Columns 2 through 80 of this card may be punched with alphanumeric information. This card is printed in the listing of input data given by the program. The comment cards may appear anywhere in the input deck. A typical use would be as a title for the aircraft tank variables.

A typical PATSIM input is shown in Figure C-1. A form that can be used for preparing and punching aircraft tank variables is shown in Figure C-2. An input listing is given in Table C-1, and tank variables are sketched in Figure C-

The output from the program is on the printer and consists of the following:

- The input data
- A detailed pattern printout
- Contour intervals - number of gallons and area in each interval
- Scaled pattern plot
- Pattern length data

	*	CL-215 RETARDANT DROP SIMULATION						
AIRCRAFT TANK VARIABLES	1.	2.	3.	5.25	3.	5.083	4.	2.58
	5.	.667	6.	5.516	7.	0.	8.	2.33
	9.	0.	10.	0.	11.	-2.47	12.	0.
	13.	22.07	14.	90.	15.	90.	16.	.841
	17.	700.	18.	1.	19.		20.	
	21.		22.		23.			
SPEED AND ALTITUDE	51.	107.	52.	300.				

Figure C-1. Example PATSIM Input

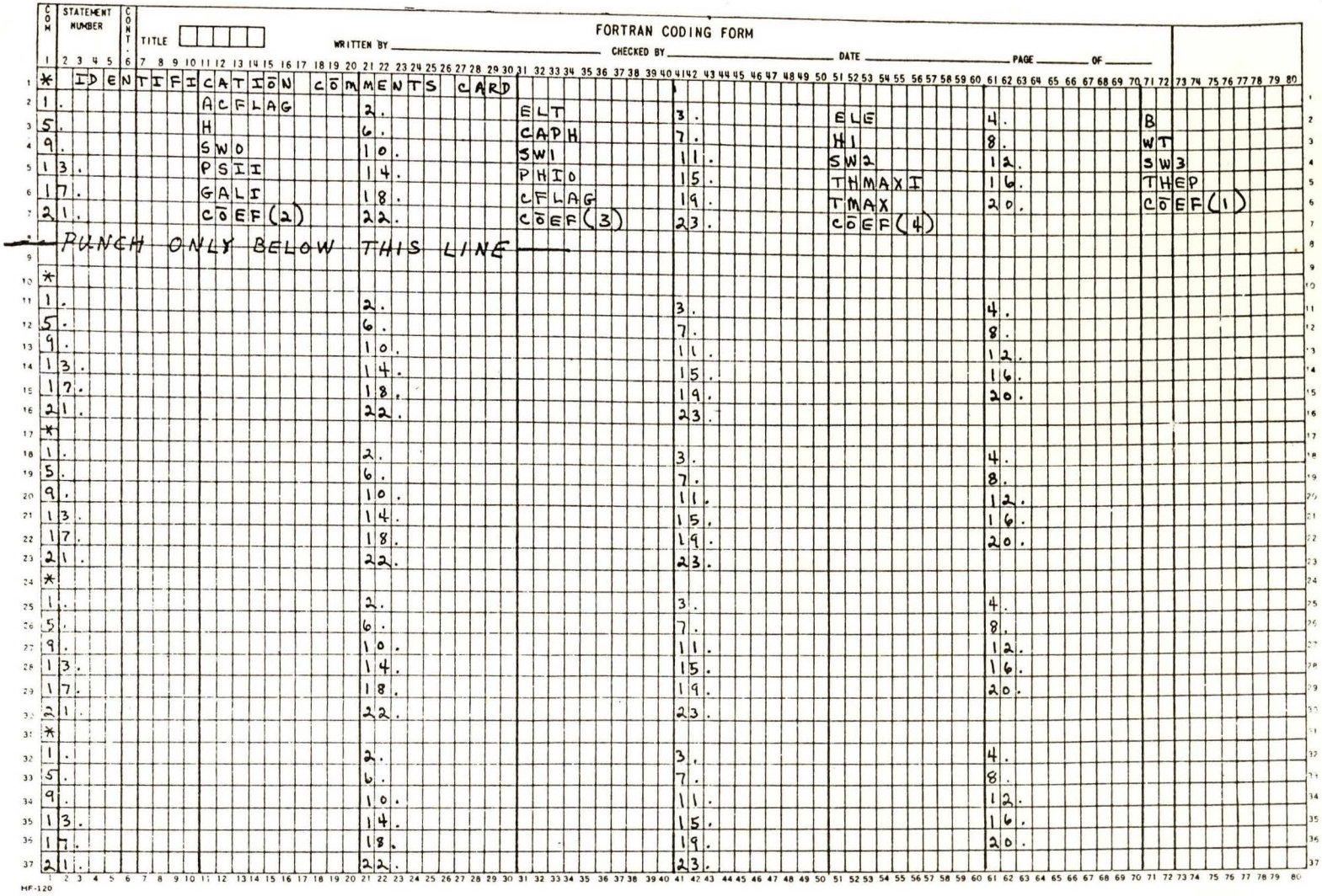

Figure C-2. Example Form for Aircraft Tank Variables

Table C-1. PATSIM Program Input

Number[a]	Name	Description	Initial Values[b]	Units
1	ACFLAG	ACFLAG = 2., program uses CL-215 tank coding ≠ 2., program uses coding for remaining tanks	0	-
2	ELT	Tank length	0	ft
3	ELE	Door opening length	0	ft
4	B	Door width	0	ft
5	H	Vertical measurement between door hinge and tank discontinuity	0	ft
6	CAPH	Initial head height when tank is full	0	ft
7	HI	Height of center tank section		ft
8	WT	Width of top of liquid when tank is full	0	ft
9	SWO	Slope of tank sides (see Figure C-3)	0	-
10	SW1	Slope of tank sides (see Figure C-3)	0	-
11	SW2	Slope of tank sides (see Figure C-3)	0	-
12	SW3	Slope of tank sides (see Figure C-3)	0	-

a The number is also the location in the A-array

b Inital value is set by the program

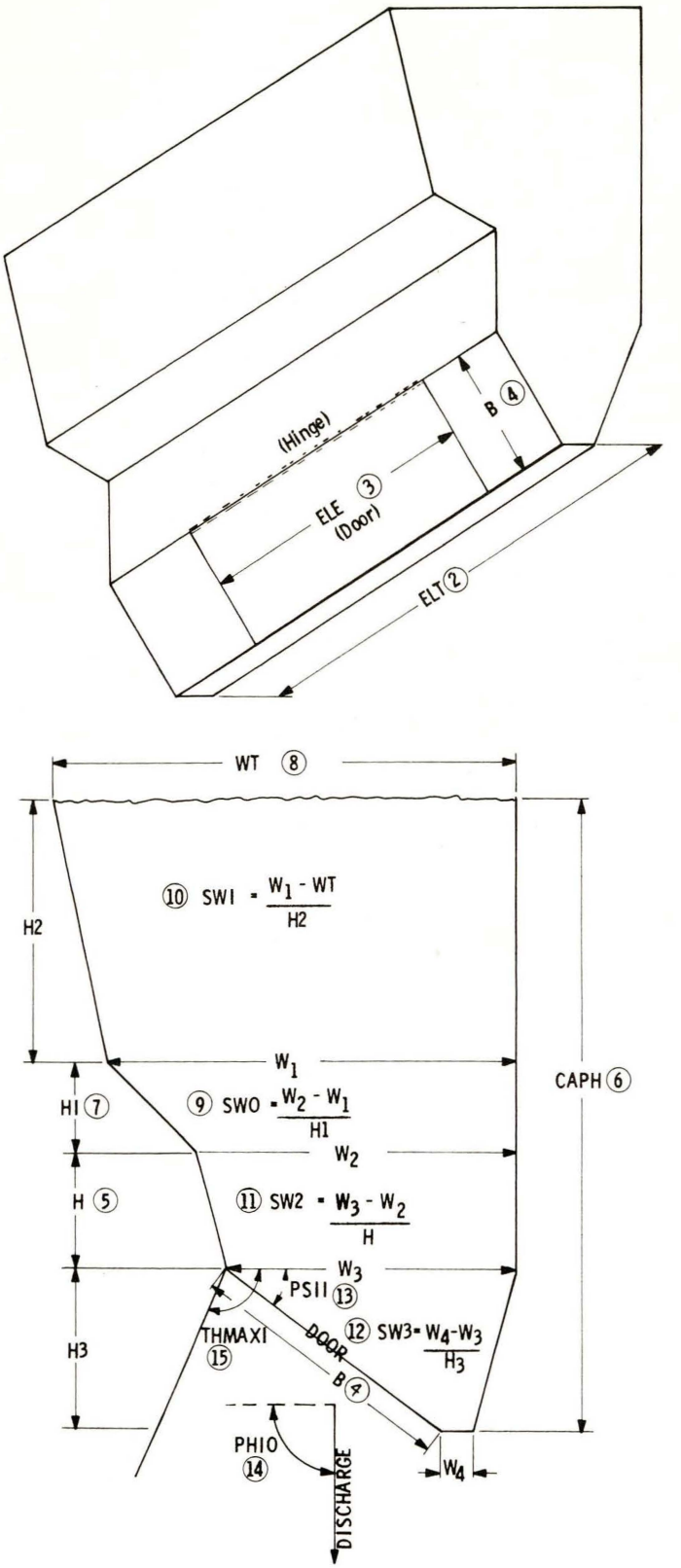

Figure C-3. Aircraft Tank Variables

REFERENCES

1. Swanson, D. H. and Helvig, T. N., "High Altitude Retardant Drop Mechanization Study," Final Report, Vols I and II, Contract 26-2888, 30 April 1973, Honeywell, Inc., Government and Aeronautical Products Division, 600 Second Street North, Hopkins, Minnesota 55343.

2. MacPherson, J. I., "An Improved Theoretical Model for the Ground Distribution of Water Released from a Fire-Bomber," National Research Council of Canada, Aeronautical Report 490 NRC No. 10202, Feb. 1965.

3. George, C. W., "Effect of Drop Height on Retardant Ground Distribution Patterns from the CL-215," USDA NFFL, Missoula, Montana (INT Research Paper in preparation).

4. Davies, O. L., Editor, The Design and Analysis of Industrial Experiments, Hafner Publishing Co., New York, 1954.

5. Simpkins, P. B. and Bales, E. L., "Water-drop Response to Sudden Accelerations," J. Fluid Mechanics, Vol. 55, Part 4 (1972).

6. Papoulis, A., The Fourier Integral and Its Applications, McGraw Hill Book Co., New York, 1962.

7. "Special Issue on FFT," IEEE Transactions on Audio and Electroacoustics, Vol AU-15, No. 2, June 1967.

☆ U.S. GOVERNMENT PRINTING OFFICE: 1974 — 677-091 / 24 REGION NO. 8